INVESTIGATIONS ON THE PERFORMANCE OF GENERALIZED QUADRATURE SPATIAL MODULATION TECHNIQUES

submitted in partial fulfilment of the requirements

for the award of the degree of

DOCTOR OF PHILOSOPHY

by

KIRAN GUNDE

(**Roll No.: 719074**)

Supervisor

Prof. S. Anuradha

Dept. of ECE

Department of Electronics and Communication Engineering

NATIONAL INSTITUTE OF TECHNOLOGY WARANGAL

September, 2023

APPROVAL SHEET

This thesis entitled "**Investigations on the Performance of Generalized Quadrature Spatial Modulation Techniques**" by **Mr. Kiran Gunde** is approved for the degree of **Doctor of Philosophy**.

Examiners

_____

_____

Supervisor

_____

Prof. S. Anuradha

Professor, Electronics and Communication Engineering Department,

NIT WARANGAL

Chairman

_____

Prof. D. Vakula

Head, Electronics and Communication Engineering Department,

NIT WARANGAL

Date:

Place:

DECLARATION

This is to certify that the work presented in the thesis entitled "**Investigations on the Performance of Generalized Quadrature Spatial Modulation Techniques**" is a bonafide work done by me under the supervision of **Prof. S. Anuradha**, Department of Electronics and Communication Engineering, National Institute of Technology Warangal, and was not submitted elsewhere for the award of any degree.

I declare that this written submission represents my ideas in my own words and where others' ideas or words have been included, I have adequately cited and referenced the original sources. I also declare that I have adhered to all principles of academic honesty and integrity and have not misrepresented or fabricated or falsified any idea/date/fact/source in my submission. I understand that any violation of the above will be cause for disciplinary action by the institute and can also evoke penal action from the sources which have thus not been properly cited or from whom proper permission has not been taken when needed.

Kiran Gunde

Roll No: 719074

Date:

Place: Warangal

Department of Electronics and Communication Engineering
National Institute of Technology
Warangal – 506 004, Telangana, India

CERTIFICATE

This is to certify that the dissertation work entitled **"Investigations on the Performance of Generalized Quadrature Spatial Modulation Techniques"**, which is being submitted by **Mr. Kiran Gunde** (Roll No.719074), is a bonafide work submitted to National Institute of Technology Warangal in partial fulfilment of the requirement for the award of the degree of *Doctor of Philosophy in Electronics and Communication Engineering.*

To the best of our knowledge, the work incorporated in this thesis has not been submitted elsewhere for the award of any degree.

Prof. S. Anuradha
Supervisor
Department of ECE
National Institute of Technology
Warangal – 506004

Dedicated to My

Family, Gurus, & Friends

Contents

ACKNOWLEDGEMENTS

I am grateful to many people who made this work possible and helped me during my Ph.D studies. I am greatly indebted to my research supervisor Prof. S. Anuradha for giving me excellent support during my research activity at NIT Warangal. She encouraged me in choosing my research topic, her vision in my research area leads to successful investigations. I am very much thankful for giving research freedom and guidance, support in non-academic matters and for the humanity shown to me. With her inimitable qualities as a good teacher, she chiseled my path towards perfection. Ever since I met her, she has been an eternal source of motivation, inspiration, encouragement and enlightenment. She is responsible for making the period of my research work as an educative and enjoyable learning experience. The thesis would not have seen the light of the day without her insistent support and cooperation.

I am also grateful to Prof. D. Vakula, Head of the Department, Department of Electronics and Communication Engineering, for her valuable suggestions and support that she shared during my research tenure.

I take this privilege to thank all my Doctoral Scrutiny Committee members, Prof. N. Vishwanathan, Professor, Department of Electrical and Electronics Engineering, Prof. L. Anjaneyulu, Professor, Department of Electronics and Communication Engineering, Dr. P. Muralidhar, Associate Professor, Department of Electronics and Communication Engineering for their detailed review, constructive suggestions and excellent advice during the progress of this research work.

I am grateful to the former Head of the ECE Department Prof. P. Sreehari Rao for his continuous support and encouragement. I would also appreciate the encouragement from

teaching, non-teaching members and fraternity of Department of ECE of NIT Warangal. They have always been encouraging and supportive.

I take this opportunity to convey my regards to my closest friends for being always next to me. Thanks to N. Mounika, HM Swetha, and Ch. Vijaya Durga Department of Electronics and Communication Engineering for their motivation and support throughout my work.

I acknowledge my gratitude to all my teachers and colleagues at various places for supporting and cooperating me to complete this work.

I would like to thank my family members (G. Venkataiah, G. Rathnamma, G. Snehalatha and G. S. Karthikeya) for giving me mental support and inspiration. They have motivated and helped me to complete my thesis work successfully.

Finally, I thank God for filling me every day with new hopes, strength, purpose and faith.

(Kiran Gunde)

ABSTRACT

Spatial modulation (SM) is a novel space-domain index modulation (IM) technique for MIMO communication. SM employs a new spatial dimension in addition to conventional MIMO techniques. In SM, the index of the transmit antenna convey extra information, which improves the spectral efficiency (SE) of the system without expanding the bandwidth of the system. A single radio frequency (RF) chain is considered for the data transmission and only one antenna is active at every symbol period, which leads to reduce the hardware complexity and cost of the system. However, there are two limitations in SM, the generalized SM (GSM) and multiple active SM (MA-SM) techniques were developed to enhance the SE by relaxing the limitations of SM. In GSM, the copy of the data symbols are transmitted on different antennas whereas in MA-SM, the different data symbols are transmitted on different antennas. A variant of SM is called quadrature SM (QSM), it improves the SE of SM by expanding spatial points on in-phase and quadrature components. QSM retains almost all the advantages of the SM. A generalized QSM (GQSM) with transmit antenna grouping was developed to increase the SE of QSM.

A modified version of the QSM technique is called a modified generalised QSM (mGQSM), which is introduced to enhance the SE of QSM by considering multiple RF chains. Using the QSM transmission principle, the mGQSM scheme can transmit the data symbols on multiple active antennas. Moreover, the proposed mGQSM scheme provides an additional one bit data rate when compared to GQSM. This thesis presents the performance of mGQSM under imperfect channel conditions over uncorrelated and correlated Rayleigh, Rician, Nakagami-m, and Weibull fading channels. For the computer simulations, we assume the correlation decay

coefficient is equal to 0.7 and various fading parameter values for the Rician, Nakagami-m, and Weibull fading channels. The BER performance of the mGQSM, GQSM, and QSM schemes are evaluated using the ML detector. Furthermore, a low complexity ZF and OB-MMSE detectors are employed for the reduced-codebook mGQSM which achieves near-ML performance with reduced complexity.

However, the SE of the conventional space modulation techniques (SMTs) is restricted to logarithmic proportional to the number of transmit antennas. Recently, a fully QSM (F-QSM) was introduced to achieve a linear proportionality between SE and number of transmit antennas by using a novel transmission mechanism. In this thesis, we propose a fully generalized QSM (FGQSM) scheme to enhance the SE of the F-QSM and mGQSM. In FGQSM, a variable number of transmit antenna combinations are used to transmit multiple data symbols. Moreover, the proposed scheme provides a linear proportionality between SE and number of transmit antennas which gives higher SE for lower number of transmit antennas. The BER performance of the FGQSM is evaluated using ML detector and compared it with mGQSM, RC-mGQSM, and QSM systems. Also, the FGQSM and F-QSM system performances are compared under imperfect channel conditions.

List of Figures

List of Tables

Nomenclature

5G	5th Generation
AWGN	Additive White Gaussian Noise
AAPs	Antenna Activation Patterns
BER	Bit Error Rate
bpcu	bits per channel use
BPSK	Binary Phase Shift Keying
CRR	Complexity Reduction Ratio
CSI	Channel State Information
CQSM	Complex Quadrature Spatial Modulation
DGSM	Double Generalized Spatial Modulation
DQSM	Double Quadrature Spatial Modulation
DSM	Double Spatial Modulation
ESM	Enhanced Spatial Modulation
FGQSM	Fully Generalized Quadrature Spatial Modulation
FGSM	Fully Generalized Spatial Modulation
FIQSM	Fully Improved Quadrature Spatial Modulation
F-QSM	Fully Quadrature Spatial Modulation
GCQSM	Generalized Complex Quadrature Spatial Modulation
GPQSM	Generalized Precoding-aided Quadrature Spatial Modulation

GSM	Generalized Spatial Modulation
GQSM	Generalized Quadrature Spatial Modulation
IAS	Inter-Antenna-Synchronization
ICI	Inter-Channel-Interference
i.i.d	Independent and Identically Distributed
IM	Index Modulation
IQSM	Improved Quadrature Spatial Modulation
ISI	Inter Symbol Interference
LOS	Line-of-Sight
LTE	Long Term Evaluation
mGQSM	Modified Generalized Quadrature Spatial Modulation
MASM	Multiple Active Spatial Modulation
MIMO	Multiple-Input Multiple-Output
MISO	Multiple-Input Single-Output
ML	Maximum-Likelihood
mmWave	Millimeter Wave
M-QAM	M-array Quadrature Amplitude Modulation
MSM	Modified Spatial Modulation
MU-MIMO	Multi User MIMO
NLOS	Non Line-of-Sight
OB-MMSE	Ordered Block Minimum Mean Squared Error
OFDM	Orthogonal Frequency-Division Multiplexing
PCQSM	Parallel Complex Quadrature Spatial Modulation
PDF	Probability Distribution Function
PEP	Pairwise Error Probability

QAM	Quadrature Amplitude Modulation
QSM	Quadrature Spatial Modulation
RC-mGQSM	Reduced Codebook Modified Generalized Quadrature Spatial Modulation
RF	Radio Frequency
RFC	Radio Frequency Chain
SE	Spectral Efficiency
SIMO	Single-Input Multiple-Output
SISO	Single-Input Single-Output
SM	Spatial Modulation
SMTs	Space Modulation Techniques
SMX	Spatial Multiplexing
SNR	Signal to Noise Ratio
SQSM	Signed Quadrature Spatial Modulation
SSK	Space Shift Keying
SVMMSE	Signal Vector-based Minimum Mean Square Error
TACs	Transmit Antenna Combinations
Wi-Fi	Wireless Fidelity
WLAN	Wireless Local Area Network
V-BLAST	Vertical Bell laboratories LAyered Space Time
ZF	Zero Forcing

Notations

N_T	Number of transmit antennas
N_R	Number of receive antennas
N_C	Number of RF chains
M	modulation order of M-QAM constellation
$\Re(\cdot)$	Real part of a complex valued quantity
$\Im(\cdot)$	Imaginary part of a complex valued quantity
R_{Tx}	Correlation matrix at the transmitter
R_{Rx}	Correlation matrix at the receiver
η_X	Spectral efficiency of the transmission technique 'X'
$\mathcal{C}_X$	Codebook for the transmission technique 'X'
$\mathbb{A}_M$	Set of M-QAM symbols
$\mathbb{S}$	Set of AAPs vectors
E_s	Energy of the signal $\mathbf{s}$
K	Rician factor
m	Nakagami parameter
β	Weibull shape parameter
ψ	Correlation decay coefficient
$sort\{\cdot\}$	Sorting function
$exp\,(\cdot)$	Exponential function

$\Gamma(\cdot)$	Gamma Function
$Q(\cdot)$	Demodulation function
$\lfloor \cdot \rfloor$	Floor operator
$\binom{\cdot}{\cdot}$	Binomial operator
$(\cdot)^H$	Hermition operator
$[\cdot]^T$	Transpose operator
$(\cdot)^{-1}$	Matrix inverse operator
$(\cdot)^\dagger$	Moore-Penrose pseudoinverse
$\{\cdot\}$	Fractional part of decimal value
$\lvert\cdot\rvert$	Absolute operator / Cardinality of a set
$\lVert \cdot \rVert$	Frobenius norm
$\lVert\mathbf{p}\rVert_0$	Zero norm of a vector $\mathbf{p}$
$\mathcal{CN}(\mu, \sigma^2)$	Complex Gaussian random variable with mean μ and variance σ^2
$Pr\{\mathbf{p}\}$	Probability of vector $\mathbf{p}$
$E_{\mathbf{H}}\{\cdot\}$	Expectation over channel $\mathbf{H}$
$\mathcal{I}$	In-phase component
$\mathcal{Q}$	Quadrature component
$\mathbf{H}$	Channel matrix
$\mathbf{h}_i$	i^{th} column of $\mathbf{H}$
$h_{i,j}$	$(i,j)^{th}$ element of $\mathbf{H}$
$\delta\mathbf{H}$	Error channel matrix
$\mathbf{n}$	AWGN Noise
$\mathbf{y}$	Received signal
σ_n^2	Noise variance
σ_h	Error variance

Chapter 1

Introduction

1.1 Multile-Input Multile-Output (MIMO)

In wireless communications, a transmitter and receiver are connected by a free-space medium. The transmitter conveys the data to receiver via communication link. There are various link configurations available based on the antennas. A "single-input single-output (SISO)" configuration is formed when the transmitter and receiver have a single antenna. A "multiple-input single-output (MISO)" configuration is formed when a transmitter has multiple antennas and communicates with a receiver that only has one antenna. A "single-input multiple-output (SIMO)" configuration is formed when the receiver has multiple antennas and transmitter has a single antenna. Finally, the configuration known as "multiple-input multiple-output (MIMO)" is created when both the transmitter and the receiver have multiple antennas [1].

MIMO systems are capable to increase the "spectral efficiency (SE)" without compromising in bandwidth and these systems can increase the reliability of the system by taking advantage of diversity gain and multiplexing gain. The diversity gain measures the reliability of the communication system and multiplexing gain measures the spatial degrees of freedom [2]. Typically, these parameters are related by so called diversity-multiplexing gain trade-off. A well known MIMO encoding technique is called spatial multiplexing (SMX),

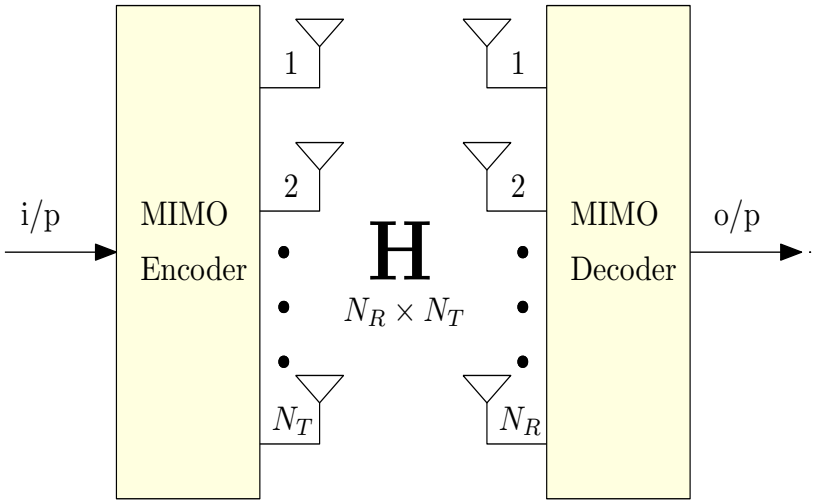

Fig. 1.1 MIMO system

also referred as "vertical Bell laboratories layered space-time architecture (V-BLAST)" [3] in which independent data bits are transmitted simultaneously one on each transmit antenna. In SMX, the number of "radio frequency (RF)" chains increases linearly with number of transmitting antennas, as a result the hardware complexity and cost of the system increases. Physical layer techniques such as "millimeter-wave (mmWave)" communications, visible light communications, MIMO, and massive MIMO are being investigated for potential deployments in fifth generation (5G) networks [4].

Fig. 1.1 shows the MIMO system being N_R receive and N_T transmit antennas. Let the channel $\mathbf{H}$ with $N_R \times N_T$ dimension and whose entries considered as "independent and identically distributed (i.i.d)" complex Gaussian random variables with mean 0 and variance 1, and they are denoted by $h_{i,j}$, it is the complex channel path gain between the j^{th} transmit antenna and i^{th} receive antenna. The information is corrupted by noise at the receiver. Let noise $\mathbf{n}$ and its entries considered as $\mathcal{CN}(0, \sigma_n^2)$, where σ_n^2 denotes the variance of the noise $\mathbf{n}$. The received signal $\mathbf{y}$ is given by,

$$\mathbf{y} = \mathbf{H}\mathbf{x} + \mathbf{n} \tag{1.1}$$

where $\mathbf{y} = [y_1\ y_2 \cdots y_{N_R}]^T$ is the received signal with $N_R \times 1$ dimension.

$\mathbf{x} = [x_1\ x_2\ \cdots x_{N_T}]^T$ is the transmitted signal with $N_T \times 1$ dimension.

$\mathbf{n} = [n_1\ n_2 \cdots n_{N_R}]^T$ is the AWGN noise with $N_R \times 1$ dimension.

$$\mathbf{H} = \begin{bmatrix} h_{11} & h_{12} & h_{13} & \cdots & h_{1N_T} \\ h_{21} & h_{22} & h_{23} & \cdots & h_{2N_T} \\ \vdots & \vdots & \ddots & \vdots & \vdots \\ h_{N_R1} & h_{N_R2} & h_{N_R3} & \cdots & h_{N_RN_T} \end{bmatrix}$$ is the channel gain matrix with $N_R \times N_T$.

where $h_{i,j} \overset{i.i.d}{\sim} \mathcal{CN}(0,1)$ is $(i,\ j)^{th}$ element of $\mathbf{H}$

Assume the perfect "channel state information (CSI)" and applies "maximum-likelihood (ML)" detection rule to estimate the transmitted signal. It is given by,

$$\hat{\mathbf{x}} = \arg\min_{\mathbf{x} \in \mathcal{C}} \|\mathbf{y} - \mathbf{H}\mathbf{x}\|^2 \tag{1.2}$$

where $\hat{\mathbf{x}}$ denotes the estimated signal of the transmitted signal $\mathbf{x}$.

1.2 Motivation

The growing demand for high spectral efficiency (SE) combined with improved quality of service in limited wireless spectrum, motivates the development of a system that can employ multiple antennas. Multiple antennas offer several attractive advantages such as diversity gain and multiplexing gain while being energy efficient. All of these advantages come by introducing the SMX. However, this system has issues of hardware complexity due to multiple RF chains and decoding complexity at the receiver due to simultaneous transmission of the

data. Moreover, SMX suffers from "inter channel interference (ICI)" and "inter symbol interference (ISI)", which further increases the system complexity. With a high demand for higher spectral efficiencies the 5G standard is anticipated and has been the subject of extensive research in recent years. 5G is expected to achieve rate upto 20 Gbps and the SE of 30 bpcu. Such high data rates necessitate the development of new spectrum and energy-efficient techniques.

Index modulation (IM) [5–8, 109] technique uses the indices of the transmission entities such as antennas, sub carriers, RF mirrors, relays, modulation types, and so on. Due to the good trade-off between the energy efficiency and SE, the IM technique has a potential for the next-generation wireless networks. Another class of MIMO systems, known as "space modulation techniques (SMTs)", employs a novel approach to overcome the issues of MIMO systems. The SMTs employ IM with a transmit entity as an antenna, as well as a new spatial constellation to improve the SE while preserving energy resources and decoding complexity. In [9], Mesleh et al. proposed the first well-known SMTs is called "spatial modulation (SM)". SM uses an additional dimension to provide extra information without expanding bandwidth. The fundamental concept of SM is to transmit the data using only one active antenna at one symbol time period, while other antennas remain silent. In SM, input data bits are divided into antenna selection block and symbol selection block. The antenna selection block selects the antenna index from the spatial constellation and the symbol selection block selects the data symbol from the signal constellation. It was demonstrated that SM can achieve high SE while preserving free ICI and reduced receiver complexity by using only one RF chain. "Quadrature SM (QSM)" is a different modulation technique of SM. In QSM the data can be separated into real and imaginary parts and these are transmitted over $\mathcal{I}$ and $\mathcal{Q}$ dimensions. QSM is also free from ICI. The generalized version of QSM technique is called "modified generalised quadrature spatial modulation (mGQSM)". The mGQSM uses multiple RF chains and transmits different data symbols on multiple active antennas. Hence the mGQSM can produce higher SE when compared to SM and QSM techniques.

1.3 Research Objectives

The main objectives of the thesis can be summarized as follows:

- To study and analyse the performance of the mGQSM and reduced codebook mGQSM (RC-mGQSM) systems over uncorrelated Nakagami-m, Rician, and Rayleigh fading channels. A ZF based low complexity detection method is evaluated for the RC-mGQSM. To compare the performance of the mGQSM with SM systems under imperfect channel conditions.

- To study and analyse the performance of the mGQSM and RC-mGQSM systems over various correlated fading channels. A low-complexity OB-MMSE detection method is used to presents the performance of the RC-mGQSM system. To compare the performance of the mGQSM with QSM systems under imperfect CSI conditions.

- To evaluate the mGQSM and RC-mGQSM system performances over uncorrelated and correlated Weibull channels with two different fading environments i.e., deep-fading and non-fading environments. To evaluate and compare the RC-mGQSM system with QSM and GQSM systems.

- To present the proposed fully generalized quadrature spatial modulation (FGQSM) performance over Rayleigh and Rician channels. Also study the fully QSM (F-QSM) scheme performance under imperfect channel conditions. To compare the BER performances of FGQSM and F-QSM systems under imperfect channel conditions.

1.4 Thesis Organization

This section provides the outline of the research work presented in each chapter. The summary of each chapter is as fallows:

- **Chapter 1** This chapter presents the introduction, motivation, research objectives, and the thesis organization.

- **Chapter 2** This chapter discusses the literature review on the space modulation techniques (SMTs).

- **Chapter 3** This chapter presents the mGQSM system performance over uncorrelated Nakagami-m, Rayleigh, and Rician channels. BER results of mGQSM and RC-mGQSM systems are compared to GQSM, QSM, and SM systems with various fading parameter values of Nakagami and Rician channels. A ZF based low complexity detection method is evaluated for the RC-mGQSM. Moreover, the performance of the mGQSM and SM systems are compared under imperfect channel conditions.

- **Chapter 4** This chapter evaluates the BER performances of the mGQSM and RC-mGQSM systems over correlated Nakagami-m, Rayleigh, and Rician channels. BER results of mGQSM and RC-mGQSM systems are compared to QSM and GQSM. Furthermore, a low-complexity OB-MMSE detector is developed for the RC-mGQSM, and it is shown that the OB-MMSE detector achieves near-ML performance. Moreover, the mGQSM and QSM systems are compared under imperfect CSI conditions. The study demonstrates that the mGQSM outperforms QSM.

- **Chapter 5** This chapter evaluates the BER results of mGQSM and RC-mGQSM systems over uncorrelated and correlated Weibull channels. Using the ML detector, the mGQSM and RC-mGQSM systems are compared to QSM and GQSM systems. The BER results of RC-mGQSM system are compared to that of QSM and GQSM systems under two different fading environment scenarios i.e., deep-fading and non-fading environments.

- **Chapter 6** This chapter presents the proposed FGQSM system performance over Rayleigh and Rician channels. A variable transmit antenna combinations are con-

sidered for the FGQSM transmission. The achievable SE of the proposed FGQSM is compared to various SMTs with different values of N_T. F-QSM performance analyzed under imperfect CSI and compared to RC-mGQSM, QSM, and SM. The ML detection is used to compare the BER results of FGQSM with mGQSM and F-QSM schemes. Moreover, the proposed FGQSM and F-QSM systems are investigated under imperfect channel conditions. The results demonstrates that the FGQSM outperforms F-QSM.

- **Chapter 7** This chapter discusses the conclusions and future scope of the research work.

Chapter 2

Space Modulation Techniques

2.1 Spatial Modulation (SM)

2.1.1 Introduction

Spatial modulation (SM) [9–13] is a space-domain energy-efficient transmission scheme for the MIMO system that has been introduced to enhance the SE of the single active antenna systems. SM uses the IM concept over space domain with the antennas as transmission entities. It creates a novel three-dimensional modulation scheme by adding a new antenna index dimension to the traditional MIMO system. The antenna index dimension of the SM scheme can provide additional information, which enhances the SE. For data transmission, a single RFC is used, and one antenna is active at any given symbol period. Since, one antenna is active the SM is free from ISI and ICI. It offers a good trade-off between the SE and computational complexity. The data bits in SM are processed by two mapping blocks, antenna mapper and symbol mapper blocks. The antenna mapper block uses the spatial constellation diagram which consist of all possible transmit antenna indices and the symbol mapper block uses the signal constellation diagram which consist of all possible data symbols.

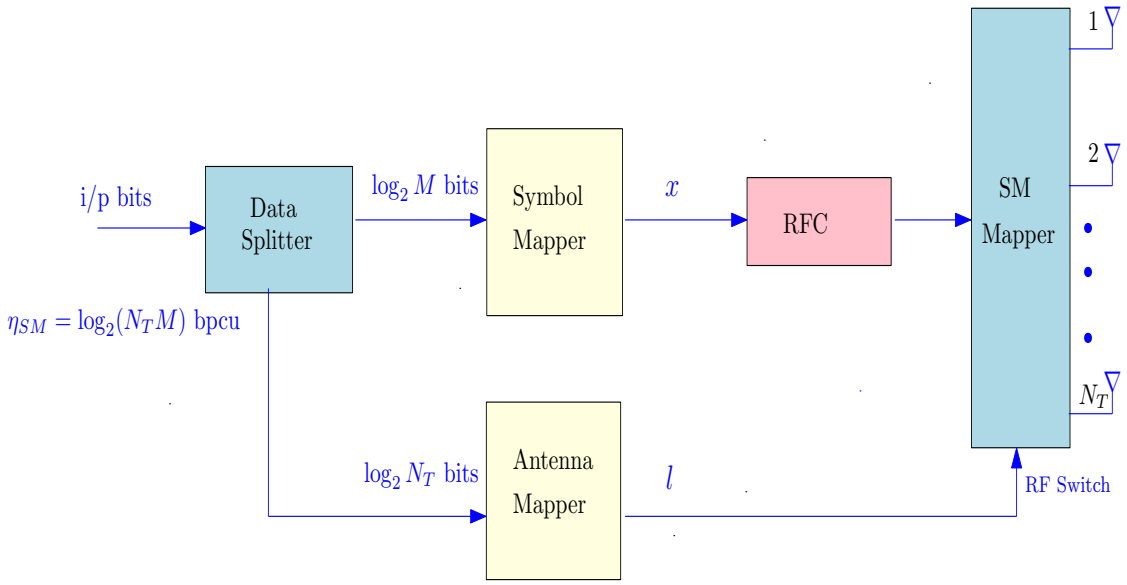

Fig. 2.1 SM transmission system diagram

The SE of the SM is given by,

$$\eta_{SM} = \log_2(N_T) + \log_2(M) \quad \text{bpcu} \tag{2.1}$$

where N_T denotes the number of transmit antennas and M denotes the order of M-QAM constellation.

Fig. 2.1 shows the SM transmission system diagram with N_T transmit antennas. The data splitter divides the inputs data bits to two parts $\log_2(N_T)$ bits and $\log_2(M)$ bits, the first, $\log_2(N_T)$ bits choose the transmit antenna index l with the help of antenna mapper block and remaining, $\log_2(M)$ bits choose the data symbol x with the help of symbol mapper block. At any time instant, the SM scheme uses one RF chain (RFC) and transmit the data symbol through the single active antenna.

SM Codebook:

The codebook consists of all possible transmitted vectors. Given N_T and M, we generate

the codebook for SM is given as,

$$\mathcal{C}_{SM} = \{\mathbf{x} = [0, \cdots, 0, x, 0, \cdots, 0]^T, l = 1, 2, \cdots, N_T; x = 1, 2, \cdots, M\}$$

where $|\mathcal{C}_{SM}| = 2^{\eta_{SM}}$ and the transmitted vector $\mathbf{x}$ is given as,

$$\mathbf{x} = [0, \cdots, 0, x, 0, \cdots, 0]^T, \|\mathbf{x}\|_0 = 1$$

where $l \in \{1, 2, \cdots, N_T\}$ and $x \in \mathbb{S}$. Table 2.1 provides the codebook for SM system with $N_T = 4$ and $M = 4$.

2.1.2 SM System Model

Assume $N_R \times N_T$ SM system being N_R receive and N_T transmit antennas. Let the channel $\mathbf{H}$ and the noise $\mathbf{n}$ being $N_R \times N_T$ and $N_R \times 1$ dimensions, respectively. The coefficients of $\mathbf{H}$ and $\mathbf{n}$ are considered as i.i.d $\mathcal{CN}(0, 1)$ and i.i.d $\mathcal{CN}(0, \sigma_n^2)$, respectively. The received signal $\mathbf{y}$ is corrupted by noise and it is given by,

$$\mathbf{y} = \mathbf{H}\mathbf{x} + \mathbf{n} \tag{2.2}$$

$$= \mathbf{h}_l x + \mathbf{n} \tag{2.3}$$

where $\mathbf{h}_l = [h_{1l}\ h_{2l} \cdots h_{N_R l}]^T$ is the l^{th} column of $\mathbf{H}$.

Assume the perfect CSI and apply the ML detection rule to estimate the data and antenna indices. It is given as,

$$(\hat{l},\ \hat{x}) = \arg\min_{l,x} \| \mathbf{y} - \mathbf{h}_l x \|^2 \tag{2.4}$$

where $\hat{l}$ denotes the estimated antenna index corresponding to estimated data symbol $\hat{x}$.

Table 2.1 Codebook for SM system with $N_T = 4$ and $M = 4$.

i/p bits	Antenna index l	Data symbol x	Transmit vector $\mathbf{x} = [\ x_1\ x_2\ x_3\ x_4]^T$
0 0 0 0	1	$+1+1j$	$[\ +1+1j\ 0\ 0\ 0]^T$
0 0 0 1	1	$-1+1j$	$[\ -1+1j\ 0\ 0\ 0]^T$
0 0 1 0	1	$+1-1j$	$[\ +1-1j\ 0\ 0\ 0]^T$
0 0 1 1	1	$-1-1j$	$[\ -1-1j\ 0\ 0\ 0]^T$
0 1 0 0	2	$+1+1j$	$[\ 0\ +1+1j\ 0\ 0]^T$
0 1 0 1	2	$-1+1j$	$[\ 0\ -1+1j\ 0\ 0]^T$
0 1 1 0	2	$+1-1j$	$[\ 0\ +1-1j\ 0\ 0]^T$
0 1 1 1	2	$-1-1j$	$[\ 0\ -1-1j\ 0\ 0]^T$
1 0 0 0	3	$+1+1j$	$[\ 0\ 0\ +1+1j\ 0]^T$
1 0 0 1	3	$-1+1j$	$[\ 0\ 0\ -1+1j\ 0]^T$
1 0 1 0	3	$+1-1j$	$[\ 0\ 0\ +1-1j\ 0]^T$
1 0 1 1	3	$-1-1j$	$[\ 0\ 0\ -1-1j\ 0]^T$
1 1 0 0	4	$-1+1j$	$[\ 0\ 0\ 0\ -1+1j]^T$
1 1 0 1	4	$+1+1j$	$[\ 0\ 0\ 0\ +1+1j]^T$
1 1 1 0	4	$+1-1j$	$[\ 0\ 0\ 0\ +1-1j]^T$
1 1 1 1	4	$-1-1j$	$[\ 0\ 0\ 0\ -1-1j]^T$

2.1.3 Example: SM Transmission

The SM transmission example with $N_T = 4$ and $M = 4$ is shown in Fig. 2.2. For the given system configuration, the SE of the SM system is given as, $\eta_{SM} = 4$ bpcu. Let 4 bits, [1 0 1 1] for the data transmission at any time instant. Using Table. 2.1, the first $\log_2 N_T = 2$ bits, [1 0] select $l = 3$ and the remaining $\log_2 M = 2$ bits, [1 1] select $x = -1 - 1j$. Therefore, the transmitted vector is given as, $\mathbf{x} = [0 \quad 0 \quad -1-1j \quad 0]^T$.

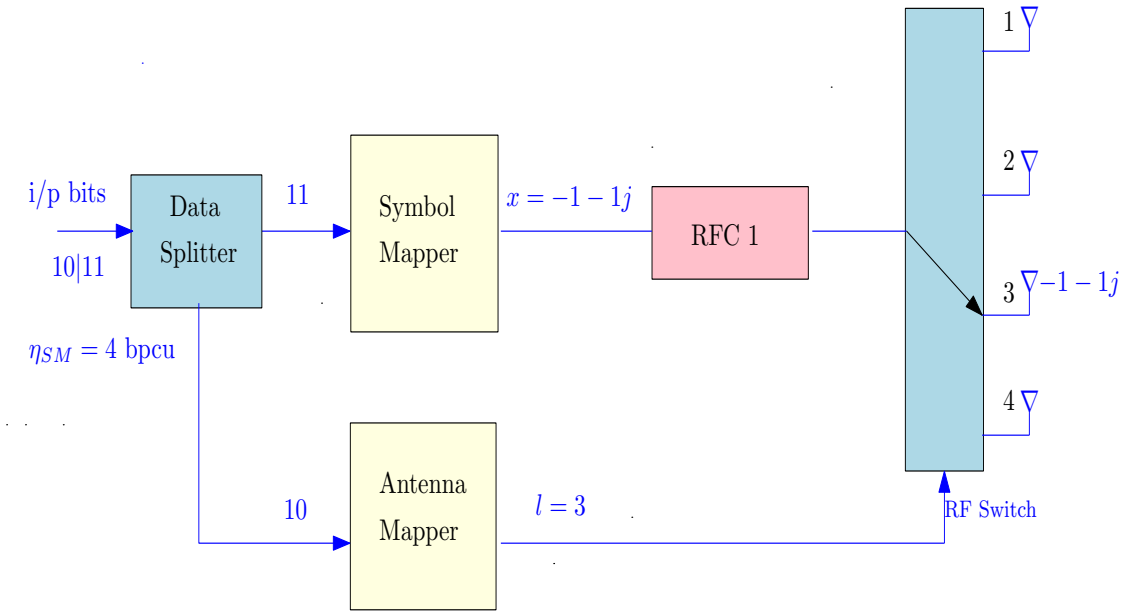

Fig. 2.2 SM transmission with $N_T = 4$ and $M = 4$

2.2 Generalized Spatial Modulation (GSM)

2.2.1 Introduction

A generalized version of SM scheme is called generalized SM (GSM) [14,15], it was introduced to improve the SE of SM by considering multiple RF chains. There are two limitations in SM, they are the number of RF chains and N_T are restricted to one and integer power of 2, respectively. These limitations are relaxed in GSM and activates multiple antennas to transmit same data symbol. Like SM, the GSM scheme completely avoids the ICI. GSM increases SE by base-two logarithm of antenna combinations and it is given by,

$$\eta_{GSM} = \left\lfloor \log_2 \binom{N_T}{N_C} \right\rfloor + \log_2 M \quad \text{bpcu} \tag{2.5}$$

where N_C denotes the number of RF chains, $1 \leqslant N_C \leqslant N_T$.

In GSM scheme, multiple RF chains and different active antennas are used to improve the

SE of SM. At any time instant, N_C out of N_T antennas are active to transmit the symbols and the remaining antennas kept silent. The total number of antenna patterns in GSM are equal to $K_{GSM} = \left\lfloor \log_2 \binom{N_T}{N_C} \right\rfloor$.

Fig. 2.3 shows the GSM transmit system diagram with N_T transmit antennas. The incoming data bits are processes in a block of η_{GSM} bits, where $\eta_{GSM} = K_{GSM} + \log_2 M$ bpcu. First, K_{GSM} bits select the active antennas $l_1, l_2, \cdots, l_{N_C}$ using the antenna mapper and remaining $\log_2 M$ bits select the data symbol x from the symbol mapper. The copy of this data symbol is transmitted on different active antennas.

GSM Codebook :

Given triplet (N_T, N_R, N_C), the codebook for the GSM system is given as,

$$\mathcal{C}_{GSM} = \{\mathbf{x} | x_l \in \mathbb{A}_M, \|\mathbf{x}\|_0 = N_C, \mathcal{I}(\mathbf{x}) \in \mathbb{S}\}$$

where $\mathbb{S}$ denotes the set of "antenna activation patterns (AAPs)", $l = 1, 2, \cdots, N_T$, and $\mathcal{I}(\mathbf{x})$ denotes the function that generate AAPs for $\mathbf{x}$. Table 2.2 provides the codebook for GSM with $N_T = 4,\ N_C = 2$ and BPSK ($M = 2$).

2.2.2 GSM System Model

Assume $N_R \times N_T$ GSM system being N_R receive and N_T transmit antennas. Let the channel $\mathbf{H}$ and the noise $\mathbf{n}$ being $N_R \times N_T$ and $N_R \times 1$ dimensions, respectively. The coefficients of $\mathbf{H}$ and $\mathbf{n}$, considered as i.i.d $\mathcal{CN}(0, 1)$ and i.i.d $\mathcal{CN}(0, \sigma_n^2)$. The received signal $\mathbf{y}$ is corrupted by noise and it is given by,

$$\mathbf{y} \;=\; \mathbf{H}\mathbf{x} + \mathbf{n} \tag{2.6}$$

We assume perfect CSI and apply ML detection rule to estimate the transmitted vector. The ML detection rule is given by,

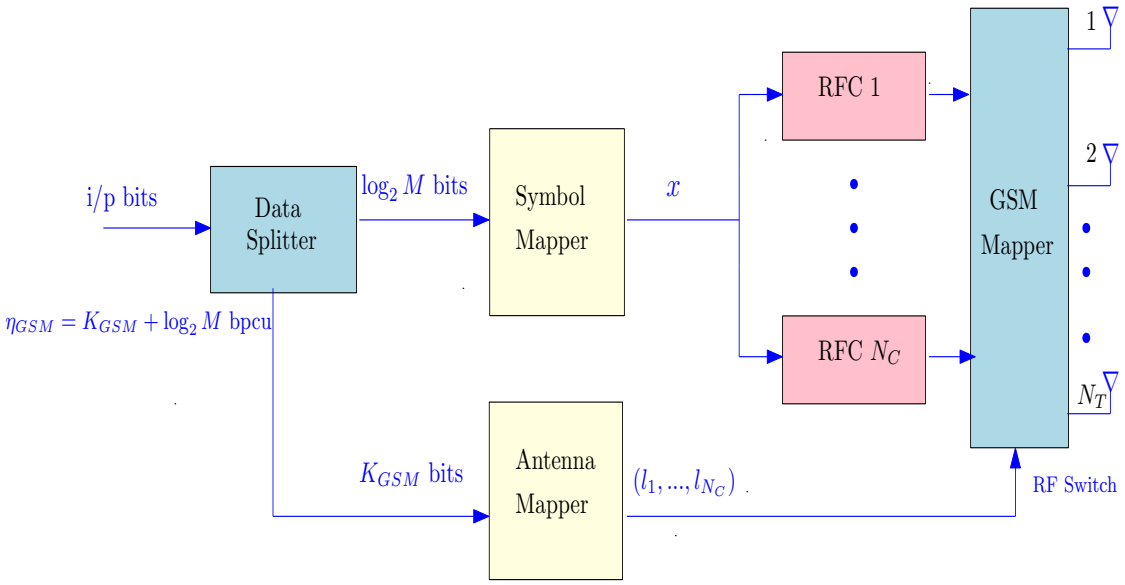

Fig. 2.3 GSM transmission system diagram

$$\widehat{\mathbf{x}} = \underset{\mathbf{x} \in \mathcal{C}_{GSM}}{\operatorname{argmin}} \|\mathbf{y} - \mathbf{H}\mathbf{x}\|^2 \tag{2.7}$$

where $\widehat{\mathbf{x}}$ denotes the estimated vector of $\mathbf{x}$.

2.2.3 Example: GSM Transmission

Fig. 2.4 shows the GSM transmission with $N_T = 4$ and $M = 2$. For $N_C = 2$, the SE of the GSM system is given as, $\eta_{GSM} = 3$ bpcu. Let us consider 3 bits, [1 0 1] for the data transmission at one time instant. Using Table. 2.2, the first $K_{GSM} = 2$ bits, [1 0] select the antenna pattern $(l_1, l_2) = (1, 4)$ and the remaining $\log_2 M = 1$ bit, [1] select the data symbol $x = -1$. The selected symbol is transmitted on antenna 1 and antenna 4. Therefore, the transmitted vector is given as, $\mathbf{x} = [\text{-1} \quad 0 \quad 0 \quad \text{-1}]^T$.

Table 2.2 Codebook for GSM system with $N_T = 4,\ N_C = 2$ and $M = 2$.

i/p bits	Antenna pattern (l_1, l_2)	Data symbol (x)	Transmit vector $\mathbf{x} = [\ x_1\ x_2\ x_3\ x_4]^T$
0 0 0	$(1,2)$	$+1$	$[\ +1\ +1\ 0\ 0]^T$
0 0 1	$(1,2)$	-1	$[\ -1\ -1\ 0\ 0]^T$
0 1 0	$(1,3)$	$+1$	$[\ +1\ 0\ +1\ 0]^T$
0 1 1	$(1,3)$	-1	$[\ -1\ 0\ -1\ 0]^T$
1 0 0	$(1,4)$	$+1$	$[\ +1\ 0\ 0\ +1]^T$
1 0 1	$(1,4)$	-1	$[\ -1\ 0\ 0\ -1]^T$
1 1 0	$(2,3)$	$+1$	$[\ 0\ +1\ +1\ 0]^T$
1 1 1	$(2,3)$	-1	$[\ 0\ -1\ -1\ 0]^T$

2.3 Multiple-Active Spatial Modulation (MA-SM)

2.3.1 Introduction

Multiple-active SM (MA-SM) [16–18] was developed to enhance the SE of the GSM scheme by considering multiple active antennas to transmit different data symbols. Like GSM scheme, the MA-SM is also relaxed the limitations of SM. MA-SM uses multiple RF chains and activates multiple active antennas to transmit different data symbols, simultaneously. SM and SMX are the special cases of MA-SM when $N_C = 1$ and $N_C = N_T$, respectively. The SE of the MA-SM is given by,

$$\eta_{MA-SM} = \left\lfloor \log_2 \binom{N_T}{N_C} \right\rfloor \ + \ N_C \log_2 M \quad \text{bpcu.} \tag{2.8}$$

In MA-SM, the N_C out of N_T antennas are active and other antennas remain silent. Therefore, the total possible antenna patterns are equal to $\binom{N_T}{N_C}$. However, it requires the

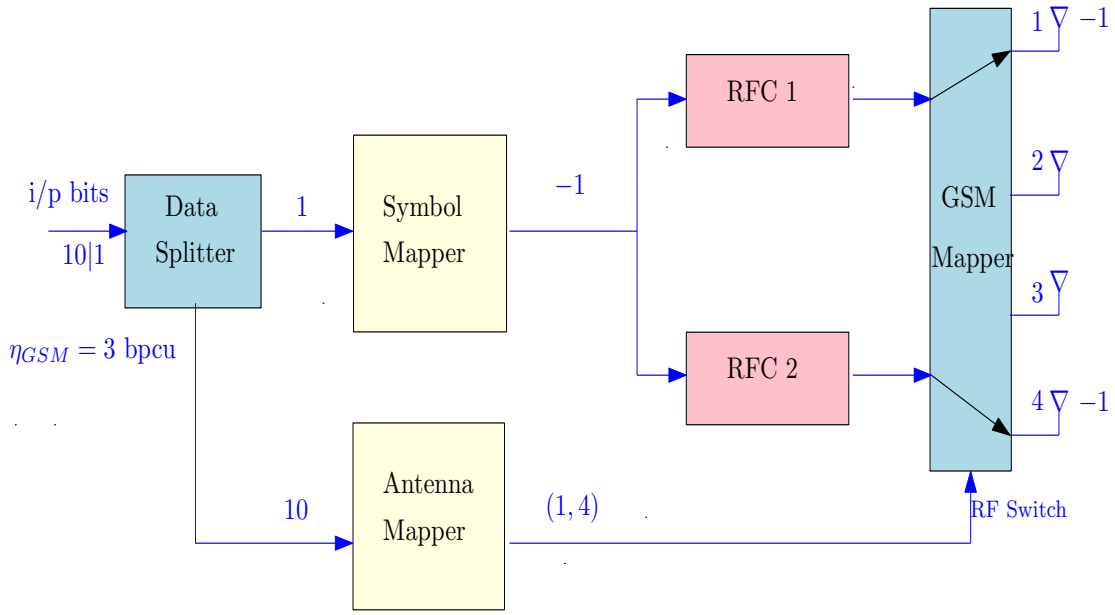

Fig. 2.4 GSM transmission with $N_T = 4, N_C = 2$, and $M = 4$

number of antenna patterns are equal to $K_{MA-SM} = \left\lfloor \log_2 \binom{N_T}{N_C} \right\rfloor$.

Fig. 2.5 shows the MA-SM transmission system with N_T transmit antennas. In MA-SM, the incoming data bits are processes in a block of η_{MA-SM} bits, where $\eta_{MA-SM} = K_{MA-SM} + N_C \log_2 M$ bpcu. The first, K_{MA-SM} bits select the active antennas $l_1, l_2, \cdots, l_{N_C}$ using antenna mapper and remaining $N_C \log_2 M$ bits select the data symbols $x_1, x_2, \cdots, x_{N_C}$ using the symbol mapper. In MA-SM, the various data symbols are transmitted on different active antennas. It can also achieve higher SE than SMX with less number of RF chains.

MA-SM Codebook :

Given triplet (N_T, N_R, N_C), the codebook for the MA-SM system is given as,

$$\mathcal{C}_{GSM} = \{\mathbf{x} | x_l \in \mathbb{A}_M, \|\mathbf{x}\|_0 = N_C, \mathcal{I}(\mathbf{x}) \in \mathbb{S}\}$$

where $\mathbb{S}$ denotes the set of AAPs, $l = 1, 2, \cdots, N_T$, and $\mathcal{I}(\mathbf{x})$ denotes the function that generate AAPs for $\mathbf{x}$. Table 2.3 provides the codebook for MA-SM with $N_T = 4$, $N_C = 2$

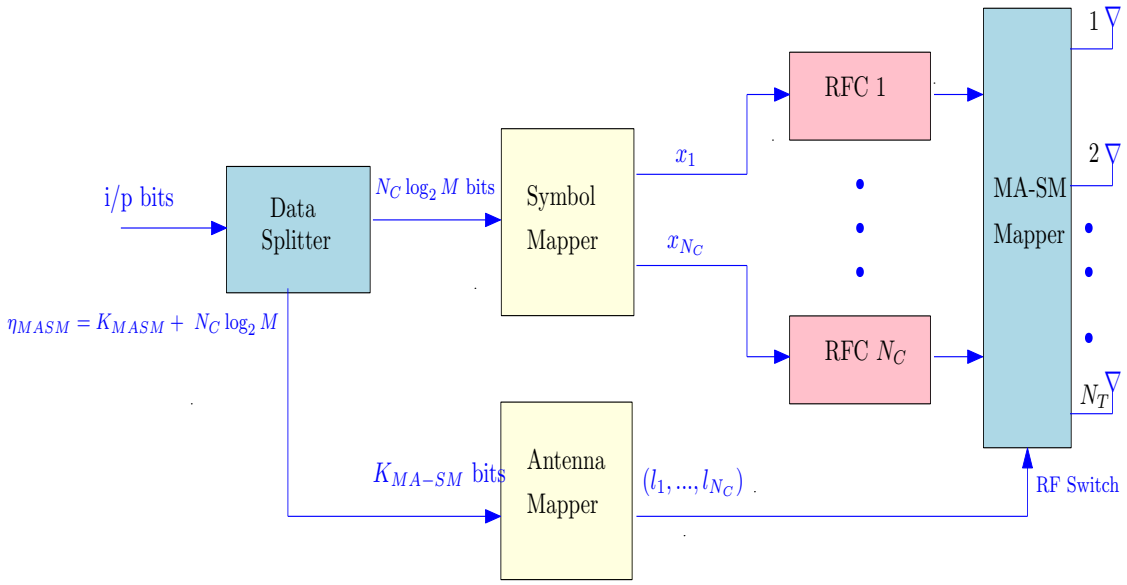

Fig. 2.5 MA-SM transmission system diagram

and BPSK ($M = 2$).

2.3.2 MA-SM System Model

Assume $N_R \times N_T$ MA-SM system being N_R receive and N_T transmit antennas. Let the channel $\mathbf{H}$ and the noise $\mathbf{n}$ being $N_R \times N_T$ and $N_R \times 1$ dimensions, respectively. The coefficients of $\mathbf{H}$ and $\mathbf{n}$, considered as i.i.d $\mathcal{CN}(0,1)$ and i.i.d $\mathcal{CN}(0,\sigma_n^2)$. The received signal $\mathbf{y}$ can be given as,

$$\mathbf{y} = \mathbf{Hx} + \mathbf{n} \tag{2.9}$$

We assume perfect CSI and perform ML detection rule to estimate the data symbols and antenna indices. It can be given as,

$$\widehat{\mathbf{x}} = \underset{\mathbf{x} \in \mathcal{C}_{MA-SM}}{\operatorname{argmin}} \|\mathbf{y} - \mathbf{Hx}\|^2 \tag{2.10}$$

Table 2.3 Codebook for MA-SM system with $N_T = 4, N_C = 2$, and $M = 2$.

i/p bits	Antenna pattern (l_1, l_2)	Data symbols (x_1, x_2)	Transmit vector $\mathbf{x} = [\ x_1\ x_2\ x_3\ x_4]^T$
0 0 0 0	$(1, 2)$	$(+1, +1)$	$[\ +1\ +1\ 0\ 0]^T$
0 0 0 1	$(1, 2)$	$(+1, -1)$	$[\ +1\ -1\ 0\ 0]^T$
0 0 1 0	$(1, 2)$	$(-1, +1)$	$[\ -1\ +1\ 0\ 0]^T$
0 0 1 1	$(1, 2)$	$(-1, -1)$	$[\ -1\ -1\ 0\ 0]^T$
0 1 0 0	$(1, 3)$	$(+1, +1)$	$[\ +1\ 0\ +1\ 0]^T$
0 1 0 1	$(1, 3)$	$(+1, -1)$	$[\ +1\ 0\ -1\ 0]^T$
0 1 1 0	$(1, 3)$	$(-1, +1)$	$[\ -1\ 0\ +1\ 0]^T$
0 1 1 1	$(1, 3)$	$(-1, -1)$	$[\ -1\ 0\ -1\ 0]^T$
1 0 0 0	$(1, 4)$	$(+1, +1)$	$[\ +1\ 0\ 0\ +1]^T$
1 0 0 1	$(1, 4)$	$(+1, -1)$	$[\ +1\ 0\ 0\ -1]^T$
1 0 1 0	$(1, 4)$	$(-1, +1)$	$[\ -1\ 0\ 0\ +1]^T$
1 0 1 1	$(1, 4)$	$(-1, -1)$	$[\ -1\ 0\ 0\ -1]^T$
1 1 0 0	$(2, 3)$	$(+1, +1)$	$[\ 0\ +1\ +1\ 0]^T$
1 1 0 1	$(2, 3)$	$(+1, -1)$	$[\ 0\ +1\ -1\ 0]^T$
1 1 1 0	$(2, 3)$	$(-1, +1)$	$[\ 0\ -1\ +1\ 0]^T$
1 1 1 1	$(2, 3)$	$(-1, -1)$	$[\ 0\ -1\ -1\ 0]^T$

where $\widehat{\mathbf{x}}$ denotes the estimated vector of $\mathbf{x}$.

2.3.3 Example: MA-SM Transmission

The MA-SM transmission with $N_T = 4$ and $M = 2$ is shown in Fig. 2.6. For $N_C = 2$, the SE of MA-SM system is given as, $\eta_{MA-SM} = 4$ bpcu. Let us consider 4 bits, [1 0 1 1] for the data transmission at one time instant. Using Table. 2.3, the first $K_{MA-SM} = 2$ bits, [1 0] select the antenna pattern $(l_1, l_2) = (1, 4)$ and the remaining $N_C \log_2 M = 2$ bits, [1 1] select the data symbols $(x_1 = -1, x_2 = -1)$. Furthermore, these data symbols are transmitted on

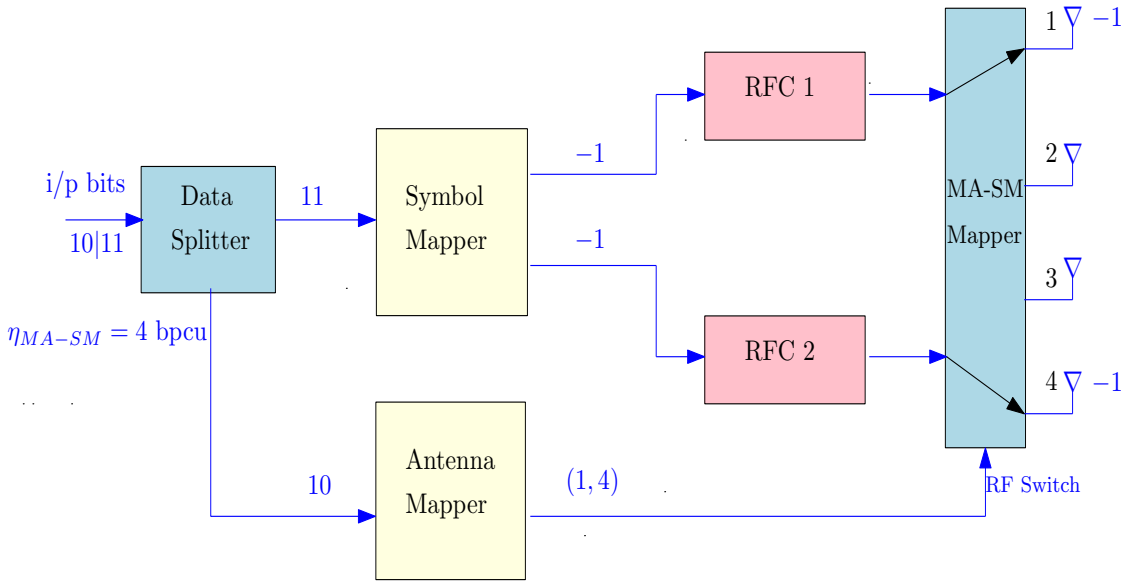

Fig. 2.6 MA-SM transmission with $N_T = 4$ and $M = 4$

antennas 1 and 4. The symbol $x_1 = -1$ is transmits on antenna 1 and the other symbol $x_2 = -1$ transmits on antenna 4. Therefore, the transmitted vector is given as, $\mathbf{x}$ = [-1 0 0 -1]^T.

2.4 Quadrature Spatial Modulation (QSM)

2.4.1 Introduction

Quadrature SM (QSM) [19–21] is a variant technique of SM. QSM enhances the SE of SM by expanding spatial points on in-phase ($\mathcal{I}$) and quadrature ($\mathcal{Q}$) components. The complex data symbol in QSM is divided into real and imaginary parts, which are then sent independently using the SM transmission principle on the same or different active antennas. QSM retains almost all the advantages of the SM. QSM uses single RF chain and the transmitted data symbols are orthogonal to each other. By taking an advantage of $\mathcal{I}$ and $\mathcal{Q}$ dimensions, QSM

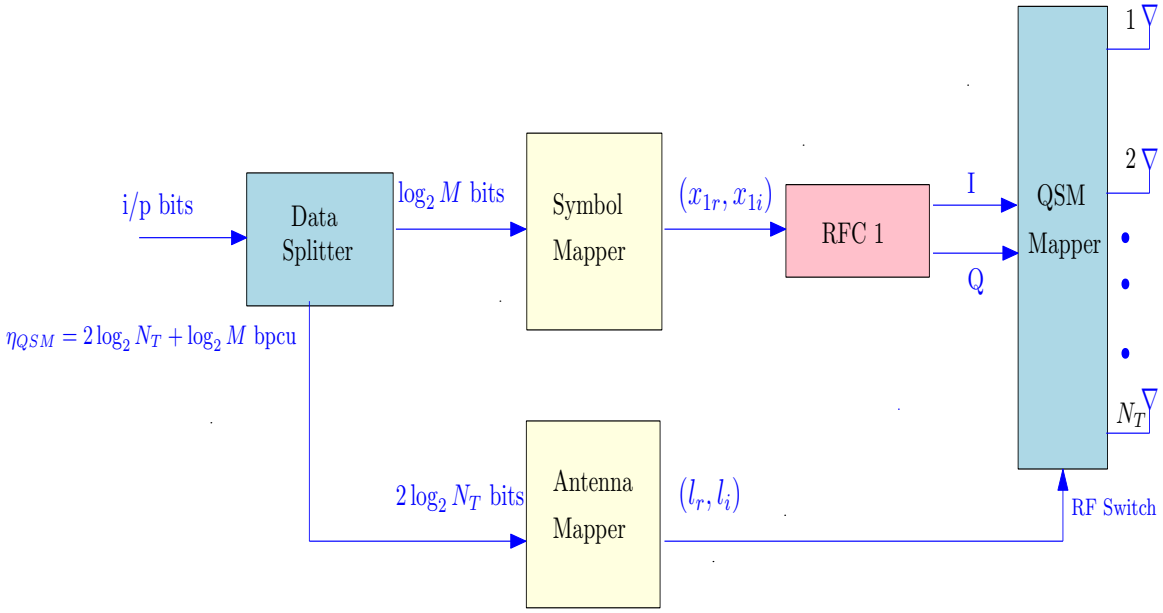

Fig. 2.7 QSM transmission system diagram

system enhances the SE of SM and it is given by,

$$\eta_{QSM} = 2\log_2 N_T + \log_2 M \quad \text{bpcu} \tag{2.11}$$

Fig. 2.7 shows the QSM transmission system with N_T transmit antennas. In QSM, the incoming data bits are processes in a block of $\eta_{QSM} = 2\log_2 N_T + \log_2 M$ bits. The $\log_2 M$ bits, select the data symbol $(x = x_r + jx_i)$ from the symbol mapper, further this symbol is divided into real (x_r) and imaginary (x_i) symbols, remaining $2\log_2 N_T$ bits, select the antenna active pattern (l_r, l_i) from antenna mapper, where the real part and imaginary part of the data symbol are transmitted on one ore two active antennas.

QSM Codebook:

We generate the codebook for QSM system with given N_T and M. The signal $\mathbf{x}$ is expressed as,

1. If one antenna is active, $\mathbf{x} = [0, ..., 0, x_r + jx_i, 0, ..., 0]^T$

where $\|\mathbf{x}\|_0 = 1$ and number of possible transmit vectors, $|\mathcal{C}_{QSM1}| = N_T$.

2. If two antennas are active, $\mathbf{x} = [0, ..., 0, x_r, 0, ..., 0, jx_i, ..., 0]^T$

   where $\|\mathbf{x}\|_0 = 2$ and number of possible transmit vectors, $|\mathcal{C}_{QSM2}| = 2^{\eta_{QSM}} - N_T$.

The total number of possible transmit vectors, $|\mathcal{C}_{QSM}| = |\mathcal{C}_{QSM1}| + |\mathcal{C}_{QSM2}| = 2^{\eta_{QSM}}$. Table. 2.4 provides the codebook for QSM with $N_T = 2$ and $M = 4$.

Table 2.4 Codebook for the QSM system with $N_T = 2$ and $M = 4$.

i/p bits	Antenna pattern (l_r, l_i)	Data symbol $(x = x_r + jx_i)$	Transmit vector $\mathbf{x} = [x_1 \ x_2]^T$
0 0 0 0	(1,1)	$-1+j$	$[-1+j \quad 0]^T$
0 0 0 1	(1,1)	$-1-j$	$[-1-j \quad 0]^T$
0 0 1 0	(1,1)	$+1+j$	$[+1+j \quad 0]^T$
0 0 1 1	(1,1)	$+1-j$	$[+1-j \quad 0]^T$
0 1 0 0	(1,2)	$-1+j$	$[-1 \quad +j]^T$
0 1 0 1	(1,2)	$-1-j$	$[-1 \quad -j]^T$
0 1 1 0	(1,2)	$+1+j$	$[+1 \quad +j]^T$
0 1 1 1	(1,2)	$+1-j$	$[+1 \quad -j]^T$
1 0 0 0	(2,1)	$-1+j$	$[+j \quad -1]^T$
1 0 0 1	(2,1)	$-1-j$	$[-j \quad -1]^T$
1 0 1 0	(2,1)	$+1+j$	$[+j \quad +1]^T$
1 0 1 1	(2,1)	$+1-j$	$[-j \quad +1]^T$
1 1 0 0	(2,2)	$-1+j$	$[0 \quad -1+j]^T$
1 1 0 1	(2,2)	$-1-j$	$[0 \quad -1-j]^T$
1 1 1 0	(2,2)	$+1+j$	$[0 \quad +1+j]^T$
1 1 1 1	(2,2)	$+1-j$	$[0 \quad +1-j]^T$

2.4.2 QSM System Model

Assume $N_R \times N_T$ QSM system being N_R receive and N_T transmit antennas. Let the channel $\mathbf{H}$ and the noise $\mathbf{n}$ being $N_R \times N_T$ and $N_R \times 1$ dimensions, respectively. The coefficients of $\mathbf{H}$ and $\mathbf{n}$, considered as i.i.d $\mathcal{CN}(0,1)$ and i.i.d $\mathcal{CN}(0,\sigma_n^2)$. The received signal $\mathbf{y}$ can be given as,

$$\begin{aligned} \mathbf{y} &= \mathbf{H}\mathbf{x} + \mathbf{n} && (2.12)\\ &= \mathbf{H}(\mathbf{x}_r + j\mathbf{x}_i) + \mathbf{n} && (2.13)\\ &= \mathbf{h}_{l_r} x_r + j\mathbf{h}_{l_i} x_i + \mathbf{n} && (2.14) \end{aligned}$$

where $\mathbf{h}_{l_r}$ is the l_r^{th} column of $\mathbf{H}$, i.e., $\mathbf{h}_{l_r} = [\mathbf{h}_{1,l_r}\ \mathbf{h}_{2,l_r} \cdots \mathbf{h}_{N_R,l_r}]^T$ and $\mathbf{h}_{l_i}$ is the l_i^{th} column of $\mathbf{H}$, i.e., $\mathbf{h}_{l_i} = [\mathbf{h}_{1,l_i}\ \mathbf{h}_{2,l_i} \cdots \mathbf{h}_{N_R,l_i}]^T$.

We assume perfect CSI at the receiver and perform ML detection rule and it is given by,

$$(\hat{l_r}, \hat{l_i}, \hat{x}_r, \hat{x}_i) = \underset{l_r, l_i, x_r, x_i \in \mathcal{C}_{QSM}}{\operatorname{argmin}} \parallel \mathbf{y} - \mathbf{h}_{l_r} x_r - j\mathbf{h}_{l_i} x_i \parallel^2 \quad (2.15)$$

where $\hat{l_r}, \hat{l_i}$ denote the estimated antenna indices corresponding to estimated data symbols $\hat{x_r}, \hat{x_i}$.

2.4.3 Example: QSM Transmission

The QSM transmission with $N_T = 2$ and $M = 4$ is shown in Fig. 2.8. For 4-QAM modulation the SE of the QSM system is given as, $\eta_{QSM} = 4$ bpcu. Let us consider 4 bits, [1 1 1 0] for the data transmission at one time instant. Using Table. 2.4, the first $2\log_2 N_T = 2$ bits, [1 1] select the antenna pattern $(l_r, l_i) = (2, 2)$ and the remaining $\log_2 M = 2$ bits, [1 0] select data symbol $x = +1 + 1j$. Furthermore, this symbol is divided into real and imaginary coefficients $(x_r = +1, x_i = +1j)$. The real symbol $x_r = +1$ is transmits on antenna 2 ($l_r = 2$) and the imaginary symbol $x_{1i} = -1$ is transmits on the same antenna 2 ($l_i = 2$). Finally, the

transmitted vector is given as, $\mathbf{x} = \mathbf{x}_r + j\mathbf{x}_i = [\ 0 \quad +1 + j1]^T$.

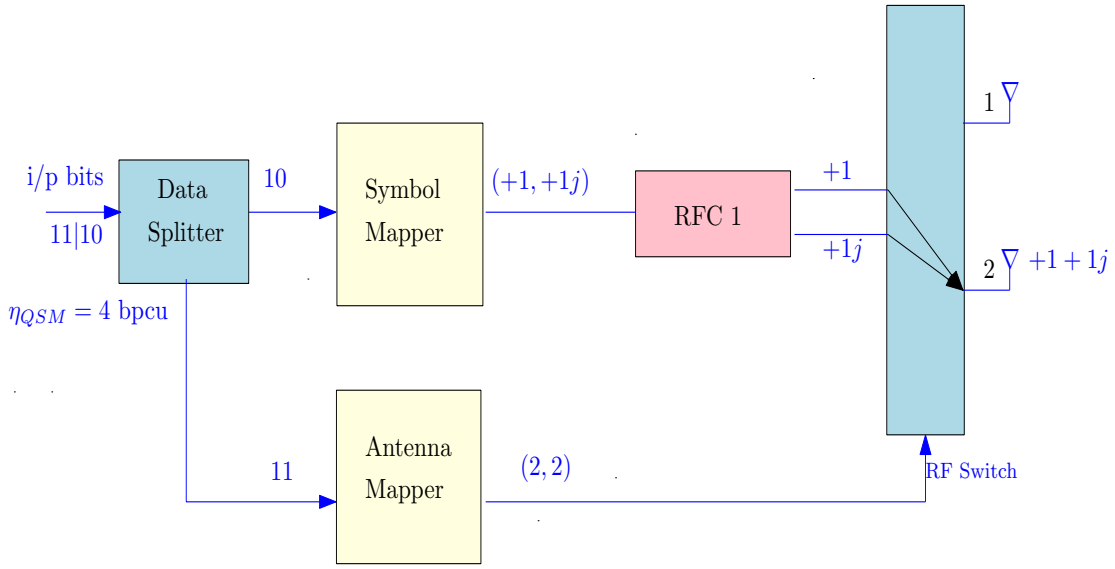

Fig. 2.8 QSM transmission with $N_T = 2$ and $M = 4$.

2.5 Generalised Quadrature Spatial Modulation (GQSM)

2.5.1 Introduction

A generalized QSM (GQSM) scheme with antenna grouping was proposed in [22], the GQSM scheme combines the transmission concepts of QSM and SMX schemes. In GQSM, the transmit antennas N_T are divided into $\mathrm{n}_B = \frac{N_T}{2}$ groups, where n_B is the number of groups. Using QSM transmission principle, each group transmits one M-QAM symbol on either one or two active antennas. Hence, the SE of GQSM system is more than the QSM and it is given by,

$$\eta_{GQSM} = \mathrm{n}_B(\log_2 M + 2) \quad \text{bpcu} \tag{2.16}$$

Fig. 2.9 shows the GQSM transmission system with N_T transmit antennas. In GQSM, the

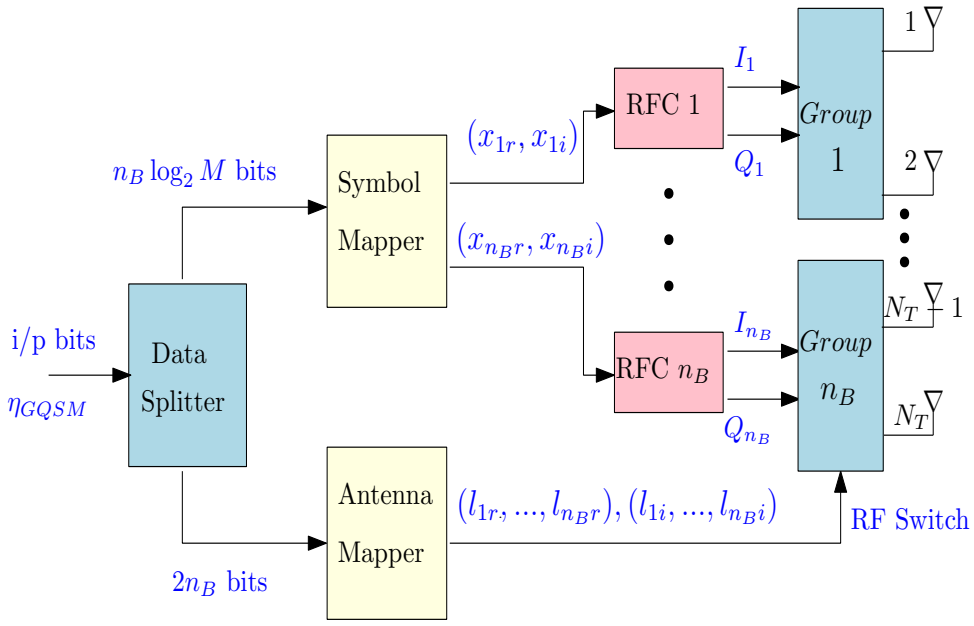

Fig. 2.9 GQSM transmission system diagram

η_{GQSM} bits are divided into two parts of bits, The first, $n_{B\log_2 M}$ bits choose the n_B complex data symbols which are then divided into real and imaginary parts for the transmission. The remaining $2n_B$ bits choose the antenna pattern $(l_{1r}, l_{2r}, \cdots, l_{n_Br})$ for the real symbols transmission and $(l_{1i}, l_{2i}, \cdots, l_{n_Bi})$ for the imaginary symbols transmission.

GQSM Codebook:

For given N_T and M, the codebook for GQSM is given as,

$\mathcal{C}_{GQSM} = \{\mathbf{x} | x_m = x_{mr} + jx_{mi}, x_{mr} \in \Re(\mathbb{A}_M), x_{mi} \in \Im(\mathbb{A}_M), \mathrm{n}_B \leq \|\mathbf{x}\|_0 \leq N_T, \mathcal{I}(\mathbf{x}) \in \mathbb{S}\}$ where $\mathbb{S}$ denotes the set of AAPs, $l = 1, 2, \cdots, N_T$, and $\mathcal{I}(\mathbf{x})$ denotes the function that generate AAPs for $\mathbf{x}$.

Table. 2.5 provide the codebook for GQSM system with $N_T = 4$ and $M = 4$, where $(l_{1r}, l_{1i})$and (l_{2r}, l_{2i}) are the antenna indices of group 1 and group 2, respectively. The spectral efficiency of GQSM is 8 bpcu and the number of groups, $\mathrm{n}_B = 2$.

Table 2.5 Codebook for the GQSM system with $N_T = 4$ and $M = 4$.

i/p bits	Antenna Group 1 $(l_{1r}, l_{1i}), (x_{1r}, x_{1i})$	Antenna Group 2 $(l_{2r}, l_{2i}), (x_{2r}, x_{2i})$
0 0 0 0	$(1,1),(-1,+1j)$	$(3,3),(-1,+1j)$
0 0 0 1	$(2,1),(-1,+1j)$	$(3,3),(-1,-1j)$
0 0 1 0	$(1,2),(-1,+1j)$	$(3,3),(+1,+1j)$
0 0 1 1	$(2,2),(-1,+1j)$	$(3,3),(+1,-1j)$
0 1 0 0	$(1,1),(-1,-1j)$	$(4,3),(-1,+1j)$
0 1 0 1	$(2,1),(-1,-1j)$	$(4,3),(-1,-1j)$
0 1 1 0	$(1,2),(-1,-1j)$	$(4,3),(+1,+1j)$
0 1 1 1	$(2,2),(-1,-1j)$	$(4,3),(+1,-1j)$
1 0 0 0	$(1,1),(+1,+1j)$	$(3,4),(-1,+1j)$
1 0 0 1	$(2,1),(+1,+1j)$	$(3,4),(-1,-1j)$
1 0 1 0	$(1,2),(+1,+1j)$	$(3,4),(+1,+1j)$
1 0 1 1	$(2,2),(+1,+1j)$	$(3,4),(+1,-1j)$
1 1 0 0	$(1,1),(+1,-1j)$	$(4,4),(-1,+1j)$
1 1 0 1	$(2,1),(+1,-1j)$	$(4,4),(-1,-1j)$
1 1 1 0	$(1,2),(+1,-1j)$	$(4,4),(+1,+1j)$
1 1 1 1	$(2,2),(+1,-1j)$	$(4,4),(+1,-1j)$

2.5.2 GQSM System Model

Assume $N_R \times N_T$ GQSM system being N_R receive and N_T transmit antennas. Let the channel $\mathbf{H}$ and the noise $\mathbf{n}$ being $N_R \times N_T$ and $N_R \times 1$ dimensions, respectively. The coefficients of $\mathbf{H}$ & $\mathbf{n}$, considered as i.i.d $\mathcal{CN}(0,1)$ and i.i.d $\mathcal{CN}(0,\sigma_n^2)$. The received signal $\mathbf{y}$ can be given as,

$$\mathbf{y} = \mathbf{H}\mathbf{x} + \mathbf{n} \tag{2.17}$$

We assume perfect CSI and apply ML detection rule to estimate the transmitted vector and it is given by,

$$\widehat{\mathbf{x}} = \underset{\mathbf{x} \in \mathcal{C}_{GQSM}}{\operatorname{argmin}} \|\mathbf{y} - \mathbf{H}\mathbf{x}\|^2 \tag{2.18}$$

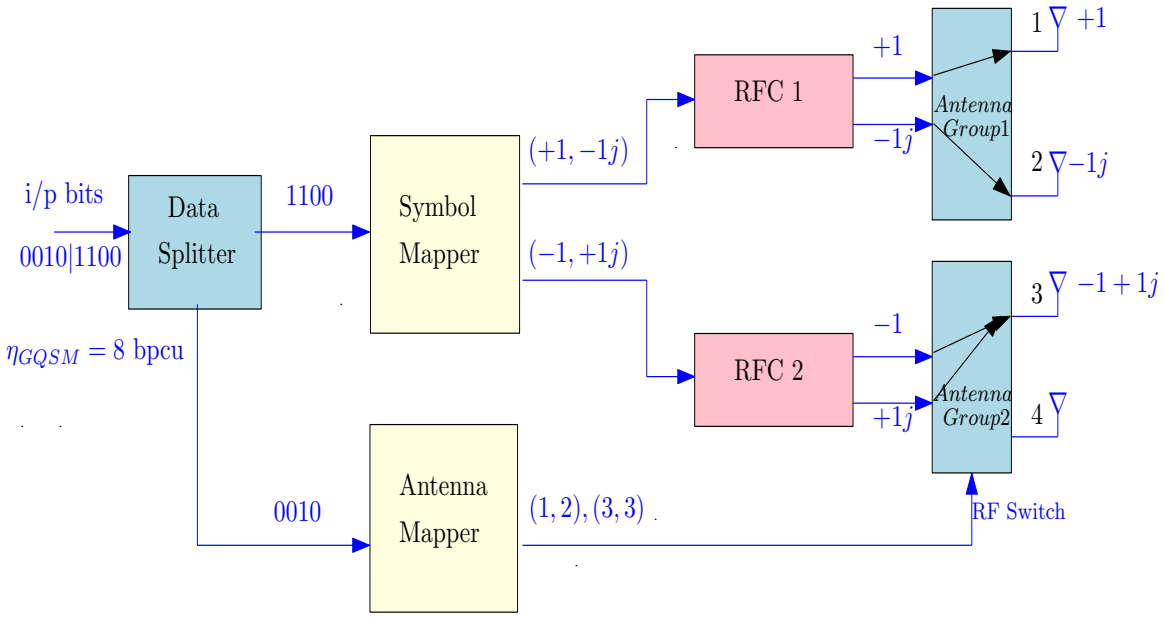

Fig. 2.10 GQSM transmission with $N_T = 4$ and $M = 4$.

where $\widehat{\mathbf{x}}$ denotes the estimated vector of $\mathbf{x}$.

2.5.3 Example: GQSM Transmission

Fig. 2.10 shows the GQSM transmission with $N_T = 4$ and $M = 4$. The SE of the GQSM is given as, $\eta_{GQSM} = 8$ bpcu. In GQSM, two groups are used for the data transmission where each group can transmit 4 bits. For GQSM transmission, let 8 bits, [0 0 1 0 1 1 0 0] at any time instant. Using Table. 2.5, the first 4 bits, [0 0 1 0] select $(l_{1r}, l_{1i}) = (1, 2)$ from antenna group 1 and $(l_{2r}, l_{2i}) = (3, 3)$ antenna group 2. Remaining 4 bits, [1 1 0 0] choose data symbols $x_1 = +1 - j1$ and $x_2 = -1 + j1$ from Table. 2.5. Therefore, antennas $l_{1r} = 1$ and $l_{2r} = 3$ transmits $x_{1r} = +1$ and $x_{2r} = -1$, respectively. Similarly, the antennas $l_{1i} = 2$ and $l_{2i} = 3$ transmits $x_{1i} = -1$ and $x_{2i} = +1$, respectively. The final vector is given as, $\mathbf{x} = \mathbf{x}_r + j\mathbf{x}_i = [+1 \quad -j1 \quad -1 + j1 \quad 0]^T$.

2.6 Literature Survey

In [23], the authors applied the IM technique for the "orthogonal frequency division multiplexing (OFDM)" systems and proposed a scheme called the "subcarrier-index modulation OFDM (SIM-OFDM)". This scheme adds a new subcarrier index dimension to the conventional 2-D signal dimension. The spectral efficiency of the SIM-OFDM is much smaller when compared to the OFDM systems.

In [24], the authors combined the OFDM with IM and introduced a new technique is called OFDM-IM. In this scheme, the data bits are conveyed by the M-QAM modulation scheme and the indices of the subcarriers. The authors in [25], introduced the different techniques to enhance the SE of OFDM-IM and also improves the diversity gain.

The authors in [26], proposed the "multiple-mode OFDM-IM (MM-OFDM-IM)". In this scheme the data is conveyed through the multiple modes and their permutations. The authors in [27], proposed the "generalized MM-OFDM-IM (GMM-OFDM-IM)" to enhance the SE of the MM-OFDM-IM.

In [28], a "layered OFDM-IM (L-OFDM-IM)" scheme was introduced. In L-OFDM-IM, the subcarriers are separated as multiple layers and the data bits are conveyed by the active subcarriers in each layer. In [29], the inactive subcarriers in the OFDM-IM scheme used to transmit signals with help of cognitive radio networks are presented. In [30] and [31], the authors proposed a low complexity detection methods for IM multiple access (IM-MA) and MIMO-OFDM-IM schemes, respectively.

In [32, 33], the authors investigated the SM performance over Nakagami channel and also derived the symbol error rate expression for SM. In [34, 35], the authors analyzed the performance of SM scheme under imperfect CSI conditions. The authors in [36], studied the effects of imperfect CSI on the error performance of the SM over Rayleigh and Rician channels.

In [37,38], the BER SM variants are compared under generalized fading channels. In [39], the authors validated the SM and SMX performances experimentally and described require-

ments and channel conditions for the experimental testbed. In [40], the SM performance improved under correlated channel conditions by using the trellis coded modulation concept where the antennas are divided into sub sets such that the spacing between antenna sub sets is maximized.

In [41], the performance of MIMO system was evaluated over Weibull channel with improved channel capacity. In [42, 43], the MIMO system was analyzed over various fading channels. The optimal detection methods were studied in [44, 45].

In [46, 47], the SM performance was evaluated over Weibull channel. In [46], the SM system studied over Weibull fading and derived the symbol error rate expression for the M-QAM SM system under low complexity receiver. In [47], the performance of various SM techniques is evaluated over Weibull non-fading and deep-fading environments.

In [48, 49], the recent advances and applications of various SM techniques are presented and also discussed the future research direction towards the spectrum and energy-efficient 5G wireless networks. The authors in [50] provide a comprehensive overview of SM research and discussed the fundamental principles and applications of various single and multidimensional entity schemes.

In [51], a simplified variant of SM technique is called "space shift keying (SSK)" was proposed, the M-QAM symbol is absent in SSK and data is conveyed by the transmitting antennas only. In [52], the generalized SSK was introduced to enhance the SE of SSK.

In [53], the Hamming SSK technique was introduced where the number of activated antennas are varied with the help of Hamming codes. In [54], binary-SSK was developed where a dual set active antennas are used to transmit real and imaginary numbers. In [55], binary generalized SSK was introduced which enhance the SE of both binary SSK and generalized SSK.

In [56], the mutual information achieved by the SM was studied, for different antenna configurations. In [57], a non-trivial bound on mutual information of SM was derived. In [58], the authors proposed a Euclidean distance based low complexity method.

In [59], the GSM performance is analyzed under correlated Rician and Rayleigh channels and also derived the closed form expression for GSM capacity. GSM avoids ISI, due to the same symbol transmission on multiple antennas. However, the rate of GSM low when compared to MASM. In [60, 111], the GSM performance was studied under imperfect CSI.

In [61], a novel "ordered block minimum mean-squared error (OB-MMSE)" detector was introduced for the GSM scheme to reduced complexity. In [62], the authors proposed a sphere decoding based low complexity detection method for GSM. Using cost metric, the proposed method eliminates the unnecessary interference caused by the symbol detection.

In [63], the enhanced SM (ESM) was introduced to increase the SE of SM by using two different signal constellations. For the data transmission, the primary constellation is considered when the single antenna is active and the secondary constellation is considered when the two antennas are active.

In [64] and [65], the QSM is analyzed under Rician and Nakagami channels, respectively. In [64], the QSM performance was studied with LOS impact. In [65], it is proved that the channel phase parameters are a significant effect on the performance of QSM. In [66], the authors demonstrated the phase distribution of Nakagami-m fading.

In [67–69], the authors studied the QSM performance with imperfect CSI conditions. In [69], the QSM performance investigated over correlated $\eta - \mu$ channels in the presence of channel imperfections. The authors in [70, 71] presented the QSM performance under imperfect CSI over correlated fading channels. In [71, 112], QSM is compared to conventional SM under imperfect CSI conditions

In [72], the reliability of the QSM cooperative decode and forward diversity systems with a multi-antenna transmitter and relay was investigated. In [73], a novel reduced-complexity sphere decoder technique was proposed for QSM decoders. It was proved to have the best QSM ML performance. In [74], the authors presented the comprehensive review of possible capacity for QSM utilizing the three-dimensional statistical channel model.

In [75], the authors analyzed the BER performance of QSM system over three different

generalized fading channels. It was shown that the influence of fading parameters on the BER performance. In [76], a low complexity "signal vector-based minimum mean square error (SVMMSE)" was proposed for QSM, a combination of signal vector-based and OB-MMSE detectors are used to detect the symbols transmitted on one and two antennas, respectively.

In [77], the authors proposed the "modified SM (MSM)" uses more than one antenna to transmit the data and avoids the effect of spatial correlation. In [78], MSM scheme was analyzed under spatially correlated channels using SVMMSE detector. It was shown that SVMMSE is close to the ML detector with reduced complexity.

In [79, 80], improved QSM (IQSM) scheme was proposed to enhance the SE of QSM by sending constellation symbol over $\mathcal{I}$ and $\mathcal{Q}$ dimensions in one symbol duration.

In [81], proposed double SM (DSM) to enhance the SE of the SM. DSM employs two modulation symbols, the first of which is transmitted directly on the selected antenna, while the other is transmitted with a rotation angle, showing that the performance of DSM outperforms QSM.

In [82], the performance of DSM was studied under imperfect CSI conditions over Nakagami, Rician, and Rayleigh channels. The OB-MMSE detector is used to analyze the performance of DSM. In [83], using the transmission concept of DSM the double QSM (DQSM) scheme was introduced to improve the rate of IQSM and results shown that DQSM is better than IQSM.

In [84], the double GSM (DGSM) was proposed to improve the transmit diversity gain and SE by combining the transmission concepts of ESM and QSM. In addition, the DGSM and QSM were compared in terms of SE and computational complexity.

In [85], a complex QSM (CQSM) was proposed to enhance SE of QSM. In CQSM, the data can be communicated using two separate symbols, the first symbol is transmitted directly, while the second symbol is a rotated it. In [86], the authors discussed that how to generate the best modulation sets to increase Euclidean distance for CQSM.

In [87], a generalized CQSM (GCQSM) was proposed. Like GSM, the spatial symbols

are created in GCQSM where each resulting combination is then divided into two subsets. In [88], the authors proposed the parallel CQSM (PCQSM) to enhance the SE of CQSM. In PCQSM, the antennas are divided into groups and transmit the two modulation symbols.

In [89], a ZF based low complexity detector was introduced for the GQSM, which achieves near-ML performance. In [90], the "generalized precoding-aided QSM (GPQSM)" was developed further to improve the SE of the QSM. In [91], the authors analyzed the performances of GSM and GQSM systems with and without the knowledge of CSI at the transmitter. Also, proposed a low complexity codebook based signal shaping method to mitigate the computational burden.

In [92], the authors derived an expression for achievable SE for GQSM scheme and compared it with various SMTs. Moreover, two low complexity detectors are introduced for GQSM.

In [93], a modified GQSM (mGQSM) scheme was introduced to enhance SE of QSM. This scheme avoids antenna grouping and enables multiple active antennas to transmit the data symbols. Moreover, a "reduced codebook mGQSM (RC-mGQSM)" was developed to decrease the complexity of mGQSM.

In [94], the authors proposed a fully GSM (FGSM) scheme to improve the SE of SM and GSM. To improve the SE, a new transmission mechanism is developed that enables the linear proportionality between the SE and N_T, whereas all other SMTs use logarithmic proportionality between the SE and N_T. In [95], the fully grouped generalized SM scheme was developed, the antennas are partitioned into groups and each group uses the FGSM concept.

In [96], the authors proposed a fully QSM (F-QSM) scheme. Like FGSM, F-QSM scheme employs a novel transmission mechanism in order to attain the linear proportionality between the SE and N_T. However, F-QSM scheme transmits $\Re(\cdot)$ and $\Im(\cdot)$ parts independently.

The complexity of F-QSM is compared to QSM with different N_T. In [97, 98, 110], the authors analyzed the F-QSM performance under correlated Rayleigh and Rician channels.

In [99], the authors discussed the required Hardware and limitations for various SMTs with minimum number of RF chains. Different schemes are compared in terms of power consumption, cost, and complexity.

In [100], fully IQSM (FIQSM) was developed to improve the SE of F-QSM. Like F-QSM, the SE of FIQSM scheme is linearly proportional with N_T. In [101], the authors presented the comprehensive study of different SMTs and provide the general mathematical framework for SMTs.

In [104–108], the signed QSM (SQSM) was proposed to enhance the SE of QSM. In SQSM, the 2 dimensional spatial constellation is extended to 4 dimesnional spatial constellation i.e. $\pm$ in-phase and quadrature phases. Furthermore, a low complexity detection methods are proposed for the SQSM.

In [113], a new hexagonal-QAM constellation was proposed, it has the advantage of maximizing the Euclidean distance when compared to conventional QAM systems. This scheme enhance error performance of GCQSM.

2.7 Conclusion

In this chapter, we have discussed the literature survey on various SMTs. The transmission concepts of SM, GSM, MA-SM, QSM, and GQSM techniques are presented in order to enhance the SE and also provided the suitable examples for the data transmission. QSM uses novel transmission concept and transmits the various data symbols single or two antennas. Hence the SE of the QSM is more than that of conventional SM techniques. The GQSM is the multiple active antenna technique that divides the antennas into groups and transmits the data using the transmission principle of QSM. In the literature, various QSM techniques were studied and found that the mGQSM and RC-mGQSM techniques can provide higher SE with minimal number of RF chains. In all the contributory chapters, we have presented the BER results of mGQSM and RC-mGQSM techniques by considering two RF chains.

Chapter 3

mGQSM Performance over Nakagami-m Fading channel

3.1 Modified Generalised Quadrature Spatial Modulation (mGQSM)

3.1.1 Introduction

"Modified generalised quadrature spatial modulation (mGQSM)" is introduced to improve the SE of QSM and SM schemes by considering multiple RF chains. By relaxing antenna grouping of GQSM, the mGQSM provides an extra SE of 1 bpcu with the constraint of $\{\log_2 \binom{N_T}{N_C}\} \geq 0.5$, where $N_C \leq \lfloor \frac{N_T}{2} \rfloor$. In mGQSM, the total number of AAPs are equal to $\binom{N_T}{N_C}^2$, from which we can choose $2^{\left\lfloor 2\log_2 \binom{N_T}{N_C} \right\rfloor}$ AAPs. Whereas in GQSM scheme, the AAPs are equal to 2^{N_T} and it is half when compared to mGQSM. At any time instant the active antennas in mGQSM are varies from N_C to $2N_C$. The SE of the mGQSM scheme is given by [93],

$$\eta_{mGQSM} = \left\lfloor 2\log_2 \binom{N_T}{N_C} \right\rfloor + N_C \log_2 M \quad \text{bpcu} \tag{3.1}$$

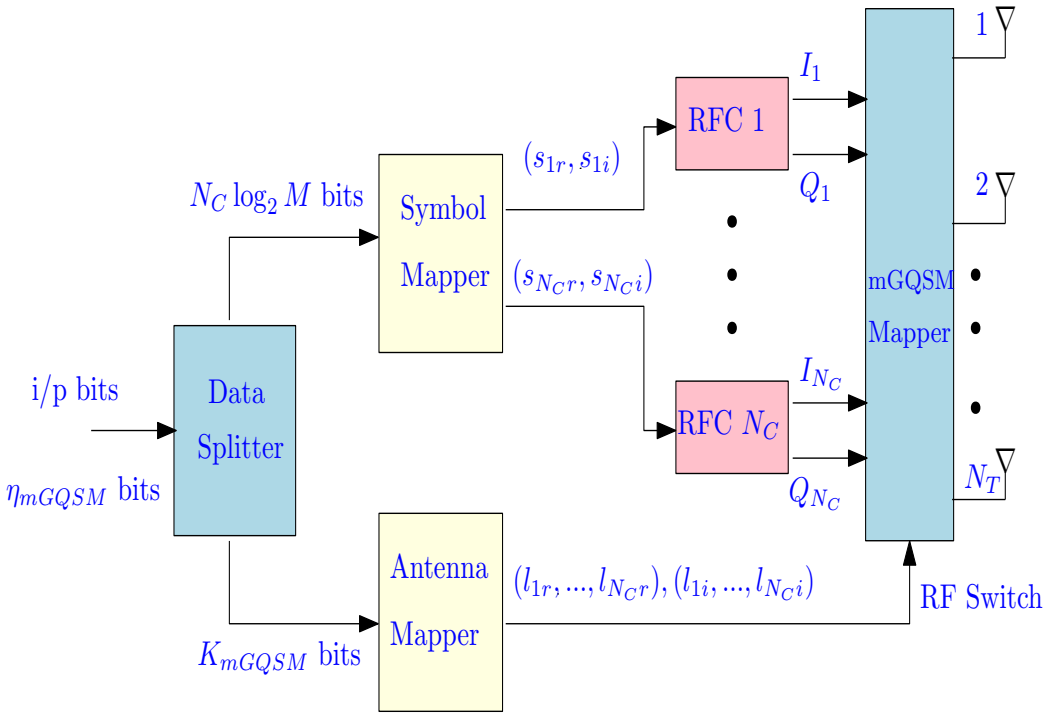

Fig. 3.1 mGQSM transmission system diagram

Fig. 3.1 shows the mGQSM transmitter system diagram with N_T transmitting antennas. The input bits in mGQSM scheme are processed by two mapping blocks, antenna mapper block and symbol mapper block. The η_{mGQSM} bits split into $K_{mGQSM} = \left\lfloor 2 \log_2 \binom{N_T}{N_C} \right\rfloor$ bits and $N_C \log_2 M$ bits. First, K_{mGQSM} bits select the transmitting antennas using the antenna mapper block, and the remaining, $N_C \log_2 M$ bits select the modulation symbols using the symbol mapper block. Furthermore, the transmitted complex symbols are grouped into $\Re(\cdot)$ and $\Re(\cdot)$ parts. Using the QSM transmission principle, these are transmitted independently on the active antennas using the AAPs selection procedure provided in the following subsection. 3.1.2.

3.1.2 Antenna Activation Patterns (AAPs) Selection

1. Given N_T.

2. Write possible N_C values, using $1 \leq N_C \leq \lfloor \frac{N_T}{2} \rfloor$.

3. Choose one value for N_C.

4. Write $\binom{N_T}{N_C}^2$ possible AAPs for the transmission of real and imaginary data symbols.

5. Form a set $\mathbb{S}$, which consist of $2^{K_{mGQSM}}$ AAPs out of $\binom{N_T}{N_C}^2$ total possible AAPs.

Codebook:

Given N_T, the codebook for mGQSM is given as,

$\mathcal{C}_{mGQSM} = \{\mathbf{s}|s_q = s_{qr}+\mathrm{j}s_{qi}, s_{qr} \in \Re(\mathbb{A}_M), s_{qi} \in \Im(\mathbb{A}_M), N_C \leq \|\mathbf{s}\|_0 \leq 2N_C, \mathcal{T}(\mathbf{s}) \in \mathbb{S}\}$, where $q = 1, 2, ..., N_C$, $\mathbb{S}$ denotes the set for the AAPs and $\mathcal{T}(\mathbf{s})$ denotes the function that provide AAPs for vector $\mathbf{s}$.

In mGQSM, the total number of possible AAPs are equal to $\binom{N_T}{N_C}^2$, out of which it can select any $2^{K_{mGQSM}}$ AAPs to transmit the data symbols. The codebook for mGQSM ($N_T = 4$, $N_C = 2$, and $M = 4$) with AAPs and data symbols are provided in Table. 3.1 and Table 3.2, respectively.

3.1.3 mGQSM System Model

Let $N_R \times N_T$ mGQSM system model being N_R receive and N_T transmit antennas. Consider the channel matrix $\mathbf{H}$ and noise vector $\mathbf{n}$ with $N_R \times N_T$ and $N_R \times 1$ dimensions, respectively. The entries of $\mathbf{n}$ are assumed to be i.i.d $\mathcal{CN}(0, \sigma_n^2)$. The characteristics of the channel matrix $\mathbf{H}$ with three different channels are discussed in the subsection 3.3. Let $h_{l_{qr}}$ and $h_{l_{qi}}$ are the l_{qr}^{th} and l_{qi}^{th} columns of $\mathbf{H}$, respectively, i.e. $h_{l_{qr}} = [h_{1,l_{qr}}, ..., h_{N_R,l_{qr}}]^T$, where $q = 1, 2, ..., N_C$. The output vector at the receiver is given by [93],

$$\begin{aligned} \mathbf{y} &= \mathbf{H}\mathbf{s} + \mathbf{n} \\ &= \sum_{q=1}^{N_C} (\mathbf{h}_{l_{qr}} s_{qr} + \mathrm{j}\mathbf{h}_{l_{qi}} s_{qi}) + \mathbf{n} \end{aligned} \tag{3.2}$$

Table 3.1 Codebook for the mGQSM AAPs with $N_T = 4$, $N_C = 2$, and $M = 4$.

i/p bits	AAPs $(l_{1r}, l_{2r}), (l_{1i}, l_{2i})$	i/p bits	AAPs $(l_{1r}, l_{2r}), (l_{1i}, l_{2i})$
00000	(1,2), (1,2)	10000	(2,4), (1,4)
00001	(1,3), (1,2)	10001	(3,4), (1,4)
00010	(1,4), (1,2)	10010	(1,2), (2,3)
00011	(2,3), (1,2)	10011	(1,3), (2,3)
00100	(2,4), (1,2)	10100	(1,4), (2,3)
00101	(3,4), (1,2)	10101	(2,3), (2,3)
00110	(1,2), (1,3)	10110	(2,4), (2,3)
00111	(1,3), (1,3)	10111	(3,4), (2,3)
01000	(1,4), (1,3)	11000	(1,2), (2,4)
01001	(2,3), (1,3)	11001	(1,3), (2,4)
01010	(2,4), (1,3)	11010	(1,4), (2,4)
01011	(3,4), (1,3)	11011	(2,3), (2,4)
01100	(1,2), (1,4)	11100	(2,4), (2,4)
01101	(1,3), (1,4)	11101	(3,4), (2,4)
01110	(1,4), (1,4)	11110	(1,2), (3,4)
01111	(2,3), (1,4)	11111	(1,3), (3,4)

where, $l_{qr}, l_{qi} = 1, 2, ..., N_T$, $q = 1, 2, ..., N_C$ and the information signal $\mathbf{s}$ is selected from the codebook, i.e. $\mathbf{s} \in \mathcal{C}_{mGQSM}$.

3.1.4 Example 1: mGQSM Transmission

Fig. 3.2 shows the mGQSM transmission with $N_T = 4$ and $M = 4$. According to AAPs selection procedure, we choose $N_C = 2$. The total number of AAPs are equal to $\binom{N_T}{N_C}^2 = \binom{4}{2}^2 = 36$ out of which any $2^{K_{mGQSM}} = 32$ AAPs are require for the data transmission

Table 3.2 Codebook for the mGQSM data symbols with $N_T = 4$, $N_C = 2$, $M = 4$.

i/p bits	Data Symbols $(x_{1r}, x_{2r}), (x_{1i}, x_{2i})$
0000	$(-1, -1), (+1j, +1j)$
0001	$(-1, -1), (+1j, -1j)$
0010	$(-1, +1), (+1j, +1j)$
0011	$(-1, +1), (+1j, -1j)$
0100	$(-1, -1), (-1j, +1j)$
0101	$(-1, -1), (-1j, -1j)$
0110	$(-1, +1), (-1j, +1j)$
0111	$(-1, +1), (-1j, -1j)$
1000	$(+1, -1), (+1j, +1j)$
1001	$(+1, -1), (+1j, -1j)$
1010	$(+1, +1), (+1j, +1j)$
1011	$(+1, +1), (+1j, -1j)$
1100	$(+1, -1), (-1j, +1j)$
1101	$(+1, -1), (-1j, -1j)$
1110	$(+1, +1), (-1j, +1j)$
1111	$(+1, +1), (-1j, -1j)$

which are given in Table. 3.1. Let 4-QAM scheme for the data transmission the SE of the mGQSM is given as, $\eta_{mGQSM} = 9$ bpcu. At one time instant, consider the 9 input data bits, [1 0 0 1 0 1 1 0 0] for the transmission. The first, $K_{mGQSM} = \left\lfloor 2 \log_2 \binom{N_T}{N_C} \right\rfloor = 5$ bits, [1 0 0 1 0] select the AAPs $(l_{1r}, l_{2r}), (l_{1i}, l_{2i}) = (1, 2), (2, 3)$ from the Table. 3.1. The remaining, $N_C \log_2 M = 4$ bits, [1 1 0 0] choose the data symbols, $s_1 = +1 - j1$ and $s_2 = -1 + j1$. Moreover, these complex data symbols are separated as real $(s_{1r} = +1, s_{2r} = -1)$ and imaginary $(s_{1i} = -1, s_{2i} = +1)$ coefficients are given in Table. 3.2. The active antennas $l_{1r} = 1$ and $l_{2r} = 2$, transmit the real symbols $s_{1r} = +1$ and $s_{2r} = -1$, respectively. Hence, the real vector is given as, $\mathbf{s}_r = [+1\ \text{-}1\ 0\ 0]^T$. Similarly, the active antennas $l_{1i} = 2$ and

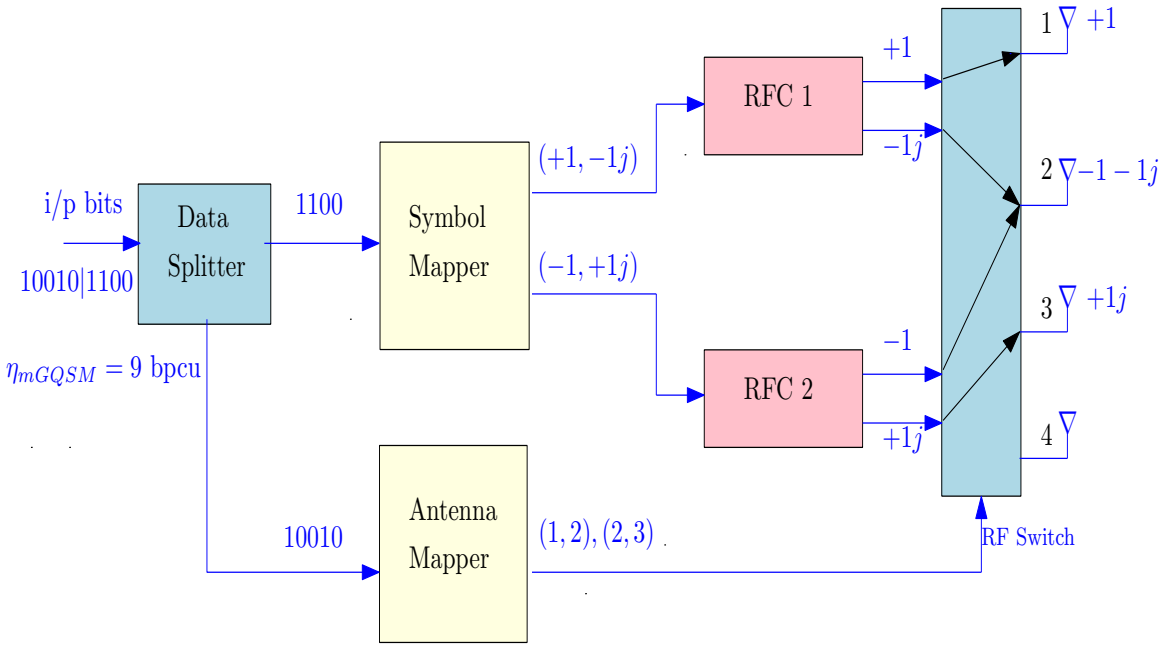

Fig. 3.2 mGQSM transmission with $N_T = 4, N_C = 2$, and $M = 4$.

$l_{2i} = 3$, transmit the symbols $s_{1i} = -1$ and $s_{2i} = +1$, respectively. Hence, the imaginary vector is given as, $\mathbf{s}_i = [0\ \text{-}1\ +1\ 0]^T$. Finally, the transmitted vector is given as, $\mathbf{s} = \mathbf{s}_r + j\mathbf{s}_i = [+1 \quad -1 - j1 \quad +j1 \quad 0\ ]^T$.

3.2 Reduced Codebook mGQSM (RC-mGQSM)

In mGQSM scheme, the maximum number of possible AAPs are considered, which increases the codebook size and the computational complexity. The RC-mGQSM scheme is introduced to minimize the computational complexity by reducing the codebook size. The RC-mGQSM system chooses a fewer number of AAPs to transmit the data symbols. As a result, the rate of RC-mGQSM decreases as the codebook size reduces. The SE of the RC-mGQSM can be given as,

$$\eta_{RC-mGQSM} = \eta_{mGQSM} - p \quad \text{bpcu} \tag{3.3}$$

Table 3.3 Spectral efficiency and computational complexity for different transmission schemes with $N_T = 4, N_R = 4$, and $M = 4$

Transmission Technique	Spectral Efficiency (bpcu)	Computational Complexity (real-valued multiplications)
SM	$\eta_{SM} = \log_2 N_T + \log_2 M = 4$	$8N_R \times 2^{\eta_{SM}} = 512$
QSM	$\eta_{QSM} = 2\log_2 N_T + \log_2 M = 6$	$8N_R \times 2^{\eta_{QSM}} = 2048$
GQSM	$\eta_{GQSM} = \frac{N_T}{2}(\log_2 M + 2) = 8$	$10N_R \times 2^{\eta_{GQSM}} = 10240$
mGQSM	$\eta_{mGQSM} = \left\lfloor 2\log_2 \binom{N_T}{N_C} \right\rfloor + N_C \log_2 M = 9$	$10N_R \times 2^{\eta_{mGQSM}} = 20480$
RC-mGQSM	$\eta_{RC-mGQSM} = \eta_{mGQSM} - p = 8\ (p = 1)$	$10N_R \times 2^{\eta_{RC-mGQSM}} = 10240$

where p denotes an integer value, $1 \leq p \leq K_{mGQSM}$.

The possible AAPs in RC-mGQSM are given as, $|\mathbb{S}| = 2^{K_{mGQSM}-p}$ which decreases as the value of p increases and thus, reduces the computational complexity. The SE and computational complexity for various SMTs with $N_R = 4, N_T = 4$, and $M = 4$ are given in Table. 3.3. For $N_C = 2$, the SE and computational complexity of the mGQSM scheme is given as, $\eta_{mGQSM} = 9$ bpcu and $10N_R \times 2^{\eta_{mGQSM}} = 20480$, real-valued multiplications, respectively. For $p = 1$, the possible AAPs in RC-mGQSM are $|\mathbb{S}| = 2^{K_{mGQSM}-p} = 2^4$. Computational complexity of RC-mGQSM is given as, $10N_R \times 2^{\eta_{RC-mGQSM}} = 10240$ which is same as complexity of GQSM for $p = 1$. For $\eta_{RC-mGQSM} = 8$ bpcu, the computational complexity of RC-mGQSM scheme is reduces by half when compared to mGQSM.

3.3 Channel Models

In this section, the frequency-flat MIMO channels are assumed. The Nakagami-m, Rician, and Rayleigh fading channels are considered for the simulations.

3.3.1 Rayleigh Fading

Non LOS paths in multipath environment is modelled as Rayleigh fading. The channel gains of $\mathbf{H}$ are considered to be i.i.d $\mathcal{CN}(0,1)$.

3.3.2 Rician Fading

When strong path, i.e. LOS path included to Rayleigh fading, the fading becomes Rician fading. It follows multipath fading with a LOS component. The channel impulse response of Rician fading is given as,

$$\mathbf{H} = \sqrt{\frac{K}{1+K}} 1_{N_R \times N_T} + \sqrt{\frac{1}{1+K}} \mathbf{H}' \tag{3.4}$$

where K denotes Rician factor,

$\mathbf{H}'$ denotes channel matrix with $N_R \times N_T$ dimension and its channel gains follows i.i.d $\mathcal{CN}(0,1)$. $1_{N_R \times N_T}$ denotes $N_R \times N_T$ matrix with all entries are equal to one.

3.3.3 Nakagami-m Fading

Several studies have presented the performance of various MIMO systems in the Nakagami-m fading environment, assuming that the phase distribution is uniform. However, except for special case m=1, where Nakagami-m fading is equivalent to Rayleigh fading, the phase distribution is not uniform [66]. We study the mGQSM system performance with non-uniform phase of Nakagami-m channel. The Nakagami-m distribution is commonly used to characterise the channels with severe to moderate fading. The Nakagami parameter m, controls the severity of the fading. The entries of $\mathbf{H}$ is given as [65, 66],

$$h_{N_R,N_T} = \sqrt{\sum_{i=1}^{m} |u_i^R|^2} + j\sqrt{\sum_{i=1}^{m} |u_i^I|^2} \tag{3.5}$$

where u_i^R, u_i^I are the zero-mean Gaussian random variables with variance $1/2m$.

The envelope of the Nakagami-m fading channel is given by,

$$p(\nu) = \frac{2m^m \nu^{2m-1}}{\Gamma(m)} e^{(-m\nu^2)} \tag{3.6}$$

where $p(\cdot)$ denotes the "probability distribution function (PDF)", and $\Gamma(\cdot)$ denotes the Gamma function.

The PDF of the phase is given as [66],

$$p(\phi) = \frac{\Gamma(m) \left|\sin(2\phi)\right|^{m-1}}{2^m \Gamma^2\left(\frac{m}{2}\right)} \tag{3.7}$$

In eq. (3.7), the phase is uniform only when $m = 1$, where Nakagami-m fading equivalent to Rayleigh fading. However, except $m = 1$, the phase distribution is not uniform [66].

At the receiver, ML detection rule is performed to jointly estimate the transmitting antenna indices and data symbols. The ML rule is given by [93],

$$\widehat{\mathbf{s}} = \underset{\mathbf{s} \in \mathcal{C}_{mGQSM}}{\arg\min} \|\mathbf{y} - \mathbf{H}\mathbf{s}\|^2. \tag{3.8}$$

$$[\widehat{l}_{qr}, \widehat{l}_{qi}, \widehat{s}_{qr}, \widehat{s}_{qi}] = \underset{l_{qr}, l_{qi}, s_{qr}, s_{qi}}{\arg\min} \|\mathbf{y} - \sum_{q=1}^{N_C} (\mathbf{h}_{l_{qr}} s_{qr} + \mathrm{j}\mathbf{h}_{l_{qi}} s_{qi})\|^2 \tag{3.9}$$

where $[\widehat{l}_{qr}, \widehat{l}_{qi}]$ are the estimated antenna indices with respect to estimated data symbols, $[\widehat{s}_{qr}, \widehat{s}_{qi}]$.

3.4 Low Complexity Detection

The computational complexity of the optimal ML detection rule is high when compared to the sub-optimal detection rules. In this section, we use ZF based low complexity detection

method which was proposed in [89]. Rewrite the received signal as follows:

$$\underbrace{\begin{bmatrix}\Re(\mathbf{y})\\ \Im(\mathbf{y})\end{bmatrix}}_{\bar{\mathbf{y}}} = \underbrace{\begin{bmatrix}\Re(\mathbf{H}) & -\Im(\mathbf{H})\\ \Im(\mathbf{H}) & \Re(\mathbf{H})\end{bmatrix}}_{\bar{\mathbf{H}}} \underbrace{\begin{bmatrix}\mathbf{s}_r\\ \mathbf{s}_i\end{bmatrix}}_{\bar{\mathbf{s}}} + \underbrace{\begin{bmatrix}\Re(\mathbf{n})\\ \Im(\mathbf{n})\end{bmatrix}}_{\bar{\mathbf{n}}} \tag{3.10}$$

the weight metric of eq. (3.10) is calculated by,

$$w_\phi = \frac{\bar{\mathbf{h}}_\phi^H \bar{\mathbf{y}}}{\bar{\mathbf{h}}_\phi^H \bar{\mathbf{h}}_\phi} \tag{3.11}$$

where $\bar{\mathbf{h}}_\phi$ denotes the ϕth column of H and $\phi \in \{1, 2, ..., 2N_T\}$. The sum of weight metrics for the αth and βth AAPs is calculated by,

$$g^\alpha = \sum_{q=1}^{N_c} \left| w_{\mathbf{l}_{qr}^\alpha} \right|, f^\beta = \sum_{q=1}^{N_c} \left| w_{(\mathbf{l}_{qi}^\beta + N_T)} \right| \tag{3.12}$$

where $\mathbf{l}_{qr}^\alpha = \left\{ l_{1i}^\alpha, l_{2i}^\alpha, ..., l_{qi}^\alpha \right\}$, and $\mathbf{l}_{qi}^\beta = \left\{ l_{1i}^\beta, l_{2i}^\beta, ..., l_{qi}^\beta \right\}$ for $1 \le \alpha, \beta \le L$, and $L = 2^{\left\lfloor \log_2 \binom{N_T}{N_C} \right\rfloor}$.

The sequential AAPs are estimated by sorting $\left[g^1, g^2, ..., g^L \right]$ and $\left[f^1, f^2, ..., f^L \right]$ as

$$[a_1, a_2, ..., a_L] = \text{sort} \left\{ \left[g^1, g^2, ..., g^L \right] \right\}, \tag{3.13}$$

and

$$[b_1, b_2, ..., b_L] = \text{sort} \left\{ \left[f^1, f^2, ..., f^L \right] \right\}, \tag{3.14}$$

where $\{a_1, b_1\}$ and $\{a_L, b_L\}$ indicate the maximal and minimal value locations, respectively. The estimated symbols with respect to the a_αth and b_βth AAPs are calculated by the ZF method is given as

$$\left[\hat{\mathbf{s}}_{qr}^{a_\alpha}, \hat{\mathbf{s}}_{qi}^{b_\beta} \right] = Q \left(\left(\tilde{\mathbf{H}}^{\mathbf{H}} \tilde{\mathbf{H}} \right)^{-1} \tilde{\mathbf{H}} \bar{\mathbf{y}} \right) \tag{3.15}$$

where $\tilde{\mathbf{H}} = \left[\bar{\mathbf{H}}_{\mathbf{l}_{qr}^{a_\alpha}}, \bar{\mathbf{H}}_{\mathbf{l}_{qi}^{b_\beta + N_T}} \right]$ and $\bar{\mathbf{H}}_{\mathbf{l}_{qr}^{a_\alpha}}$ and $\bar{\mathbf{H}}_{\mathbf{l}_{qi}^{b_\beta + N_T}}$ are the $\mathbf{l}_{qr}^{a_\alpha}$th and $\mathbf{l}_{qi}^{b_\beta + N_T}$th columns of $\bar{\mathbf{H}}$,

respectively.

The Euclidean distances are sequentially calculated by,

$$\epsilon\left(a_{\alpha}, b_{\beta}\right) = \left\| \bar{\mathbf{y}} - \tilde{\mathbf{H}} \begin{bmatrix} \hat{\mathbf{s}}_{qr}^{a_{\alpha}} \\ \hat{\mathbf{s}}_{qi}^{b_{\beta}} \end{bmatrix} \right\|^2 \tag{3.16}$$

The detection complexity is high for large values of L. The authors in [89], presents the threshold V_{th} to stop the calculating Euclidean distances in eq. (3.16), i.e. $\epsilon\left(a_{\alpha}, b_{\beta}\right) < V_{th}$ which results in estimated symbols $\left[\hat{\mathbf{s}}_{qr}^{a_{\alpha}}, \hat{\mathbf{s}}_{qi}^{b_{\beta}}\right]$ with respect to the transmit antenna indices $\left[\hat{\mathbf{l}}_{qr}^{\alpha}, \hat{\mathbf{l}}_{qi}^{\beta}\right]$.

3.5 mGQSM System with Imperfect CSI

This section describes the mGQSM system performance under imperfect CSI. To detect the transmitted symbols, receivers require the perfect knowledge of the CSI. In practical systems, the perfect knowledge of the channel $\mathbf{H}$ is not available. Because of the noise the perfect CSI cannot be provided and resulting channel estimation errors will cause a degradation of the receiver's performance. The estimated channel $\hat{\mathbf{H}}$ is different from the true channel $\mathbf{H}$ and it is given as, $\hat{\mathbf{H}} = \mathbf{H} + \delta\mathbf{H}$, where $\delta\mathbf{H}$ is the error channel matrix. At the receiver, the ML detection rule make decision with $\delta\mathbf{H}$ in addition to the $\mathbf{H}$. The elements of $\delta\mathbf{H}$ are assumed as $\overset{i.i.d}{\sim} \mathcal{CN}(0, \sigma_h)$, where σ_h is the error variance. The ML decision rule for the input signal $\mathbf{s}$ is given as,

$$\hat{\mathbf{s}} = \underset{\mathbf{s} \in \mathcal{C}_{mGQSM}}{\arg\min} \|\mathbf{y} - (\mathbf{H} + \delta\mathbf{H})\mathbf{s}\|^2 \tag{3.17}$$

where $\hat{\mathbf{s}}$ denote as estimated signal of the input signal $\mathbf{s}$.

3.6 Performance Analysis and Simulation Results

3.6.1 Performance Analysis

The conditional pairwise error probability (PEP) for determining $\widehat{\mathbf{s}}$ when $\mathbf{s}$ is transmitted on the given channel, H can be determined by [89],

$$\begin{aligned} Pr\left\{\mathbf{s} \to \widehat{\mathbf{s}} \mid \mathbf{H}\right\} &= Pr\left\{\left\|\mathbf{y}-\mathbf{H}\mathbf{s}\right\|^2 > \left\|\mathbf{y}-\mathbf{H}\widehat{\mathbf{s}}\right\|^2\right\} \\ &= Q\left(\sqrt{\frac{\left\|\mathbf{H}\left(\mathbf{s}-\widehat{\mathbf{s}}\right)\right\|^2}{2N_o}}\right) \end{aligned}$$

The unconditional PEP is given as,

$$Pr\left\{\mathbf{s} \to \widehat{\mathbf{s}}\right\} = E_{\mathbf{H}}\left\{Pr\left\{\mathbf{s} \to \widehat{\mathbf{s}} \mid \mathbf{H}\right\}\right\}$$

Upper bound on BER is calculated as,

$$P_e \leq \frac{1}{\eta_{RC-mGQSM} 2^{\eta_{RC-mGQSM}}} \sum_{\mathbf{s}} \sum_{\widehat{\mathbf{s}} \neq \mathbf{s}} d\left\{\mathbf{s} \to \widehat{\mathbf{s}}\right\} Pr\left\{\mathbf{s} \to \widehat{\mathbf{s}}\right\}$$

where, $d\left\{\mathbf{s} \to \widehat{\mathbf{s}}\right\}$ denotes the number of bit errors between $\mathbf{s}$ and $\widehat{\mathbf{s}}$.

3.6.2 Simulation Results

This section presents the comparison of mGQSM and RC-mGQSM system performances with GQSM, QSM, and SM systems over Nakagami-m, Rayleigh, and Rician channels. We set the threshold $V_{th} = N_R\sigma_n^2$ for the low complexity detection method. In the figures the doublet denotes as(N_T, N_C) and the triplet denotes as (N_T, N_R, N_C). For the computer simulations, we assume the number of receiving antennas are equal to 4, i.e. $N_R = 4$. Consider $N_C = 2$ for mGQSM, RC-mGQSM, and GQSM schemes and $N_C = 1$ for QSM and SM schemes. We

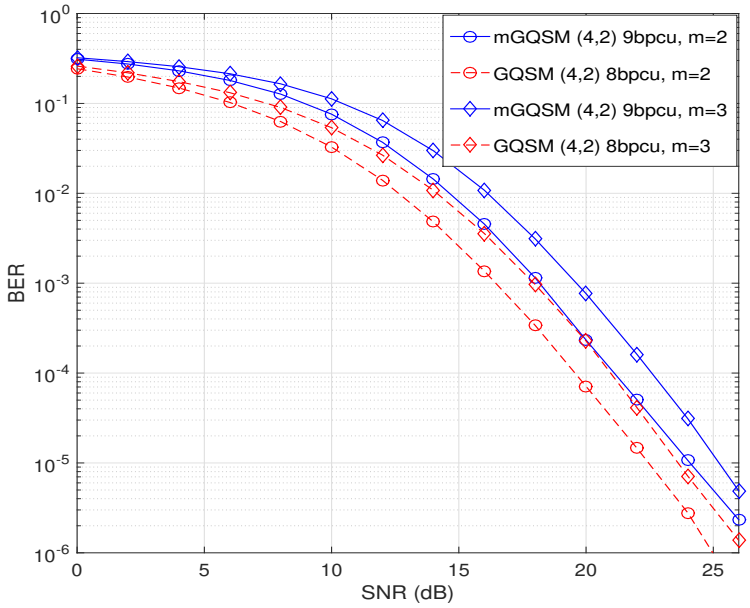

Fig. 3.3 BER versus SNR for the mGQSM and GQSM systems over Nakagami channel ($m = 2, 3$) with the same system configuration.

compare all the schemes at the BER of 10^{-4}.

Fig. 3.3 presents the performance of mGQSM and GQSM systems over Nakagami-m fading with $m = 2$ and $m = 3$. Consider the $N_R \times N_T$ system model with $N_R = 4$, $N_T = 4$ and 4-QAM modulation for both the schemes. At any time instant, the SE of mGQSM and GQSM schemes are equal to 9 bpcu and 8 bpcu, respectively. At the BER of 10^{-4}, we noticed that the mGQSM system performance loses 1 dB SNR over GQSM for both the values $m = 2$ and $m = 3$. However, the mGQSM scheme can provide an extra 1 bpcu rate over GQSM scheme.

In Fig. 3.4 the performance of RC-mGQSM scheme is compared with the performance of GQSM and QSM schemes with different Nakagami parameter values, $m = 2$ and $m = 3$. The RC-mGQSM system performance is compared with the GQSM and QSM system performances with the same SE of 8 bpcu. At the BER of 10^{-4}, we noticed that the RC-mGQSM performance loses nearly 1 dB SNR over GQSM with the same modulation scheme and gain 2.5 dB SNR over QSM for both the values $m = 2$ and $m = 3$.

Fig. 3.5 compares the RC-mGQSM to GQSM, QSM, and SM schemes over Nakagami fading channel with the Nakagami-m parameter, $m = 4$. We consider 4×4 system model and the same SE of 8 bpcu. We noticed that the RC-mGQSM gain nearly 1.5 dB and 2 dB SNR values over SM ($M = 64$) and QSM ($M = 16$) schemes, respectively. When compared to GQSM with the same 4-QAM modulation, the performance of RC-mGQSM degrades by around 0.5 dB SNR. Moreover, at low SNR, SM outperforms GQSM and RC-mGQSM schemes by 1.5 dB and 2 dB SNR, respectively. However, the performance of SM scheme degrades at high SNR values. Since, the error in detecting the active antenna index dominates at low SNR, whereas the error in detecting data symbols dominates at high SNR [65]. As a result, SM outperforms the RC-mGQSM, GQSM, and QSM at low SNR due to its smaller spatial constellation size. These methods, on the other hand, perform better at high SNR since the data constellation size is smaller than the SM.

Figs. 3.6 and 3.7 present the BER comparison of RC-mGQSM system with various SM systems over Rayleigh channel. In Fig. 3.6, we fix $N_T = 4$ and compared the performance of different SM systems with the same SE of 8 bpcu. We observed that the RC-mGQSM performance with 4-QAM modulation outperforms MA-SM ($M = 8$), QSM ($M = 16$), and GSM ($M = 64$) by nearly 2 dB, 3 dB, and 5 dB SNRs, respectively. However, the performance of RC-mGQSM degrades by 0.5 dB SNR when compared to GQSM. In Fig. 3.7, we fix $M = 4$ and compared the schemes with the same SE of 8 bpcu. We observed that the RC-mGQSM performance loses nearly 1.5 dB and 2 dB SNRs over QSM and SM, respectively. However, the QSM and SM schemes require 8 and 64 transmit antennas, respectively. Whereas the RC-mGQSM scheme requires only 4 transmit antennas to attain that performance.

Fig. 3.8 presents the mGQSM and GQSM performances over Rician channel with Rician factor values are equal to 3 dB and 5 dB. Consider the $N_R \times N_T$ system model with $N_R = 4$, $N_T = 4$ and 4-QAM modulation for both the schemes. At any time instant, the SE of mGQSM and GQSM schemes are equal to 9 bpcu and 8 bpcu, respectively. We observed that the mGQSM system performance loses 1.5 dB SNR value over GQSM for both the values

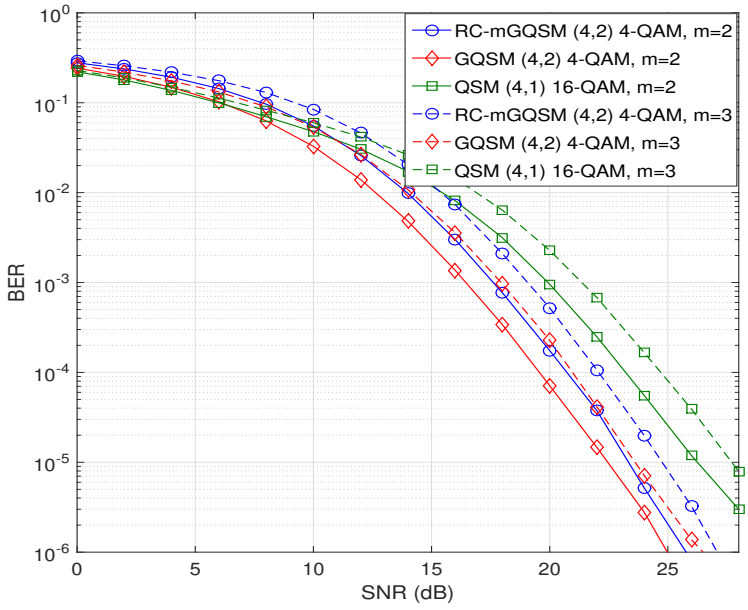

Fig. 3.4 BER versus SNR for the RC-mGQSM, GQSM, and QSM systems over Nakagami channel ($m = 2, 3$) with the same SE of 8 bpcu.

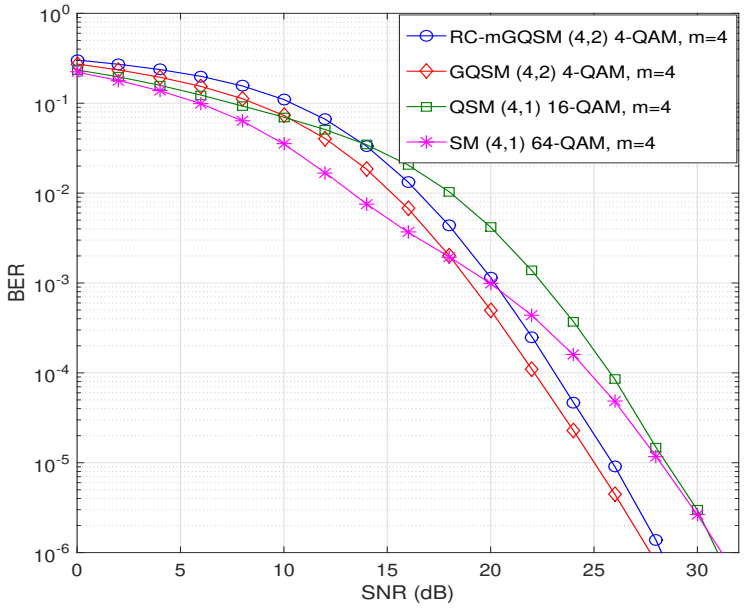

Fig. 3.5 BER versus SNR for the RC-mGQSM, GQSM, QSM, and SM systems over Nakagami channel ($m = 4$) with the same SE of 8 bpcu.

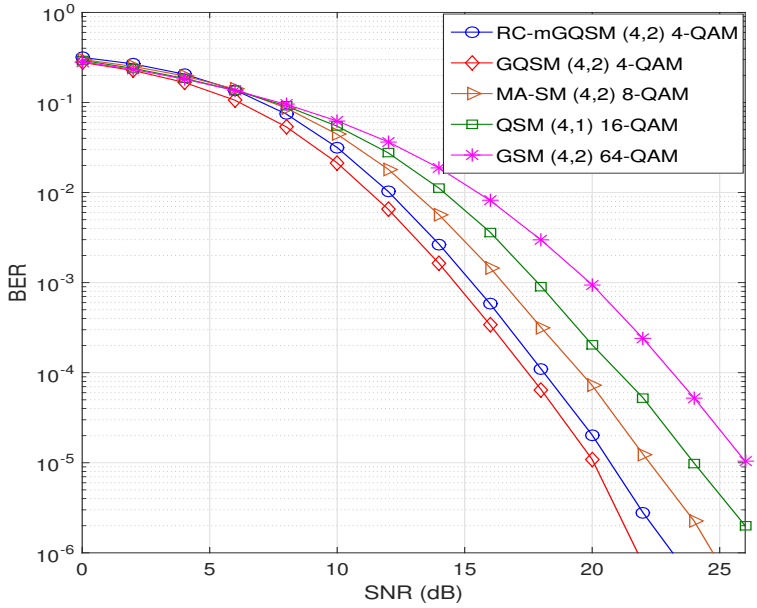

Fig. 3.6 BER versus SNR for the RC-mGQSM, GQSM, QSM, and SM systems over Rayleigh channel with the same SE of 8 bpcu.

$K = 3$ dB and $K = 5$ dB.

Figs. 3.9 and 3.10 present the RC-mGQSM system performance comparison with GQSM, QSM, and SM system performances under Rician fading with $K = 3$ dB and $K = 5$ dB, respectively. In Fig. 3.9, we consider $N_T = 4$ for all the schemes and compare the performance of the schemes with the same SE of 8 bpcu. We noticed that the RC-mGQSM performance gain nearly 2.5 dB and 2 dB SNR values over QSM ($M = 16$) and SM ($M = 64$), respectively, and loses 1 dB SNR value over GQSM ($M = 4$) for $K = 3$ dB. In Fig. 3.10, we compared all the schemes with the same modulation scheme and the same rate of 8 bpcu. We noticed that the RC-mGQSM performance loses 1.5 dB SNR over QSM and 1 dB SNR over GQSM for the Rician factor, $K = 5$ dB. However, the QSM scheme requires 8 transmit antennas. Whereas RC-mGQSM scheme requires only 4 transmit antennas to attain that performance.

Fig. 3.11 presents the RC-mGQSM scheme with low complexity detection method [89]. We consider 4×4 system model with $N_T = 4$, $N_R = 4$, and $N_C = 2$. By comparing the performance of the RC-mGQSM system with optimal ML detection and low complexity detection

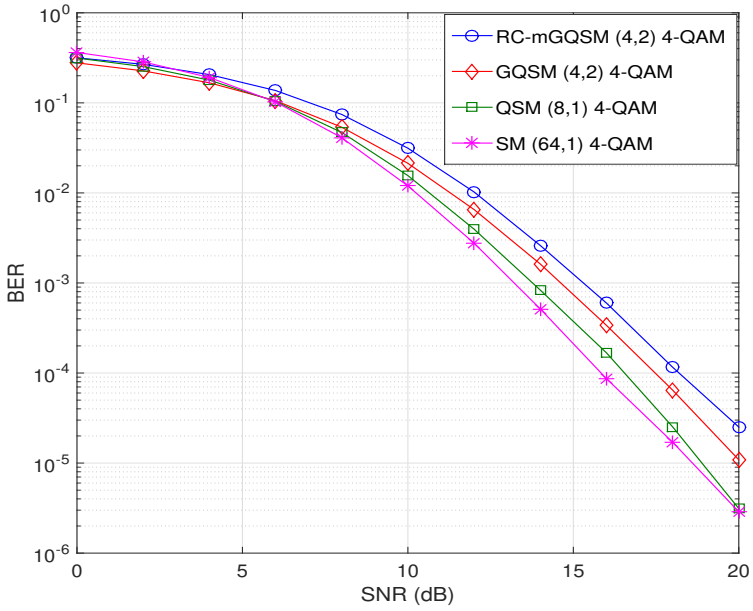

Fig. 3.7 BER versus SNR for the RC-mGQSM, GQSM, QSM, and SM systems over Rayleigh channel with the different N_T values and the same SE of 8 bpcu.

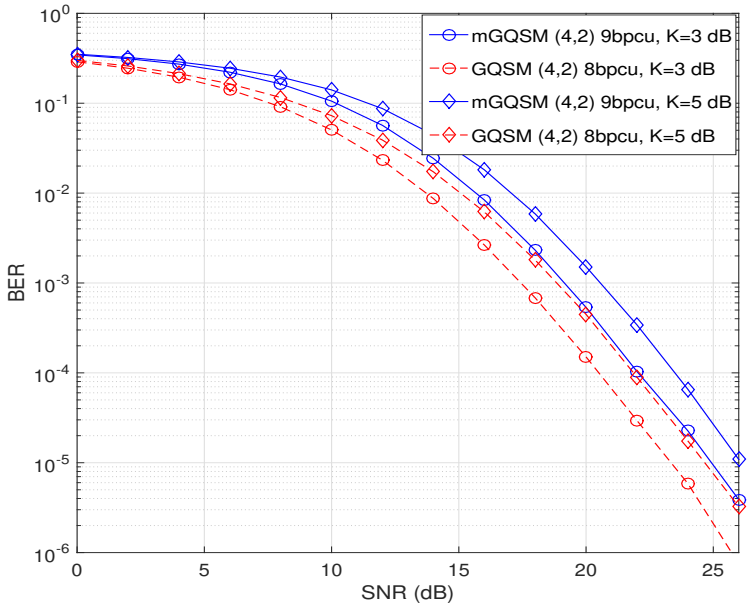

Fig. 3.8 BER versus SNR for the mGQSM and GQSM systems over Rician channel ($K = 3, 5$) dB with the same system configuration.

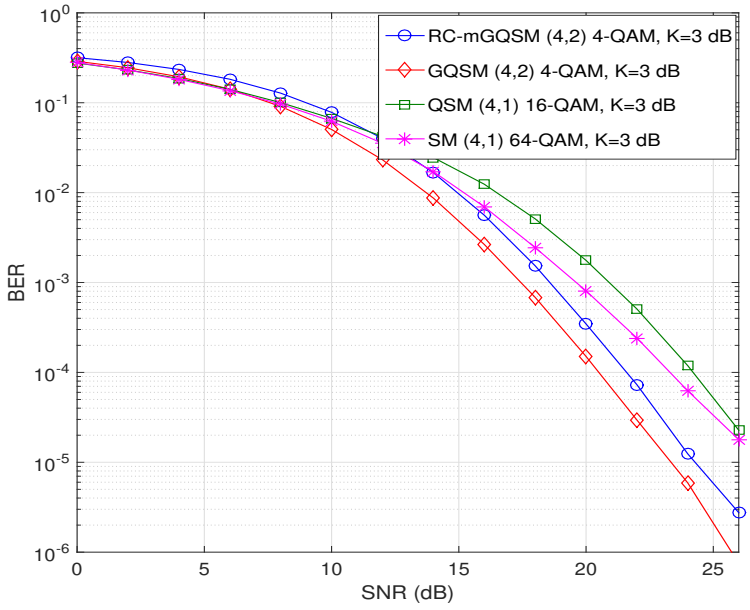

Fig. 3.9 BER versus SNR for the RC-mGQSM, GQSM, QSM, and SM systems over Rician channel ($K = 3$) dB with the same SE of 8 bpcu.

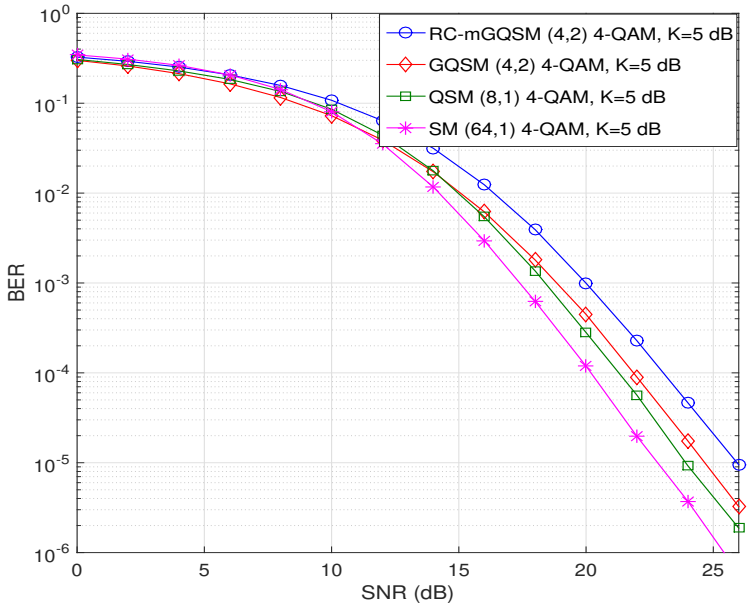

Fig. 3.10 BER versus SNR for the RC-mGQSM, GQSM, QSM, and SM systems over Rician channel ($K = 5$) dB with different N_T values and the same SE of 8 bpcu.

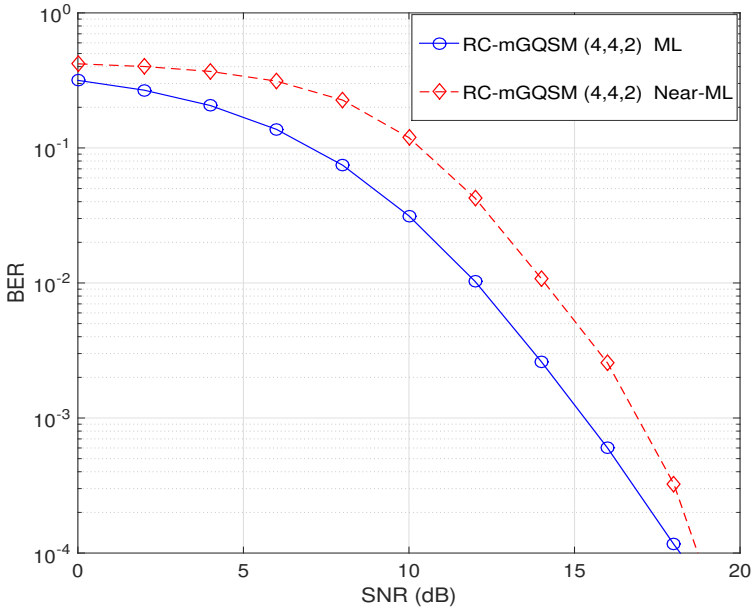

Fig. 3.11 BER versus SNR for the RC-mGQSM with low complexity detection method [89] with SE of 8 bpcu.

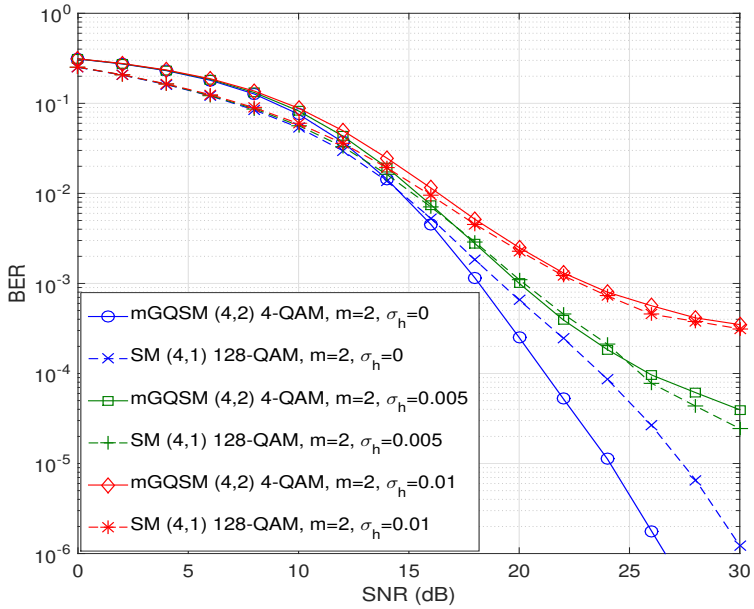

Fig. 3.12 BER versus SNR for the mGQSM and SM systems over Nakagami-m channel ($m = 2$) with $\sigma_h = (0, 0.005, 0.01)$ and the SE of 9 bpcu.

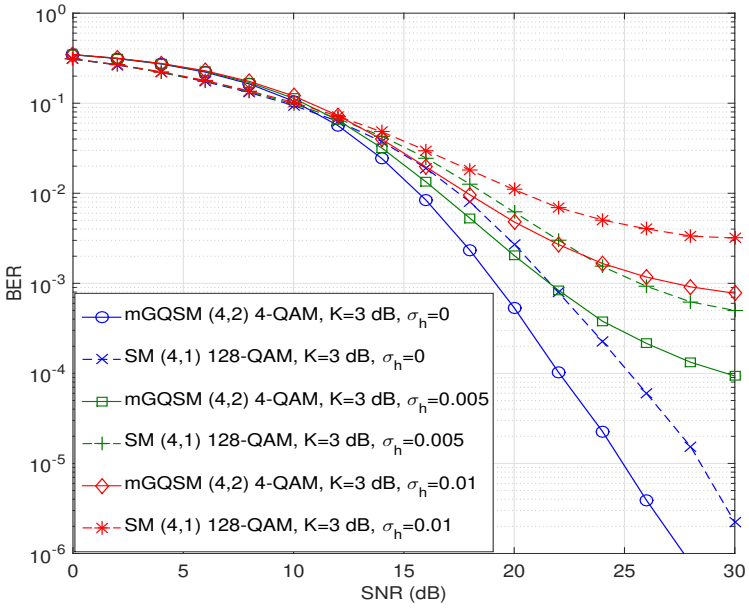

Fig. 3.13 BER versus SNR for the mGQSM and SM systems over Rician channel ($K = 3$) dB with $\sigma_h = (0, 0.005, 0.01)$ and the SE of 9 bpcu.

methods, we noticed that the RC-mGQSM degrades by 1.5 dB SNR when compared to the RC-mGQSM with ML detection at BER of 10^{-3}. However, the computational complexity of the system decreases with the low complexity detection method.

Fig. 3.12 presents the mGQSM and SM systems over Nakagami-m ($m = 2$) channel with imperfect CSI. Let the 4×4 system model, 4-QAM modulation for mGQSM, and 128-QAM for SM. In addition to the true channel $\mathbf{H}$, we use $N_R \times N_T$ error channel $\delta\mathbf{H}$, the elements of $\delta\mathbf{H}$ are modelled as i.i.d $\mathcal{CN}(0, \sigma_h)$, where the variance of the error channel matrix, σ_h is assumed as 0.005 and 0.01. At BER of 10^{-3}, we noticed that the mGQSM system error performance with $\sigma_h = 0.005$ loses nearly 2 dB SNR value when compared to the mGQSM performance with $\sigma_h = 0$. Whereas SM performance loses nearly 1 dB SNR for $\sigma_h = 0.005$. Table. 3.4 shows the BER results of imperfect mGQSM and SM systems over Nakagami channel ($m = 2$). At SNR of 18 dB, we noticed that the BER values for the imperfect SM and mGQSM systems are 0.0028 and 0.0027, respectively for $\sigma_h = 0.005$. Similarly, for the remaining σ_h values we found that mGQSM system with imperfect channel outperforms the

Table 3.4 BER Vs. SNR for imperfect SM & mGQSM systems.

SNR	BER					
	SM			mGQSM		
(dB)	$\sigma_h = 0$	$\sigma_h = 0.005$	$\sigma_h = 0.01$	$\sigma_h = 0$	$\sigma_h = 0.005$	$\sigma_h = 0.01$
18	0.0018	0.0028	0.0045	0.0011	0.0027	0.0051
20	0.0006	0.0011	0.0023	0.0002	0.0010	0.0025
24	8.6E-05	0.0002	0.0007	1.1E-05	0.0001	0.0007

SM.

Fig. 3.13 presents the BER performance of mGQSM and SM systems over Rician fading channel with imperfect channel conditions. We assume a 4×4 system model and Rician factor, $K = 3$ dB. The values for the imperfect channel variance, σ_h are considered as 0, 0.005, and 0.01. However, the special case σ_h=0 is considered as the perfect channel, i.e. there is no error added to the true channel $\mathbf{H}$. We compare both the systems with the same SE of 9 bpcu, where SM scheme requires 128-QAM modulation and mGQSM scheme requires only 4-QAM modulation to attain the same SE. At the BER of 10^{-3}, we noticed that the mGQSM and SM system performances with error variance, $\sigma_h = 0.005$ degrade the performance by 2.5 dB and 4 dB SNR when compared to mGQSM and SM system performances with $\sigma_h = 0$. Similarly, for the error variance, $\sigma_h = 0.01$, the mGQSM system shows better performance when compared to that SM.

3.7 Conclusion

In this chapter, we presented the mGQSM and RC-mGQSM system performances under Nakagami-m, Rayleigh, and Rician fading channels. We described the mGQSM system model with a suitable example. Using the ML-detection algorithm, the performance of the mGQSM

and RC-mGQSM schemes are presented and compared with the performances of the GQSM, QSM, and SM schemes with various values for the Nakagami parameter and Rician factor. For m=4, the RC-mGQSM outperforms SM ($M = 64$) by $\sim$ 1.5 dB and QSM ($M = 16$) by $\sim$2 dB SNRs. RC-mGQSM performance with 4-QAM modulation outperforms MA-SM ($M = 8$), QSM ($M = 16$), and GSM ($M = 64$) by $\sim$ 2 dB, 3 dB, and 5 dB SNRs, respectively. A low complexity detection method is presented for the RC-mGQSM scheme. We also study and compared the performances of the mGQSM and SM schemes under imperfect channel conditions.

Chapter 4

mGQSM Performance over Correlated Fading Channels

4.1 mGQSM System Model

Consider $N_R \times N_T$ system for the mGQSM with N_T transmit and N_R receive antennas. Let the correlated channel $\mathbf{H}$ and the noise $\mathbf{n}$ being $N_R \times N_T$ and $N_R \times 1$ dimensions, respectively. The entries of $\mathbf{n}$ are considered to be i.i.d $\mathcal{CN}(0, \sigma_n^2)$. The characteristics of $\mathbf{H}$ with various fading channels are described in the section. 4.2. Let $\mathbf{h}_{l_{qr}}$ and $\mathbf{h}_{l_{qi}}$ be the l_{qr}^{th} and l_{qi}^{th} columns of $\mathbf{H}$, respectively, i.e., $\mathbf{h}_{l_{qr}} = [h_{1,l_{qr}}, \cdots, h_{N_R,l_{qr}}]^T$ and $\mathbf{h}_{l_{qi}} = [h_{1,l_{qi}}, \cdots, h_{N_R,l_{qi}}]^T$; $q = 1, \cdots, N_C$. The received signal is given by,

$$\begin{aligned} \mathbf{y} &= \sqrt{E_s}\mathbf{H}\mathbf{s} + \mathbf{n} \\ &= \sqrt{E_s}\sum_{q=1}^{N_C}(\mathbf{h}_{l_{qr}} s_{qr} + \mathrm{j}\mathbf{h}_{l_{qi}} s_{qi}) + \mathbf{n} \end{aligned} \tag{4.1}$$

where $l_{qr}, l_{qi} = 1, \cdots, N_T$; $q = 1, \cdots, N_C$ and the $\mathbf{s}$ input signal.

4.2 Correlated Fading Channels

In this section, we assume correlated fading channels and the correlation matrix is modelled using the Kronecker channel model [102] and it is given by,

$$\mathbf{H} = R_{Rx}^{\frac{1}{2}} \tilde{\mathbf{H}} R_{Tx}^{\frac{1}{2}} \tag{4.2}$$

where, $\tilde{\mathbf{H}}$ denotes the uncorrelated channel matrix and the R_{Tx} and R_{Rx} are denote the correlation matrices at transmitter and receiver, respectively.

The matrices R_{Tx} and R_{Rx} are generated using the exponential decay model [103] and they are given by,

$$R_{Tx} = \begin{bmatrix} 1 & \rho_t & \rho_t^2 & \cdots & \rho_t^{N_T-1} \\ \rho_t & 1 & \rho_t & \ddots & \vdots \\ \rho_t^2 & \rho_t & 1 & \ddots & \rho_t^2 \\ \vdots & \ddots & \ddots & \ddots & \rho_t \\ \rho_t^{N_T-1} & \cdots & \rho_t^2 & \rho_t & 1 \end{bmatrix} \tag{4.3}$$

$$R_{Rx} = \begin{bmatrix} 1 & \rho_r & \rho_r^2 & \cdots & \rho_r^{N_R-1} \\ \rho_r & 1 & \rho_r & \ddots & \vdots \\ \rho_r^2 & \rho_r & 1 & \ddots & \rho_r^2 \\ \vdots & \ddots & \ddots & \ddots & \rho_r \\ \rho_r^{N_R-1} & \cdots & \rho_r^2 & \rho_r & 1 \end{bmatrix} \tag{4.4}$$

where $\rho_z = \exp(-\psi)$ and ψ denotes the correlation decay coefficient, and z denotes r or t.

The characteristics of the uncorrelated channel matrix $\tilde{\mathbf{H}}$ with three different channels are discussed in the following subsections.

At the receiver, we use ML detector to estimate the indices of the transmitting antennas corresponding to the data symbols, which is given as,

$$\widehat{\mathbf{s}} = \underset{\mathbf{s}\in\mathcal{C}_{mGQSM}}{\arg\min} \left\| \mathbf{y} - \sqrt{E_s}\mathbf{H}\mathbf{s} \right\|^2. \tag{4.5}$$

$$\left[\widehat{l}_{qr}, \widehat{l}_{qi}, \widehat{s}_{qr}, \widehat{s}_{qi}\right] = \underset{l_{qr},l_{qi},s_{qr},s_{qi}\in\mathcal{C}_{mGQSM}}{\arg\min} \left\| \mathbf{y} - \sqrt{E_s}\sum_{q=1}^{N_C} \left(\mathbf{h}_{l_{qr}} s_{qr} + \mathrm{j}\mathbf{h}_{l_{qi}} s_{qi}\right) \right\|^2 \tag{4.6}$$

where, $\widehat{l}_{qr}$ and $\widehat{l}_{qi}$ are the estimated antenna indices for the estimated symbols, $\widehat{s}_{qr}$ and $\widehat{s}_{qi}$.

4.3 Low-Complexity Detection: OB-MMSE

In comparison to sub-optimal detectors, the optimal ML detector has a larger computational complexity. This section introduces a low-complexity sub-optimal "ordered block minimum mean-squared error (OB-MMSE)" [61] detection algorithm for the RC-mGQSM. In OB-MMSE, the ordered AAPs are obtained by sorting the weighting factors. Then, a block MMSE equalization method is used to detect the possible AAPs sequentially. The received signal can rewrite as,

$$\underbrace{\begin{bmatrix} \Re(\mathbf{y}) \\ \Im(\mathbf{y}) \end{bmatrix}}_{\bar{\mathbf{y}}} = \underbrace{\begin{bmatrix} \Re(\mathbf{H}) & -\Im(\mathbf{H}) \\ \Im(\mathbf{H}) & \Re(\mathbf{H}) \end{bmatrix}}_{\bar{\mathbf{H}}} \underbrace{\begin{bmatrix} \mathbf{s}_r \\ \mathbf{s}_i \end{bmatrix}}_{\bar{\mathbf{s}}} + \underbrace{\begin{bmatrix} \Re(\mathbf{n}) \\ \Im(\mathbf{n}) \end{bmatrix}}_{\bar{\mathbf{n}}} \tag{4.7}$$

the weight metric of eq. (4.9) is given by,

$$z_k = \left(\bar{\mathbf{h}}_k\right)^{\dagger} \bar{\mathbf{y}} \tag{4.8}$$

where, $\left(\bar{\mathbf{h}}_k\right)^{\dagger} = \frac{\bar{\mathbf{h}}_k^H}{\bar{\mathbf{h}}_k^H \bar{\mathbf{h}}_k}$ and $k \in \{1, 2, \cdots, 2N_T\}$.

The weight factors are given by,

$$g^{\alpha} = \sum_{q=1}^{N_C} \left| z_{\mathbf{l}_{qr}^{\alpha}} \right|^2 \tag{4.9}$$

$$f^{\beta} = \sum_{q=1}^{N_C} \left| z_{\left(\mathbf{l}_{qi}^{\beta}+N_T\right)} \right|^2 \tag{4.10}$$

where $\mathbf{l}_{qr}^{\alpha} = \left\{ l_{1r}^{\alpha}, l_{2r}^{\alpha}, \cdots, l_{qr}^{\alpha} \right\}$, and $\mathbf{l}_{qi}^{\beta} = \left\{ l_{1i}^{\beta}, l_{2i}^{\beta}, \cdots, l_{qi}^{\beta} \right\}$ for $1 \leq \alpha, \beta \leq N$; $N = 2^{\left\lfloor \log_2 \binom{N_T}{N_C} \right\rfloor}$.

After calculating g^{α} and f^{β}, sort the weighting factor values as follows,

$$[a_1, a_2, \cdots, a_N] = \text{sort}\left\{ \left[g^1, g^2, \cdots, g^N \right] \right\} \tag{4.11}$$

and

$$[b_1, b_2, \cdots, b_N] = \text{sort}\left\{ \left[f^1, f^2, \cdots, f^N \right] \right\} \tag{4.12}$$

where $\{a_N, b_N\}$ and $\{a_1, b_1\}$ denotes the indices of minimum and maximum values, respectively. The OB-MMSE detector is used to determine the estimated symbols corresponding to a_{α}^{th} and b_{β}^{th} AAPs as follows,

$$\left[\hat{\mathbf{s}}_{qr}^{a_\alpha}, \hat{\mathbf{s}}_{qi}^{b_\beta} \right] = Q\left(\left(\left(\hat{\mathbf{H}} \right)^H \hat{\mathbf{H}} + N_0 \mathbf{I}_{2N_C \times 2N_C} \right)^{-1} \left(\hat{\mathbf{H}} \right)^H \bar{\mathbf{y}} \right) \tag{4.13}$$

where $\hat{\mathbf{H}} = \left[\bar{\mathbf{H}}_{\mathbf{l}_{qr}^{a_\alpha}}, \bar{\mathbf{H}}_{\mathbf{l}_{qi}^{b_\beta+N_T}} \right]$, $\bar{\mathbf{H}}_{\mathbf{l}_{qr}^{a_\alpha}}$ and $\bar{\mathbf{H}}_{\mathbf{l}_{qi}^{b_\beta+N_T}}$ denote the $\mathbf{l}_{qr}^{a_\alpha}$th and $\mathbf{l}_{qi}^{b_\beta+N_T}$th columns of $\bar{\mathbf{H}}$, respectively.

The block MMSE detector in eq. (4.15) will stop once the output satisfies,

$$d(a_\alpha, b_\beta) = \left\| \bar{\mathbf{y}} - \tilde{\mathbf{H}} \begin{bmatrix} \hat{\mathbf{s}}_{qr}^{a_\alpha} \\ \hat{\mathbf{s}}_{qi}^{b_\beta} \end{bmatrix} \right\|_F^2 \leq V_{th} \tag{4.14}$$

where V_{th} represents the threshold which is expressed as $V_{th} = 2N_R N_o$. For large values of N, the detection complexity is high. The authors in [61], presents the threshold V_{th} for stopping the calculation of $d(a_\alpha, b_\beta)$ in eq. (4.16), i.e. $d(a_\alpha, b_\beta) \leq V_{th}$ which results in estimated symbols $\left[\hat{\mathbf{s}}_{qr}^{a_\alpha}, \hat{\mathbf{s}}_{qi}^{b_\beta} \right]$ with respect to the transmit antenna indices $\left[\hat{\mathbf{l}}_{qr}^{\alpha}, \hat{\mathbf{l}}_{qi}^{\beta} \right]$.

Algorithm 1 OB-MMSE detection

Input: $\bar{\mathbf{y}}, \bar{\mathbf{H}}, N_T, N_C, V_{th} = 2N_R N_o, L = 2^N$
Calculate z_k by (4.11)
Obtain g^{α} from (4.12)
Obtain f^{β} from (4.13)
$[a_1, a_2, \cdots, a_N] = \arg \text{ sort } \left\{ \left[g^1, g^2, \cdots, g^N \right] \right\}$
$[b_1, b_2, \cdots, b_N] = \arg \text{ sort } \left\{ \left[f^1, f^2, \cdots, f^N \right] \right\}$
Initial $q = 1$;
while $q < L$ do
    Calculate $\left[\tilde{\mathbf{s}}_{qr}^{a_\alpha}, \tilde{\mathbf{s}}_{qi}^{b_\beta} \right]$ by (4.16)
    Compute $d(a_\alpha, b_\beta)$ from (4.17)
if $d(a_\alpha, b_\beta) \leq V_{th}$
    $\hat{\mathbf{I}} = \left[\tilde{\mathbf{l}}_{qr}^{\alpha}, \tilde{\mathbf{l}}_{qi}^{\beta} \right]$, $\hat{\mathbf{s}} = \left[\tilde{\mathbf{s}}_{qr}^{a_\alpha}, \tilde{\mathbf{s}}_{qi}^{b_\beta} \right]$; break;
else
    $q = q + 1$;
end if
end while
if $q > L$
    $u = \arg \min_{q} \ d(a_\alpha, b_\beta)$, $q \in \{1, \cdots, L\}$
    $\hat{\mathbf{I}} = \left[\tilde{\mathbf{l}}_{ur}^{\alpha}, \tilde{\mathbf{l}}_{ui}^{\beta} \right]$, $\hat{\mathbf{s}} = \left[\tilde{\mathbf{s}}_{ur}^{a_\alpha}, \tilde{\mathbf{s}}_{ui}^{b_\beta} \right]$;
end if
Output: detected $\left(\left[\hat{\mathbf{l}}_{qr}^{\alpha}, \hat{\mathbf{l}}_{qi}^{\beta} \right], \left[\hat{\mathbf{s}}_{qr}^{a_\alpha}, \hat{\mathbf{s}}_{qi}^{b_\beta} \right] \right)$

4.4 mGQSM System with Imperfect CSI:

This section studies the mGQSM scheme with imperfect CSI. We consider correlated Rayleigh, Rician ($K = 5$ dB), and Nakagami-m ($m = 2$) channels. To illustrate the mGQSM performance with imperfect CSI, we employ an $N_R \times N_T$ error channel, $\delta\mathbf{H}$ in addition to the perfect channel $\mathbf{H}$. The coefficients of $\delta\mathbf{H}$ are assumed to be $\overset{i.i.d}{\sim} \mathcal{CN}(0, \sigma_h)$. The ML rule under imperfect CSI can be given as,

$$\hat{\mathbf{s}} = \underset{\mathbf{s} \in \mathcal{C}_{mGQSM}}{\arg \min} \left\| \mathbf{y} - \sqrt{E_s}(\mathbf{H} + \delta\mathbf{H})\mathbf{s} \right\|^2 \tag{4.15}$$

where $\hat{\mathbf{s}}$ denote the estimated signal of $\mathbf{s}$.

4.5 Example 2: mGQSM Transmission

Fig. 4.1 shows the mGQSM transmission with $N_T = 4$ and $M = 4$. According to AAPs selection, we choose $N_C = 2$. To transmit data symbols, mGQSM scheme can choose any $2^{\left\lfloor 2\log_2 \binom{N_T}{N_C} \right\rfloor} = 32$ possible AAPs out of $\binom{N_T}{N_C}^2 = \binom{4}{2}^2 = 36$ total number of AAPs. The possible AAPs for the mGQSM is shown in Table. 3.1. Let the 4-QAM ($M = 4$) modulation for the mGQSM transmission with the SE of 9 bpcu. Assume the input bits, [0 1 0 0 1 1 1 1 0] at particular time. First, $K_{mGQSM} = \left\lfloor 2\log_2 \binom{N_T}{N_C} \right\rfloor = 5$ bits, [0 1 0 0 1] choose the AAPs, $(l_{1r}, l_{2r}), (l_{1i}, l_{2i}) = (2,3), (1,3)$ from the Table. 3.1, where $l_{qr}, l_{qi}; q = 1, \cdots, N_C$ denote the antenna indices with respect to the $\Re(\mathbf{s})$ and $\Im(\mathbf{s})$. The remaining, $N_C \log_2 M = 4$ bits, [1 1 1 0] choose the complex symbols, $(s_1, s_2) = (+1 - j1, +1 + j1)$ from the M-QAM constellation. Furthermore, these are formed as, $(s_{1r}, s_{2r}) = (+1, +1)$ and $(s_{1i}, s_{2i}) = (-1, +1)$, which are given in Table. 3.2. First two antennas $(l_{1r}, l_{2r}) = (2, 3)$, transmit the corresponding symbols $(s_{1r}, s_{2r}) = (+1, +1)$. Likewise, remaining antennas $(l_{1i}, l_{2i}) = (1, 3)$, transmit the corresponding symbols $(s_{1i}, s_{2i}) = (-1, +1)$. Therefore, the transmitted vectors for the $\Re(\mathbf{s})$ and $\Im(\mathbf{s})$, become, $\mathbf{s}_r = [0\ +1\ +1\ 0]^T$ and $\mathbf{s}_i = [-1\ 0\ +1\ 0]^T$, respectively. Finally, the transmitted vector is, $\mathbf{s} = \mathbf{s}_r + j\mathbf{s}_i = [-j1 \quad +1 \quad +1 + j1 \quad 0\ ]^T$.

4.6 Simulation Results and Complexity Analysis

This section presents the BER performance of mGQSM and RC-mGQSM schemes over correlated Rayleigh, Rician, and Nakagami-m channels and compares them with the QSM and GQSM. The mGQSM and QSM are studied and compared under imperfect CSI scenarios. Moreover, the OB-MMSE detector is introduced for the RC-mGQSM and compared to that of the ML detector.

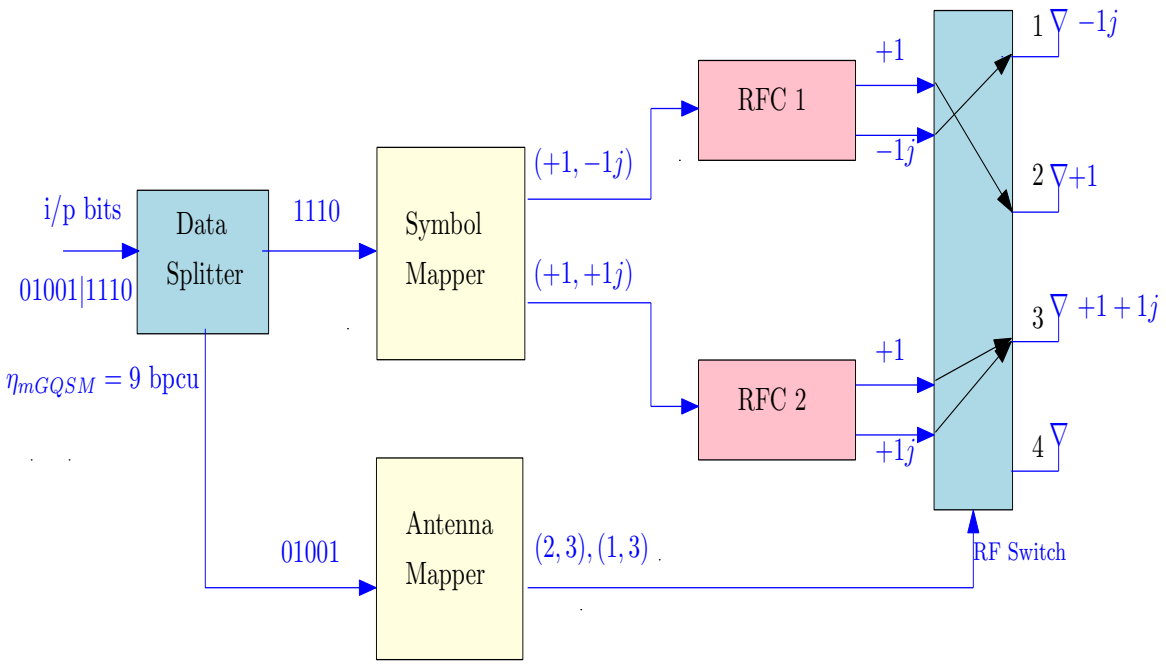

Fig. 4.1 mGQSM transmission with $N_T = 4$ and $M = 4$.

4.6.1 Simulation Results

In this subsection, we use 10^6 data symbols to calculate the BER. The elements of noise $\mathbf{n}$ are observed to be i.i.d $\mathcal{CN}(0, \sigma_n^2)$. For all the simulations, we use $N_R \times N_T$ system being $N_T = 4$ and $N_R = 4$, and 4-QAM modulation for the mGQSM and RC-mGQSM. At the BER of 10^{-3}, we compare the BER performances of different schemes using the correlation decay coefficient, $\psi = 0.7$ at both the transmitter and receiver sides.

Fig. 4.2 presents the BER comparison of RC-mGQSM, GQSM, and QSM schemes over correlated Rayleigh channel. We use 4×4 system and 4-QAM ($M = 4$) modulation for RC-mGQSM and GQSM schemes and 16-QAM ($M = 16$) modulation for QSM. We compare these three schemes with the fixed SE of 8 bpcu. By comparing the BER results, we noticed that the BER of the RC-mGQSM gain 2 dB SNR over QSM and performance degrades by $\sim$ 0.5 dB SNR over GQSM. However, the mGQSM gains an additional 1-bit data rate over GQSM for the fixed system configuration. Figs. 4.3 and 4.4 shows the RC-mGQSM and QSM

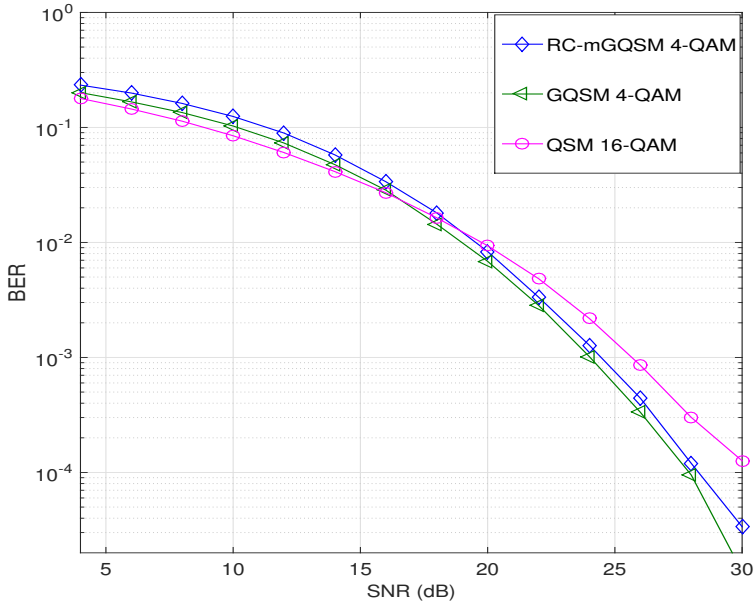

Fig. 4.2 BER Vs. SNR of RC-mGQSM, GQSM, and QSM systems over correlated Rayleigh channel with same SE of 8 bpcu.

performances over correlated Rician channel with $K = 3$ dB and $K = 5$ dB, respectively. We consider $N_C = 2$, 4-QAM ($M = 4$) modulation for the RC-mGQSM, and 16-QAM ($M = 64$) modulation for the QSM. The BER of the RC-mGQSM outperforms QSM by $\sim$2 dB SNR for $K = 3$ dB and $\sim$1.5 dB SNR for $K = 5$ dB. The BER comparison of RC-mGQSM and QSM over correlated Nakagami fading with $m = 2$ and $m = 3$ are shown in Figs. 4.5 and 4.6. Let $N_C = 2$ for the RC-mGQSM. By comparing both the schemes, the RC-mGQSM scheme outperforms QSM by $\sim$1.5 dB SNR for $m = 2$ and $\sim$1 dB SNR for $m = 3$.

The mGQSM performance over correlated Nakagami-m and Rician channels with various values of m and K are shown in Figs. 4.7 and 4.8, respectively. Consider mGQSM with $N_C = 2$ and 4-QAM modulation. We compare mGQSM performance with various parameter values of Nakagami fading and noticed that the mGQSM performance with $m = 1$ gain $\sim$1.5 dB and $\sim$4 dB SNRs over mGQSM performance with $m = 2$ and $m = 4$, respectively. For the Rician fading, we compare mGQSM performance with different values of Rician factor, i.e. K= 3 dB, 5 dB, and 10 dB. The mGQSM with $K = 3$ dB gain $\sim$1 dB and $\sim$6 dB SNRs

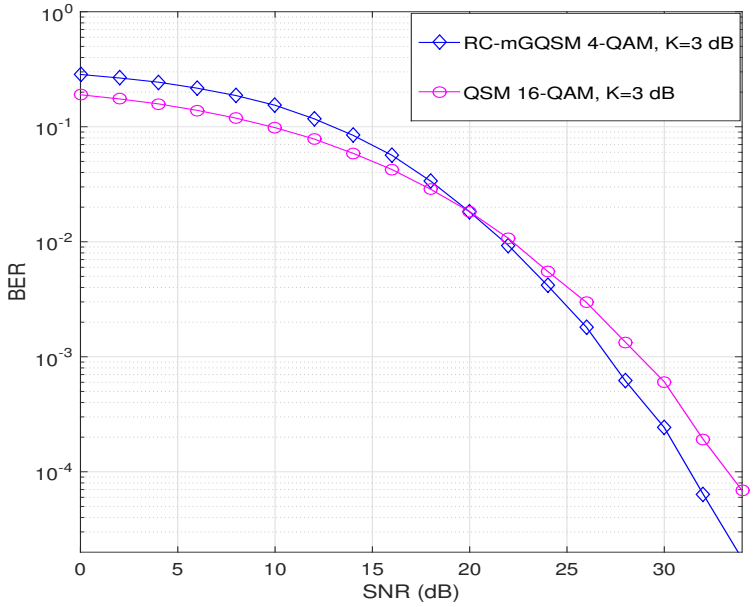

Fig. 4.3 BER Vs. SNR of RC-mGQSM and QSM systems over correlated Rician channel ($K = 3$) dB with same SE of 8 bpcu.

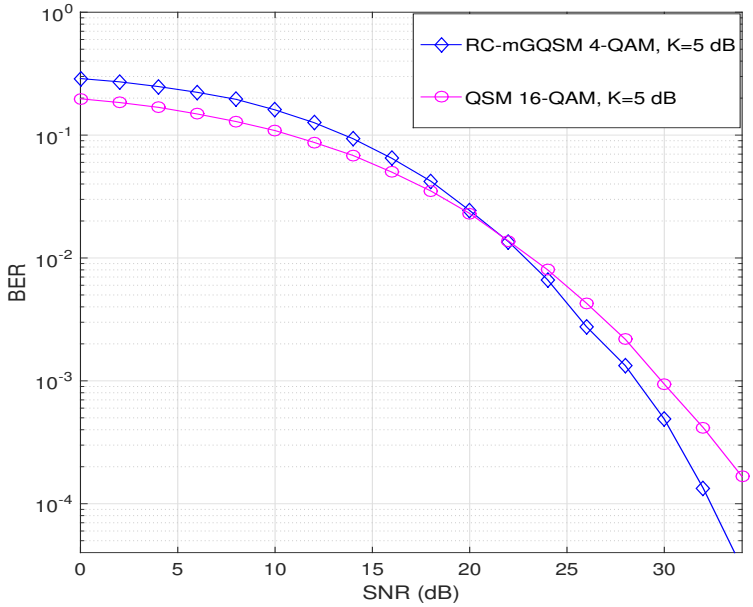

Fig. 4.4 BER Vs. SNR of RC-mGQSM and QSM systems over correlated Rician channel ($K = 5$) dB with same SE of 8 bpcu.

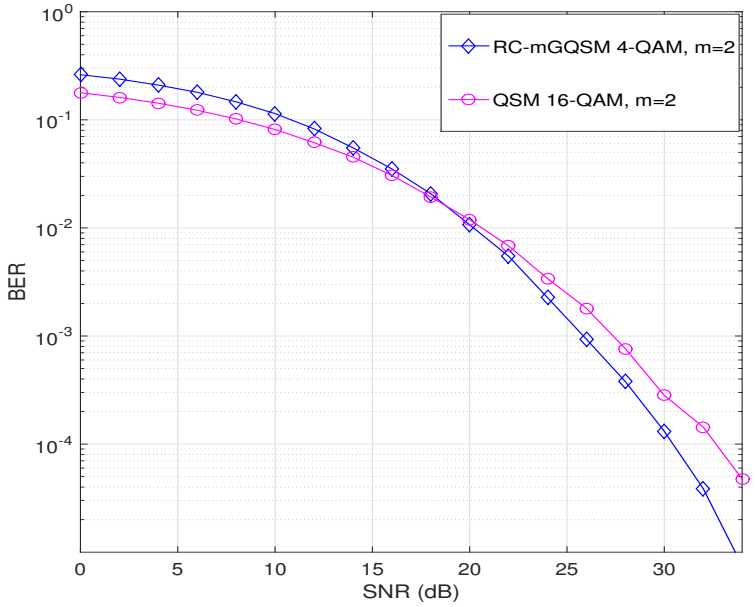

Fig. 4.5 BER Vs. SNR of RC-mGQSM and QSM systems over correlated Nakagami channel ($m = 2$) with same SE of 8 bpcu.

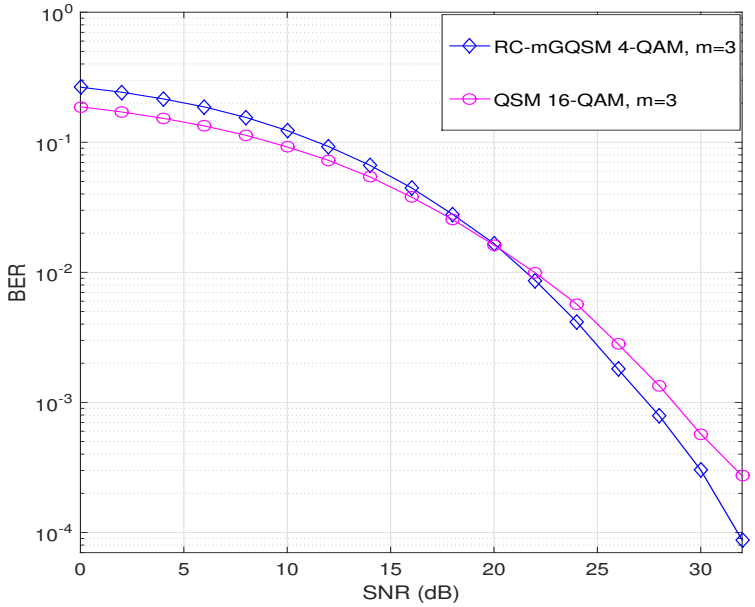

Fig. 4.6 BER Vs. SNR of RC-mGQSM and QSM systems over correlated Nakagami channel ($m = 3$) with same SE of 8 bpcu.

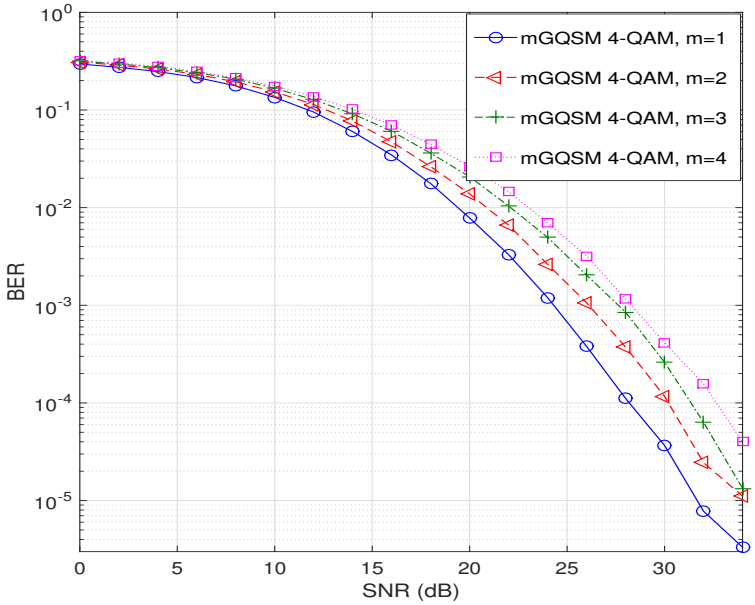

Fig. 4.7 BER Vs. SNR of mGQSM system over correlated Nakagami channel ($m = 1, 2, 3, 4$) with SE of 9 bpcu.

over mGQSM performance with $K = 5$ dB and $K = 10$ dB, respectively.

Fig. 4.9 presents the BER performance comparison of OB-MMSE [61] and ML detectors for the RC-mGQSM. Assume 4×4 system and $N_C = 2$ for the RC-mGQSM. The BER results of RC-mGQSM with OB-MMSE detector degrades by $\sim$1.5 dB SNR over RC-mGQSM performance with ML detector. However, the OB-MMSE detector achieves near-ML performance with reduced computational complexity.

The comparison of mGQSM and QSM systems under imperfect CSI over correlated Rician (K=5 dB), Rayleigh, and Nakagami-m (m=2) channels are shown in Figs. 4.10, 4.11, and 4.12, respectively. We consider 4-QAM ($M = 4$) modulation for the mGQSM and 32-QAM ($M = 32$) modulation for the QSM. We compare mGQSM and QSM schemes with the same SE of 9 bpcu. Assume the error variance, $\sigma_h = (0.001, 0.002)$. The BER values for perfect and imperfect QSM and mGQSM schemes over correlated channels with $\sigma_h = 0.001$ are given in Table. 4.1. We compute the BER values of mGQSM and QSM schemes with the SNR values of 16 dB, 22 dB, 28 dB. At SNR of 16 dB, we noticed that the BER values for the QSM

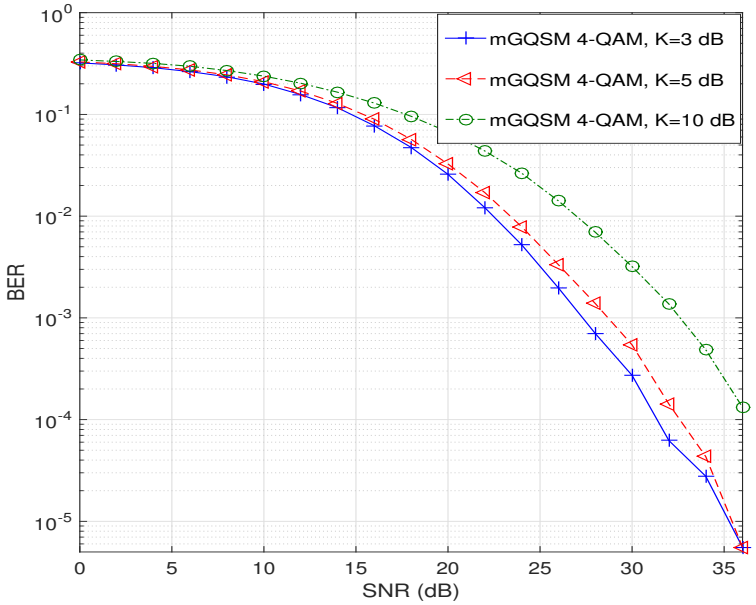

Fig. 4.8 BER Vs. SNR of mGQSM system over correlated Rician channel ($K = 3, 5, 10$) dB with SE of 9 bpcu.

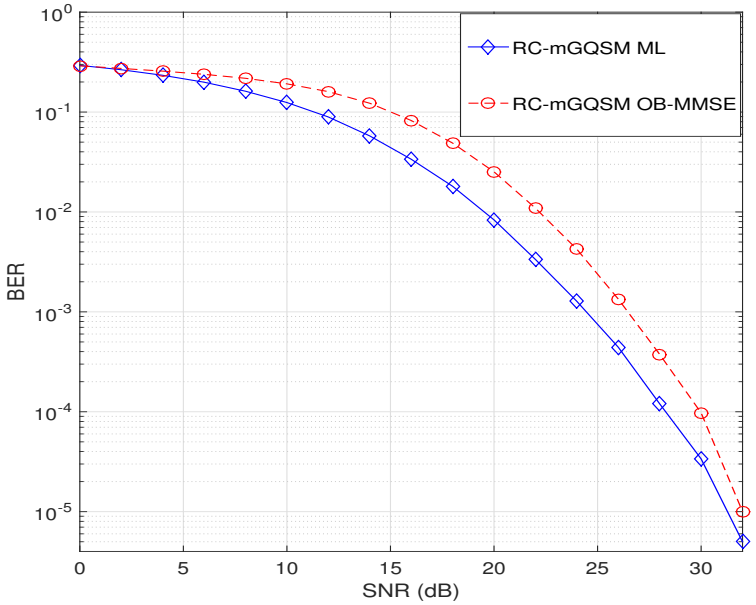

Fig. 4.9 BER Vs. SNR of RC-mGQSM system with low-complexity OB-MMSE [61] with SE of 8 bpcu.

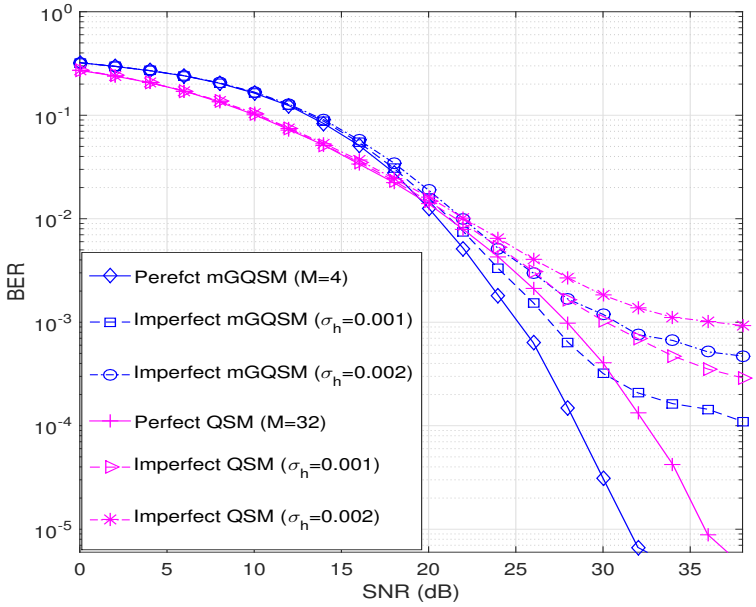

Fig. 4.10 BER Vs. SNR of mGQSM and QSM systems over correlated Rayleigh channel with $\sigma_h = (0.001, 0.002)$ and same SE of 9 bpcu.

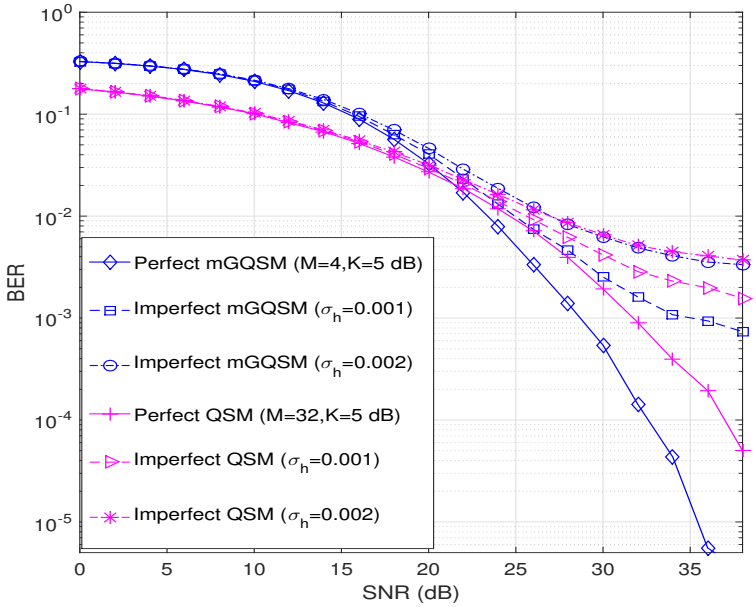

Fig. 4.11 BER Vs. SNR of mGQSM and QSM systems over correlated Rician channel ($K = 5$) dB with $\sigma_h = (0.001, 0.002)$ and same SE of 9 bpcu.

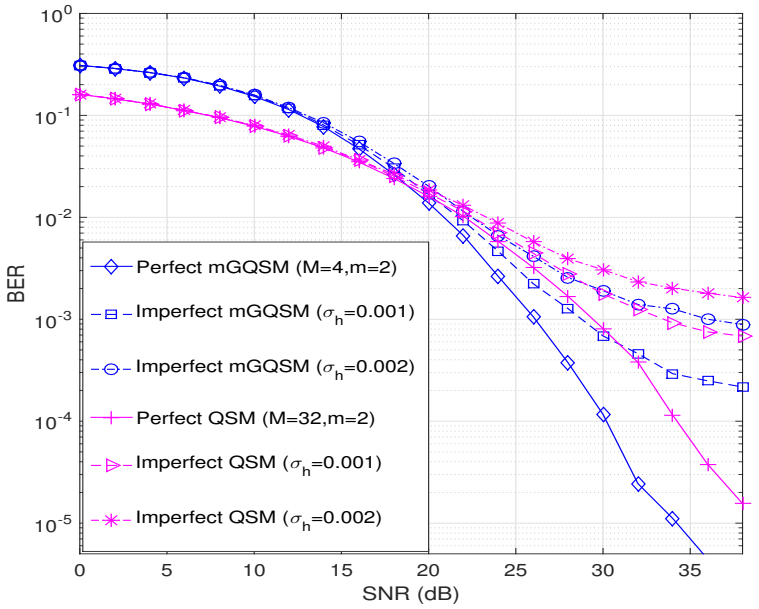

Fig. 4.12 BER Vs. SNR of mGQSM and QSM systems over correlated Nakagami channel ($m = 2$) with $\sigma_h = (0.001, 0.002)$ and same SE of 9 bpcu.

and mGQSM are 0.0338 and 0.0513, respectively and at SNR of 28 dB, the BER values for the QSM and mGQSM are 0.0009 and 0.0001, respectively over Rayleigh fading. Similarly, for the remaining channels, we noticed that the mGQSM under imperfect channel conditions presents better BER performance over the QSM at high SNR values.

4.6.2 Complexity Analysis

In this subsection, we compare the computational complexity of OB-MMSE to that of ML detector for the RC-mGQSM, the computational complexity is measured by the number of real-valued multiplications [76]. In OB-MMSE, calculating z_k requires $(4N_R + 1)2N_T$ real-valued multiplications, calculating g^{α} and f^{β} requires $4N$ real-valued multiplications, V_{th} requires 2 real-valued multiplications, and calculating MMSE detector requires $(2N_R N_T^2 + 11N_R N_T + 4N_R + N_T M^{N_C} + 16)P + 2N_R 2^{\eta_{RC-mGQSM}}$ real-valued multiplications, where P is the average number of MMSE detectors. Hence, the computational complexity of OB-MMSE,

Table 4.1 BER Vs. SNR for perfect and imperfect QSM & mGQSM systems

SNR (dB)	QSM						mGQSM					
	Rayleigh		Rician [K=5 dB]		Nakagami-m [m=2]		Rayleigh		Rician [K=5 dB]		Nakagami-m [m=2]	
	Perfect (BER)	Imperfect (BER)	Perfect (BER)	Imperfect (BER)	Perfect (BER)	Imperfect (BER)	Perfect (BER)	Imperfect (BER)	Perfect (BER)	Imperfect (BER)	Perfect (BER)	Imperfect (BER)
16	0.0338	0.0352	0.0517	0.0535	0.0348	0.0362	0.0513	0.0547	0.0896	0.0953	0.0470	0.0513
22	0.0078	0.0090	0.0186	0.0206	0.0102	0.0114	0.0051	0.0075	0.0170	0.0232	0.0066	0.0092
28	0.0009	0.0016	0.0039	0.0061	0.0016	0.0027	0.0001	0.0006	0.0013	0.0046	0.0003	0.0012

$C_{OB-MMSE}$ is given as,

$$(2N_R N_T^2+11N_R N_T+4N_R+N_T M^{N_C}+16)P+2N_R 2^{\eta_{RC-mGQSM}}+(4N_R+1)2N_T+4N+2 \quad (4.16)$$

The complexity of OB-MMSE and ML detectors are compared using the complexity reduction ration (CRR), it is defined as,

$$CRR = \frac{C_{ML} - C_{OB-MMSE}}{C_{ML}} \quad (4.17)$$

where, C_{ML} denoted as the computational complexity of the ML detector for the RC-mGQSM, it is given as $10N_R 2^{\eta_{RC-mGQSM}}$ [93], where $\eta_{RC-mGQSM}$ denotes the SE of the RC-mGQSM, it is given as, $\eta_{RC-mGQSM} = \eta_{mGQSM} - 1$ bpcu. For the 4×4 system and 4-QAM modulation, we have $C_{OB-MMSE} = 5402$ and $C_{ML} = 10240$ with $N_C = 2$ and $P = 8$. We calculate the CRR using eq. (4.19), we observed that the computational complexity of the OB-MMSE detector is reduced by 47% compared to that of the ML detector for the 4×4 RC-mGQSM with 4-QAM modulation.

4.7 Conclusion

In this chapter, the BER performances of the mGQSM and RC-mGQSM schemes are investigated under correlated Nakagami-m, Rayleigh, and Rician channels. An appropriate example is used to describe the mGQSM transmission system. ML method is used to compare the BER results of the mGQSM and RC-mGQSM schemes to that of the QSM and GQSM with various fading parameters of Nakagami and Rician channels. We observed that the proposed RC-mGQSM scheme outperforms QSM by $\sim$ 2 dB SNR for $K = 3$ dB and $\sim$ 1.5 dB SNR for $m = 2$. Under Rayleigh channel, the RC-mGQSM, GQSM, and QSM are compared with the fixed SE of 8 bpcu, we noticed that the RC-mGQSM gain 2 dB SNR over QSM and performance degrades by $\sim$ 0.5 dB SNR over GQSM. However, the RC-mGQSM uses more number of active antennas when compared to GQSM for the fixed system configuration. Furthermore, a low-complexity OB-MMSE detector is developed for the RC-mGQSM, and it is shown that the OB-MMSE detector achieves near-ML performance with reduced computational complexity of 47% when compared to the ML detector. Moreover, the mGQSM and QSM are evaluated and compared under imperfect CSI conditions. The study demonstrates that the mGQSM performs better than the QSM at high SNR values.

Chapter 5

mGQSM Performance over Correlated Weibull Fading Channel

5.1 mGQSM System Model

Consider $N_R \times N_T$ mGQSM system model being N_R receive and N_T transmit antennas. Assume the noise vector $\mathbf{n}$ has a dimension of $N_R \times 1$ and its entries follows i.i.d $\mathcal{CN}(0, \sigma_n^2)$. Let the correlated Weibull channel $\mathbf{H}$ being the dimension of $N_R \times N_T$. In the following section, the characteristics of H is described. Let $\mathbf{h}_{l_{jr}}$ be the l_{jr}^{th} and $\mathbf{h}_{l_{ji}}$ be the l_{ji}^{th} column vectors of $\mathbf{H}$. $\mathbf{h}_{l_{jr}} = [h_{1,l_{jr}}, \cdots, h_{N_R,l_{jr}}]^T$ and $\mathbf{h}_{l_{ji}} = [h_{1,l_{ji}}, \cdots, h_{N_R,l_{ji}}]^T$; $j = 1, 2, \cdots, N_C$. The received signal $\mathbf{y}$ can be given as,

$$\begin{aligned} \mathbf{y} &= \sqrt{E_s}\mathbf{H}\mathbf{s} + \mathbf{n} \\ &= \sqrt{E_s}\sum_{j=1}^{N_C}(\mathbf{h}_{l_{jr}} s_{jr} + \mathrm{j}\mathbf{h}_{l_{ji}} s_{ji}) + \mathbf{n} \end{aligned} \tag{5.1}$$

where $l_{jr}, l_{ji} = 1, 2, \cdots, N_T$ and $\mathbf{s} \in \mathcal{C}_{mGQSM}$.

5.2 Weibull Fading Channel

Weibull fading channel is characterized by the PDF which is given by,

$$f(x;\lambda,\beta) = \frac{\beta}{\lambda}\Big(\frac{x}{\lambda}\Big)^{\beta-1} e^{-(\frac{x}{\lambda})^{\beta}} \tag{5.2}$$

where λ and β denote the Weibull scale and shape parameters, respectively. The complex envelope of Weibull channel can be given as [41],

$$\bar{h}_{N_R,N_T} = (U + jV)^{2/\beta} \tag{5.3}$$

where U and V are the Gaussian in-phase and quadrature components, respectively. The Weibull distribution exhibits good fit to practical channel measurements for indoor and outdoor environment scenarios. The fading severity is controlled by the parameter β. For the simulations, we consider deep fade environment when $\beta = 0.5$ and the non-fading environment when $\beta = 5$. The negative exponential and Rayleigh distributions are the special cases of Weibull fading when $\beta = 1$ and $\beta = 2$, respectively.

In this section, we assume a correlated fading channel and compute correlation matrix using Kronecker channel model [102], which is given by,

$$\mathbf{H} = R_{Rx}^{\frac{1}{2}} \bar{\mathbf{H}} R_{Tx}^{\frac{1}{2}} \tag{5.4}$$

where $\bar{\mathbf{H}}$ is uncorrelated channel matrix, and R_{Tx} and R_{Rx} are the correlation matrices at the transmitter and receiver, respectively.

The matrices R_{Tx} and R_{Rx} are generated using the exponential decay model [103] and they are given in chapter. 4, eq. (4.3) and eq. (4.4), respectively.

ML detection rule for the input signal $\mathbf{x}$ can be given as,

$$\widehat{\mathbf{s}} = \underset{\mathbf{s}\in\mathcal{C}_{mGQSM}}{\arg\min} \left\| \mathbf{y} - \sqrt{E_s}\mathbf{H}\mathbf{s} \right\|^2. \tag{5.5}$$

$$\left[\widehat{l}_{jr}, \widehat{l}_{ji}, \widehat{s}_{jr}, \widehat{s}_{ji}\right] = \underset{\mathbf{s}\in\mathcal{C}_{mGQSM}}{\arg\min} \left\| \mathbf{y} - \sqrt{E_s} \sum_{j=1}^{N_C} \left(\mathbf{h}_{l_{jr}} s_{jr} + \mathrm{j}\mathbf{h}_{l_{ji}} s_{ji} \right) \right\|^2 \tag{5.6}$$

where $\widehat{l}_{jr}$ and $\widehat{l}_{ji}$ represent the estimated antenna indices corresponding to the estimated symbols, $\widehat{s}_{jr}$ and $\widehat{s}_{ji}$.

5.3 mGQSM System with Imperfect CSI

This section discusses the uncoded mGQSM system performance with imperfect CSI. In addition to Weibull channel $\mathbf{H}$, we use $N_R \times N_T$ dimension error channel $\delta\mathbf{H}$ for the imperfect channel. The entries of $\delta\mathbf{H}$ are modelled as i.i.d. $\mathcal{CN}(0, \sigma_h)$. We consider Weibull non-fading environment ($\beta = 5$) scenario. At the receiver, the ML decoding algorithm make a decision with respect to the $\delta\mathbf{H}$.

ML decoding algorithm for the signal vector $\mathbf{s}$ is given as,

$$\hat{\mathbf{s}} = \underset{\mathbf{s}\in\mathcal{C}_{mGQSM}}{\arg\min} \|\mathbf{y} - \sqrt{E_s}(\mathbf{H} + \delta\mathbf{H})\mathbf{s}\|^2 \tag{5.7}$$

where $\hat{\mathbf{s}}$ denote estimated signal vector for the input signal $\mathbf{s}$.

5.4 Example 3: mGQSM Transmission

Fig. 5.1 shows the mGQSM transmission with $N_T = 4$ and $M = 4$. According to AAPs selection [93], we choose $N_C = 2$. To transmit data symbols, mGQSM scheme can choose any $2^{\left\lfloor 2\log_2 \binom{N_T}{N_C} \right\rfloor} = 32$ possible AAPs out of $\binom{N_T}{N_C}^2 = \binom{4}{2}^2 = 36$ total number of AAPs. The possible AAPs for the mGQSM is shown in chapter 3, Table. 3.1. Let the 4-QAM ($M = 4$) modulation for the mGQSM transmission with the SE of 9 bpcu. Consider the input bits, [1 0 0 0 1 0 0 1 0] at one channel use. First, $\left\lfloor 2\log_2 \binom{N_T}{N_C} \right\rfloor = 5$ bits, [1 0 0 0 1] choose the AAPs, $(l_{1r}, l_{2r}) = (3, 4)$ for real, and $(l_{1i}, l_{2i}) = (1, 4)$ for imaginary parts, while remaining,

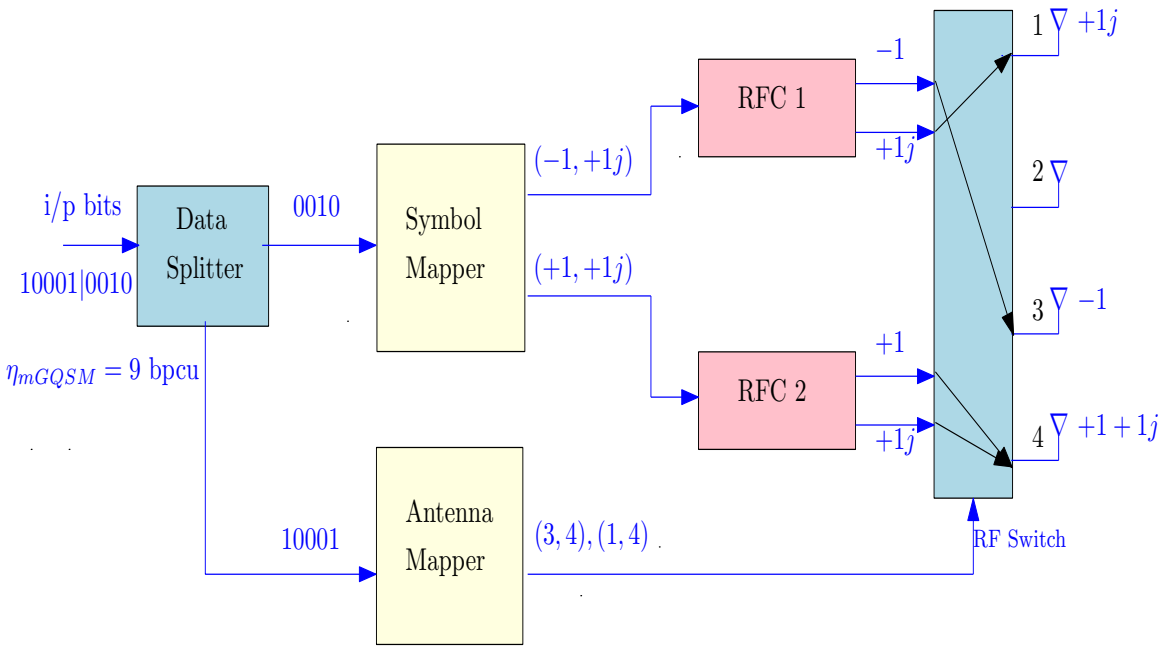

Fig. 5.1 mGQSM transmission with $N_T = 4$ and $M = 4$.

$N_C \log_2 M = 4$ bits, [0 0 1 0] choose data symbols $s_1 = -1 + j1$ and $s_2 = +1 + j1$. The antennas $l_{1r} = 3$ and $l_{2r} = 4$ transmit the real symbols, $s_{1r} = -1$ and $s_{2r} = +1$ with the transmission vector, $\mathbf{s}_r = [0\ 0\ \text{-}1\ +1]^T$. Likewise, the antennas $l_{1i} = 1$ and $l_{2i} = 4$ transmit the imaginary symbols, $s_{1i} = +1$ and $s_{2i} = +1$ with the transmission vector, $\mathbf{s}_i = [+1\ 0\ 0\ +1]^T$. Finally, the transmission vector is given as, $\mathbf{s} = \mathbf{s}_r + j\mathbf{s}_i = [+1 \quad 0 \quad -1 \quad +1 + j1\ ]^T$.

5.5 Simulation Results

This section illustrates the BER performance of the mGQSM and RC-mGQSM systems over uncorrelated and correlated Weibull fading channel. Consider Weibull fading channel with two different fading environment scenarios which depend on the Weibull shape parameter β, deep fade environment with $\beta = 0.5$ and the non-fading environment with $\beta = 5$. The entries of the noise vector $\mathbf{n}$ are follows as i.i.d. $\mathcal{CN}(0, \sigma_n^2)$. We use 10^5 data symbols to calculate BER with different SNR values and also assume the correlation decay coefficient $\phi = 0.7$ at

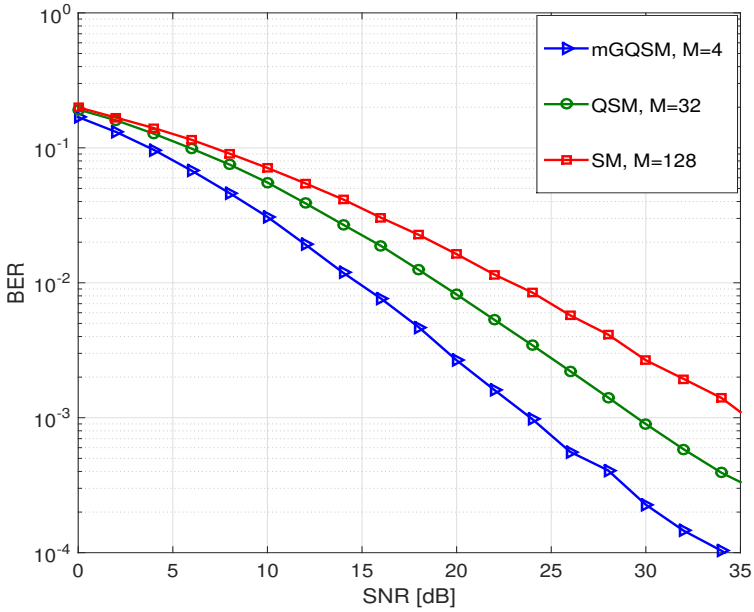

Fig. 5.2 BER Vs. SNR for mGQSM, QSM and SM systems over Weibull channel ($\beta = 0.5$) with same SE of 9 bpcu

both the transmitter and receiver sides. For the simulations, we consider $N_T = 4$, $N_R = 4$ system model for all the systems, and $N_C = 2$ for mGQSM and RC-mGQSM systems. We compare all the schemes at the BER of 10^{-3}.

The error performance comparison of mGQSM, QSM, and SM systems with Weibull deep fade ($\beta = 0.5$) and the non-fading ($\beta = 5$) environment scenarios are shown in Figs. 5.2 and 5.3, respectively. We compare the error performance of systems with the same SE of 9 bpcu. In Fig. 5.2, we noticed that mGQSM system performance with 4-QAM ($M = 4$) scheme gain in SNR of ∼4 dB over QSM with 32-QAM ($M = 32$) and ∼8 dB over SM with 128-QAM ($M = 128$). In Fig. 5.3, we noticed that mGQSM system performance with 4-QAM ($M = 4$) scheme gain in SNR of ∼2 dB over QSM with 32-QAM ($M = 32$) and ∼4 dB over SM with 128-QAM ($M = 128$) modulation.

The comparison of RC-mGQSM, QSM, and SM with Weibull deep fade ($\beta = 0.5$) and non-fading ($\beta = 5$) environment scenarios are shown in Figs. 5.4 and 5.5, respectively. We compare the error performance of systems with the same SE of 8 bpcu. In Fig. 5.4, we

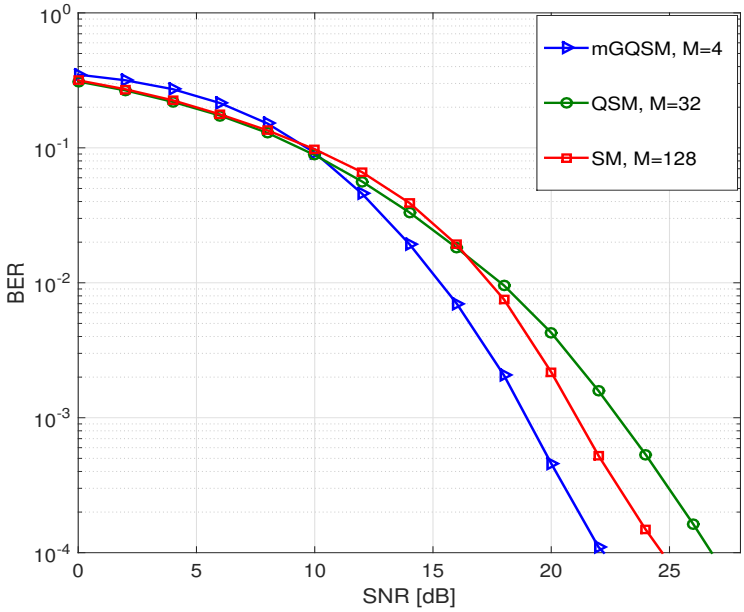

Fig. 5.3 BER Vs. SNR for mGQSM, QSM and SM systems over Weibull channel ($\beta = 5$) with same SE of 9 bpcu

noticed that RC-mGQSM system performance with 4-QAM ($M = 4$) scheme gain in SNR of ∼2 dB over QSM with 16-QAM ($M = 16$) and ∼6 dB over SM with 64-QAM ($M = 64$). In Fig. 5.5, we noticed that RC-mGQSM system performance with 4-QAM ($M = 4$) scheme gain in SNR of ∼3 dB over QSM with 16-QAM ($M = 16$) and ∼0.8 dB over SM with 64-QAM ($M = 64$) modulation. The mGQSM performance under imperfect CSI is shown in Fig. 5.6. We consider a non-fading environment ($\beta = 5$) scenario and $N_R \times N_T$ dimension error channel $\delta\mathbf{H}$, with the variance σ_h varies from 0.01 to 0.05. For 4-QAM ($M = 4$) scheme, we compared the mGQSM system performance with different error channel variances. We noticed that mGQSM system performance with error channel variance 0.01 and 0.02 are loses ∼2 dB and ∼6 dB SNR values, respectively. Hence, the system performance degrades by adding an error channel to the perfect channel.

A comparison of mGQSM and QSM performances over uncorrelated and correlated Weibull fading ($\beta = 0.5$) channel are shown in Figs. 5.7 and 5.8, respectively. We assume 4-QAM modulation for mGQSM and 32-QAM modulation for QSM and compare both the systems

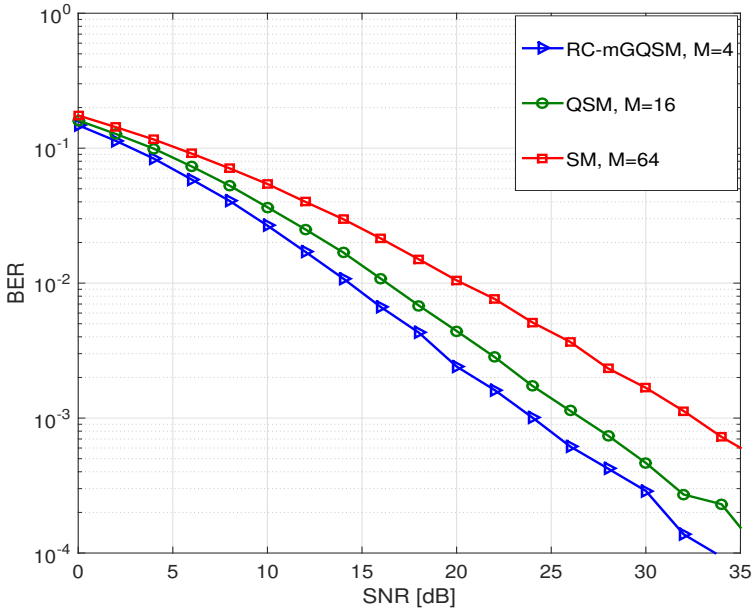

Fig. 5.4 BER Vs. SNR for RC-mGQSM, QSM and SM systems over Weibull channel ($\beta = 0.5$) with same SE of 8 bpcu

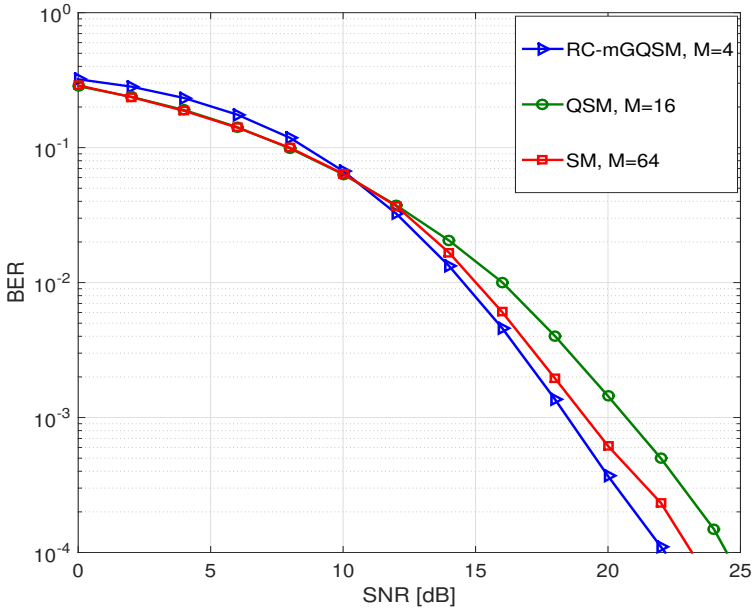

Fig. 5.5 BER Vs. SNR for RC-mGQSM, QSM and SM systems over Weibull channel ($\beta = 5$) with same SE of 8 bpcu

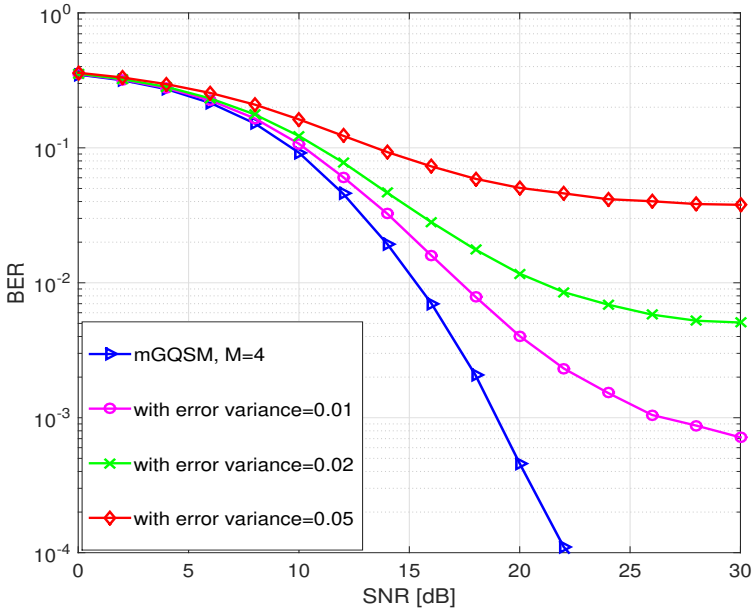

Fig. 5.6 BER Vs. SNR for mGQSM system over Weibull channel ($\beta = 5$) with error variances are equal to 0.01, 0.02, 0.05 and the SE of 9 bpcu.

at same SE of 9 bpcu. In Fig. 5.7, we can see that mGQSM performance gain ∼4 dB SNR over QSM. In Fig. 5.8, we found that mGQSM outperforms QSM by ∼3 dB SNR at the same BER.

Figs. 5.9 and 5.10 presents the comparison of RC-mGQSM, GQSM, and QSM systems over correlated Weibull channel with $\beta = 0.5$ and $\beta = 5$, respectively. We consider 4-QAM modulation for RC-mGQSM and GQSM systems, 16-QAM modulation for QSM system. In Fig. 5.9, we found that RC-mGQSM system performance gain about ∼0.5 dB SNR over QSM and degrade the performance in SNR of ∼1.5 dB over GQSM at BER of 10^{-4}. In Fig. 5.10, RC-mGQSM outperforms QSM by ∼1.5 dB SNR and degrades ∼1.6 dB SNR over GQSM at the same BER. Fig. 5.11 presents the mGQSM performance over different fading channels i.e. Rayleigh, Rician ($K = 3, 10$) dB, Nakagami ($m = 2, 4$), and Weibull ($\beta = 5$). We noticed that the mGQSM performance shows better under Reyleigh channel and gain ∼2 dB and ∼3 dB SNRs over mGQSM with $m = 2$ and $K = 3$ dB. Also, observed that the mGQSM shows poor performances as increases the values of m and K.

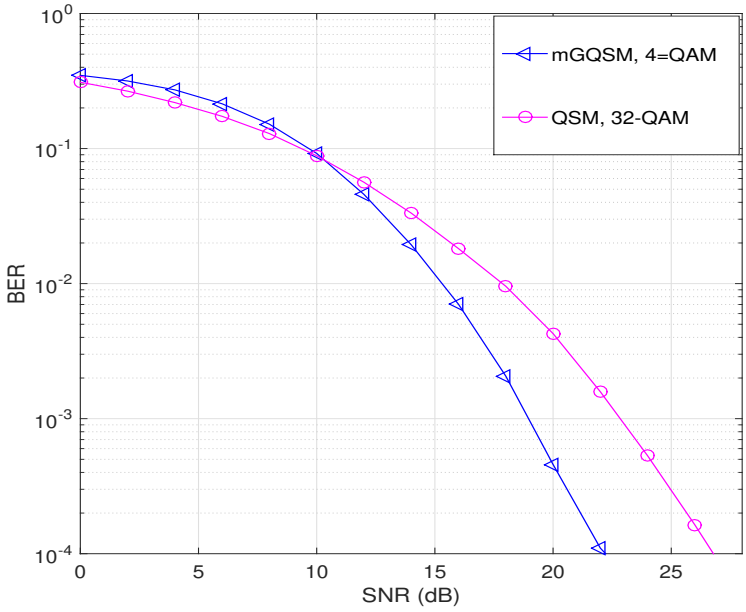

Fig. 5.7 BER Vs. SNR for mGQSM and QSM systems over Weibull channel ($\beta = 5$) with SE of 9 bpcu.

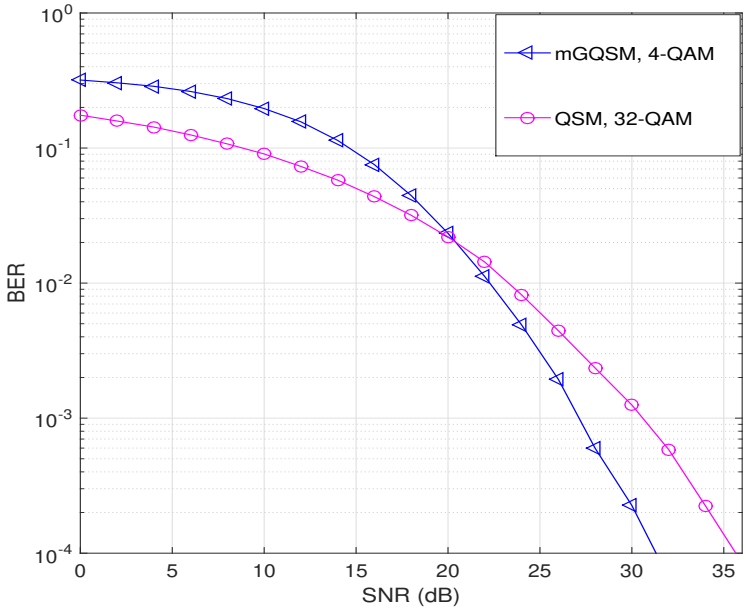

Fig. 5.8 BER Vs. SNR for mGQSM and QSM systems over correlated Weibull channel ($\beta = 5$) with SE of 9 bpcu.

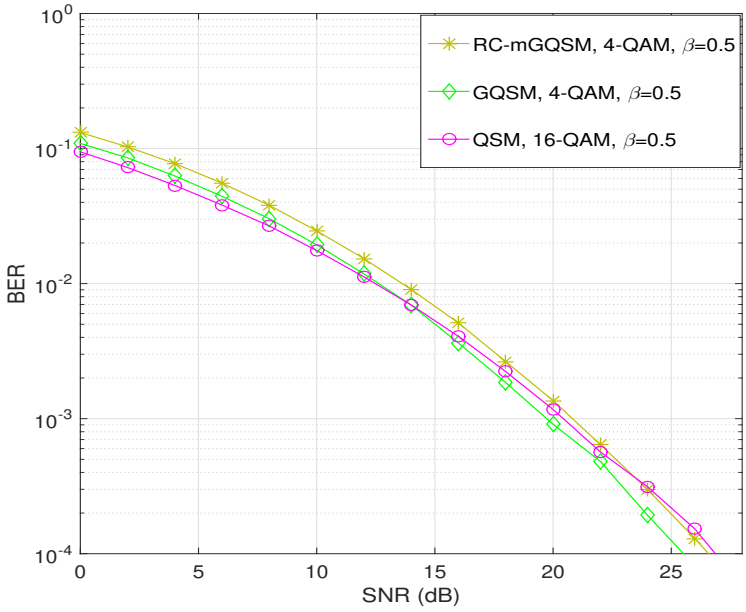

Fig. 5.9 BER Vs. SNR of RC-mGQSM, GQSM and QSM systems over correlated Weibull channel ($\beta = 0.5$) with SE of 8 bpcu.

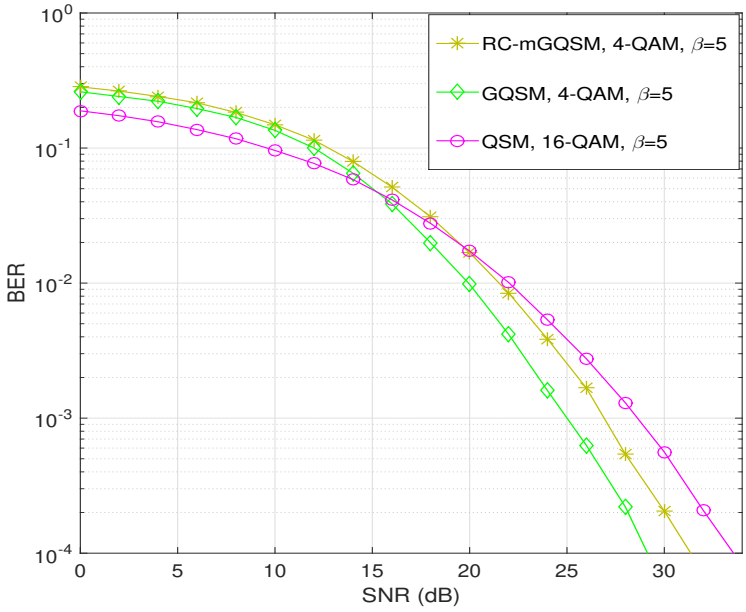

Fig. 5.10 BER Vs. SNR of RC-mGQSM, GQSM and QSM systems over correlated Weibull channel ($\beta = 0.5$) with SE of 8 bpcu.

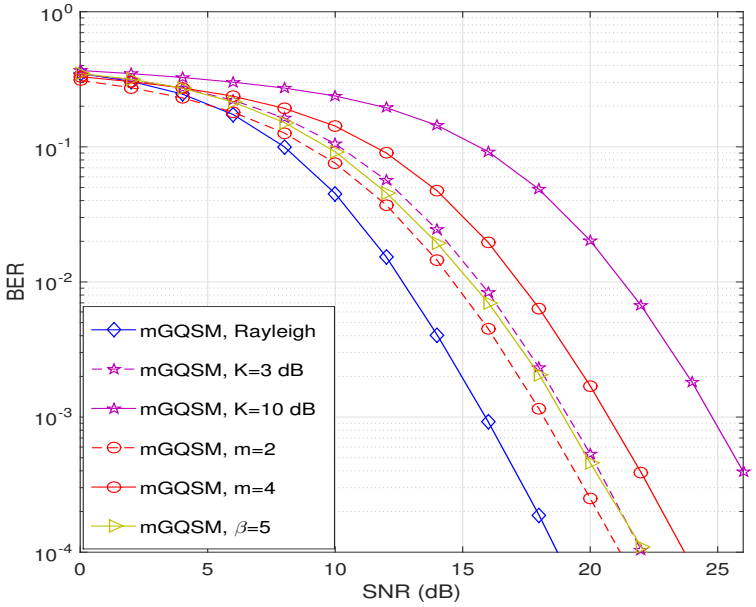

Fig. 5.11 BER Vs. SNR of mGQSM system over different fading channels with the same SE of 9 bpcu.

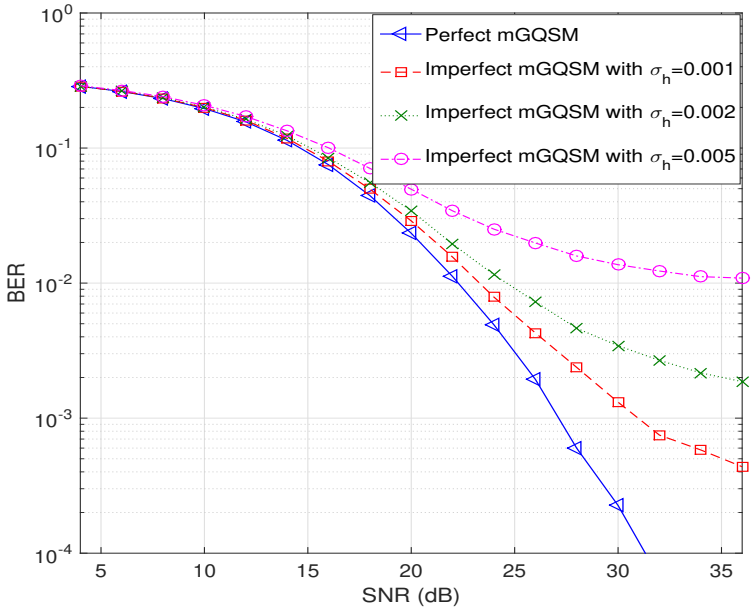

Fig. 5.12 BER Vs. SNR of mGQSM system over correlated Weibull channel ($\beta = 5$) with $\sigma_h = 0.001, 0.002, 0.005$ and the SE of 9 bpcu.

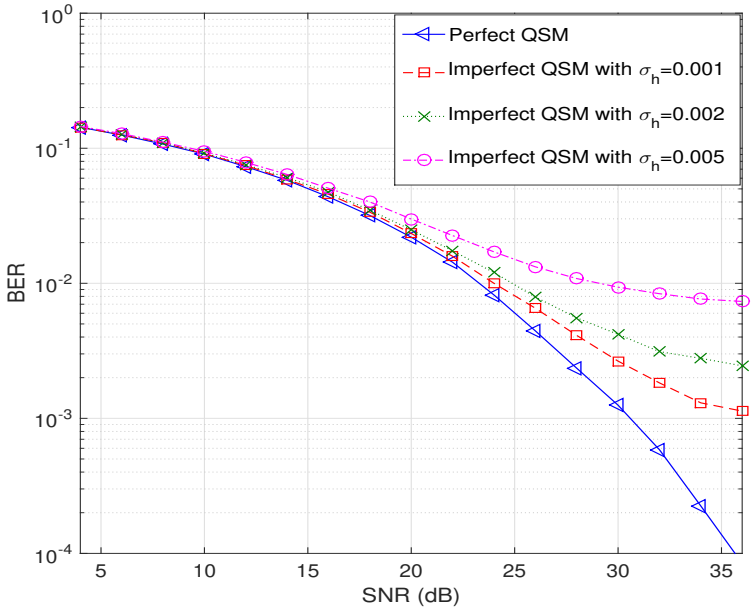

Fig. 5.13 BER Vs. SNR of QSM system over correlated Weibull channel ($\beta = 5$) with $\sigma_h = 0.001, 0.002, 0.005$ and the SE of 9 bpcu.

A comparison of mGQSM and QSM system performances over correlated Weibull fading ($\beta = 5$) with imperfect CSI are shown in the Figs. 5.12 and 5.13, respectively. We consider 4-QAM modulation for mGQSM and 32-QAM modulation for QSM. We assume the values for the error variance, $\sigma_h = \{0.001, 0.002, 0.005\}$. Table. 5.1 shows the BER values for perfect and imperfect mGQSM and QSM systems over correlated Weibull fading channel with SNR values of 18 dB, 24 dB, 30 dB. At SNR of 18 dB, we noticed that the BER values for the imperfect ($\sigma_h = 0.001$)QSM and mGQSM systems are 0.0336 and 0.0496, respectively, while at SNR of 30 dB, the BER values for QSM and mGQSM systems are 0.0026 and 0.0013, respectively. Similarly, for the remaining σ_h values we found that mGQSM system with imperfect channel outperforms the QSM at high SNR values.

Table 5.1 BER Vs SNR for the QSM and mGQSM systems with imperfect CSI.

SNR (dB)	BER							
	QSM				mGQSM			
	$\sigma_h = 0$	$\sigma_h = 0.001$	$\sigma_h = 0.002$	$\sigma_h = 0.005$	$\sigma_h = 0$	$\sigma_h = 0.001$	$\sigma_h = 0.002$	$\sigma_h = 0.005$
18	0.0317	0.0336	0.0348	0.0400	0.0444	0.0496	0.0555	0.0707
24	0.0081	0.0099	0.0120	0.0170	0.0049	0.0078	0.0115	0.0250
30	0.0012	0.0026	0.0041	0.0093	0.0002	0.0013	0.0034	0.0136

5.6 Conclusion

In this chapter, the BER results of mGQSM and RC-mGQSM systems are presented over uncorrelated and correlated Weibull fading channels. A relevant example is used to explain the mGQSM transmission system. Using the ML detector, mGQSM and RC-mGQSM systems are illustrated and compared to QSM and GQSM systems. We considered Weibull non-fading and deep-fading environments with β equal to 5 and 0.5, respectively. The BER results of RC-mGQSM system are compared to that of QSM and GQSM systems under different fading scenarios. RC-mGQSM outperforms QSM by $\sim$1.5 dB SNR and degrades $\sim$1.6 dB SNR over GQSM. The mGQSM outperforms QSM by $\sim$3 dB SNR and $\sim$4 dB SNR for correlated and uncorrelated Weibull channels, respectively. Furthermore, the mGQSM performance is demonstrated under imperfect CSI and compared to QSM. The computational complexity of the mGQSM increases with the SE.

Chapter 6

Fully Generalized Quadrature Spatial Modulation

6.1 Fully Quadrature Spatial Modulation (F-QSM)

6.1.1 Introduction

Fully QSM (F-QSM) [96] scheme was proposed to improve the SE of QSM. F-QSM scheme employs a novel transmission mechanism in order to attain the linear proportionality between the SE and N_T. Whereas all other SMTs use logarithmic proportionality between SE and N_T. The transmission diagram of F-QSM is shown in [96]. The input bits split into 3 blocks, the first block consists of data bits which are equal to $\log_2 M$ bits. Using these bits the data symbol, S is selected from the QAM modulation. Furthermore, the symbol S is separated as real $S_{\Re}$ and imaginary $S_{\Im}$ symbols. The remaining two blocks consists of spatial bits which are equal to $(N_T - 1)$ bits per each block. Using these spatial bits the transmit antenna combinations (TACs) is selected. The first $(N_T - 1)$ bits choose a TACs to transmit the $S_{\Re}$, and remaining $(N_T - 1)$ bits choose a same or different TACs to transmit the $S_{\Im}$. Therefore, the SE of F-QSM scheme can be given as [96],

Table 6.1 Transmit antenna combinations (TACs) for F-QSM with $N_T = 4$

Possible Bits	**Transmit Antenna Combinations (TACs)**
000	1
001	2
010	3
011	4
100	$(1, 2)$
101	$(1, 3)$
110	$(1, 4)$
111	$(2, 3)$

$$\eta_{F-QSM} = 2(N_T - 1) + \log_2 M \quad \text{bpcu} \tag{6.1}$$

From eq. (6.1), we can observe that the SE of F-QSM is linearly proportional with N_T, while the conventional SMTs SE is logarithmically proportional with N_T. Hence, F-QSM scheme provide higher spectral efficiencies over SM and QSM with fewer N_T values. For example, Let $N_T = 4$ and $M = 4$, then the SE of F-QSM becomes 8 bpcu. To attain the SE of 8 bpcu, SM and QSM schemes require $N_T = 64$ and $N_T = 8$, respectively.

Let the input bits [1 1 0 0 0 0 1 1] for F-QSM scheme with 8 bpcu transmission. Where the first, two bits [1 1] map the M-QAM data symbol S. Furthermore, the data symbol S is separated as $S_{\Re}$ and $S_{\Im}$. Remaining, spatial bits split into 2 equal blocks, the first block of bits, [0 0 0] choose the transmit antenna 1 and second block of bits, [0 1 1] choose the transmit antenna 4 using the Table. 6.1. Finally, the symbols, $S_{\Re}$ and $S_{\Im}$ are transmitted by the antennas 1 and 4, respectively. Hence, the $N_T \times 1$ dimension transmission vector is given as, $\mathbf{S} = [S_{\Re}\ 0\ 0\ jS_{\Im}]^T$. Similarly, for the other possible transmitted vectors are given in Table. 6.2.

Table 6.2 Codebook for the F-QSM transmission with $N_T = 4$ and $M = 4$

i/p Bits		**Transmission Data**			
Data Bits	Spatial Bits	Antenna-1	Antenna-2	Antenna-3	Antenna-4
$b_1 b_2$	000000	S	-	-	-
$b_1 b_2$	000001	$S_{\Re}$	$S_{\Im}$	-	-
$b_1 b_2$	000010	$S_{\Re}$	-	$S_{\Im}$	-
$b_1 b_2$	000011	$S_{\Re}$	-	-	$S_{\Im}$
$b_1 b_2$	111100	$S_{\Im}$	S	$S_{\Re}$	-
$b_1 b_2$	111101	$S_{\Im}$	$S_{\Re}$	S	-
$b_1 b_2$	111110	$S_{\Im}$	$S_{\Re}$	$S_{\Re}$	$S_{\Im}$
$b_1 b_2$	111111	-	S	S	-

6.1.2 F-QSM System Model

Consider $N_R \times N_T$ system model being N_R receive and N_T transmit antennas. Let the Rayleigh channel, $\mathbf{H}$ and the noise $\mathbf{n}$ with dimensions $N_R \times N_T$ and $N_R \times 1$, respectively. The channel gains of $\mathbf{H}$ and $\mathbf{n}$ follows i.i.d $h_{N_R,N_T} \sim \mathcal{CN}(0,1)$ and $n_{N_R,1} \sim \mathcal{CN}(0,\sigma_n^2)$. The received signal is given by,

$$\begin{aligned} \mathbf{y} &= \mathbf{HS} + \mathbf{n} \\ &= \mathbf{h}_{l_{\Re}} S_{\Re} + j\mathbf{h}_{l_{\Im}} S_{\Im} + \mathbf{n} \end{aligned} \tag{6.2}$$

and

$$\mathbf{h}_{l_{\Re}} = \sum_{p=1}^{N_c} \mathbf{h}_p, \quad \mathbf{h}_{l_{\Im}} = \sum_{q=1}^{N_c} \mathbf{h}_q \tag{6.3}$$

where $\mathbf{h}_p$, $\mathbf{h}_q$ denotes the p^{th} and q^{th} columns of $\mathbf{H}$, respectively, and $N_C = 1, 2, \cdots, \left\lceil \frac{N_T}{2} \right\rceil$.

At the receiver, we use the ML detection algorithm by assuming perfect CSI and it is given by,

$$[\widehat{l}_{\Re}, \widehat{l}_{\Im}, \widehat{S}_{\Re}, \widehat{S}_{\Im}] = \underset{l_{\Re}, l_{\Im}, S_{\Re}, S_{\Im}}{\arg\min} \|\mathbf{y} - (\mathbf{h}_{l_{\Re}} S_{\Re} + j\mathbf{h}_{l_{\Im}} S_{\Im})\|^2 \tag{6.4}$$

where $\widehat{l}_{\Re}$ and $\widehat{l}_{\Im}$ are the detected antenna indices of $\widehat{S}_{\Re}$ and $\widehat{S}_{\Im}$.

6.2 Fully Generalized Quadrature Spatial Modulation (FGQSM)

6.2.1 Introduction

In this section, we propose a fully generalised QSM (FGQSM) scheme to enhance the SE of F-QSM and mGQSM by considering variable number of TACs and multiple RF-chains. The logarithmic proportionality between SE and N_T of conventional SMTs is vanquished in FGQSM and achieves a linear proportionality by using variable number of TACs. Moreover, the SE of FGQSM improves over symbol and spatial constellations for F-QSM and mGQSM, respectively. The transmission system diagram of FGQSM with N_T transmit antennas is shown in Fig. 6.1. The input data bits split into 3 group of bits, the first $N_C \log_2 M$ bits encode data symbols $S_1, \cdots, S_{N_C}$ using symbol mapper and $1 < N_C \leq \left\lfloor \frac{N_T}{2} \right\rfloor$. The remaining two group of spatial bits, $2(N_T - 1)$ choose the TACs with the help of antenna mapper. The first $(N_T - 1)$ bits choose one TACs to transmit the symbols, $S_{1\Re}, \cdots, S_{N_C\Re}$, and remaining $(N_T - 1)$ bits choose the same or different TACs to transmit symbols, $S_{1\Im}, \cdots, S_{N_C\Im}$. Hence, the SE of FGQSM is given by,

$$\eta_{FGQSM} = 2(N_T - 1) + N_C \log_2 M \quad \text{bpcu} \tag{6.5}$$

From eq. (6.5), we observe that the SE of FGQSM is linearly proportional with N_T,

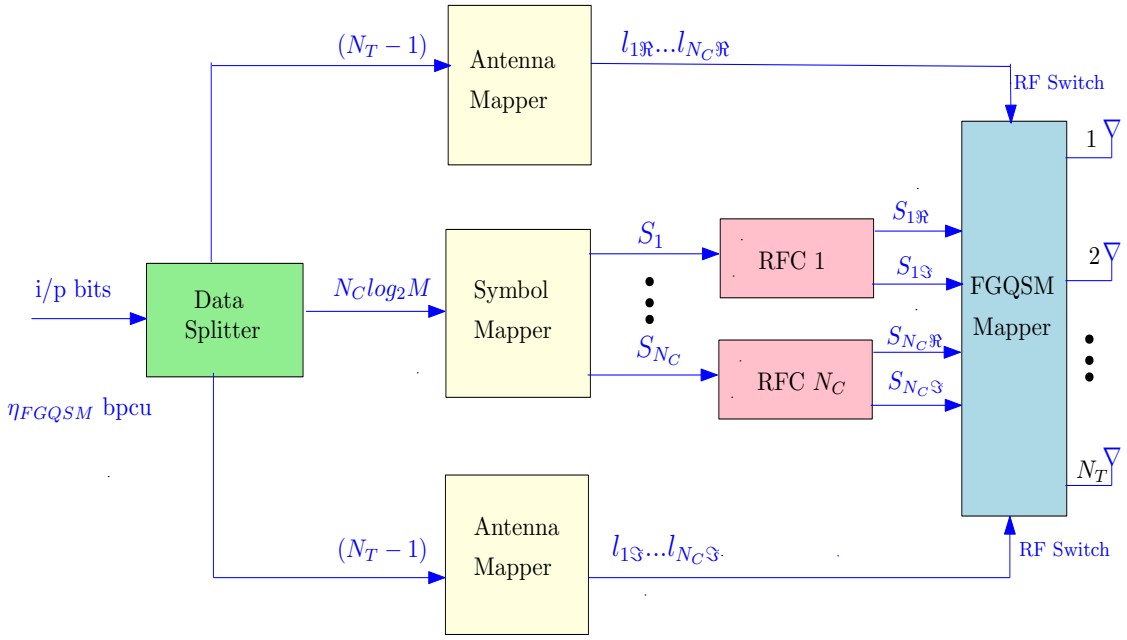

Fig. 6.1 FGQSM transmission system diagram

while the SE of the conventional SMTs is logarithmic proportional with N_T. Therefore, the FGQSM scheme provide higher data rates over conventional SMTs with fewer N_T values. For example, Let $N_T = 4$ and $M = 4$, then the SE of FGQSM becomes 10 bpcu. To attain the same SE of 10 bpcu, mGQSM ($N_C = 2$), F-QSM, and QSM schemes require $N_T = 5$, $N_T = 5$ and $N_T = 16$, respectively.

Fig. 6.2 shows the FGQSM transmission with $N_T = 4$ and $M = 4$. Let the input bits $\left[\underbrace{0\,1\,1\,0\,1}_{spatial\ bits}\ \underbrace{0\,1\,0\,0\,1}_{data\ bits}\right]$ for FGQSM ($N_T = 4, M = 4$) with 10 bpcu transmission. Where the first, four data bits $\left[\underbrace{1\,0\,0\,1}_{b_1 b_2 b_3 b_4}\right]$ map the M-QAM symbols ($S_1 = +1 + 1j, S_2 = -1 - 1j$). Furthermore, these data symbols are separated as ($S_{1\Re} = +1, S_{2\Re} = -1$) and ($S_{1\Im} = +1j, S_{2\Im} = -1j$). Remaining, spatial bits are split into 2 equal parts, the first part of bits, [0 1 1] choose the TACs $(2, 4)$ and the second part of bits, [0 1 0] choose the TACs $(1, 4)$ using the Table. 6.3. Finally, the symbols, ($S_{1\Re} = +1, S_{2\Re} + -1$) and ($S_{1\Im} = +1j, S_{2\Im} = -1j$) are transmitted by the TACs $(2, 4)$ and $(1, 4)$, respectively. Hence, the $N_T \times 1$ dimension transmission vector

Table 6.3 Transmit antenna combinations (TACs) for FGQSM with $N_T = 4$

Possible Bits	**Transmit Antenna Combinations (TACs)**
000	$(1, 2)$
001	$(1, 3)$
010	$(1, 4)$
011	$(2, 4)$
100	$(1, 2, 3)$
101	$(1, 2, 4)$
110	$(2, 3, 4)$
111	$(1, 2, 3, 4)$

Table 6.4 Codebook for the FGQSM transmission with $N_T = 4$ and $M = 4$

i/p Bits		**Transmission Data**			
Data Bits	Spatial Bits	Antenna $-$ 1	Antenna $-$ 2	Antenna $-$ 3	Antenna $-$ 4
$b_1b_2b_3b_4$	000000	$S_{1\Re} + jS_{1\Im}$	$S_{2\Re} + jS_{2\Im}$	-	-
$b_1b_2b_3b_4$	000001	$S_{1\Re} + jS_{1\Im}$	$S_{2\Re}$	$jS_{2\Im}$	-
$b_1b_2b_3b_4$	000010	$S_{1\Re} + jS_{1\Im}$	$S_{2\Re}$	-	$jS_{2\Im}$
$b_1b_2b_3b_4$	000011	$S_{1\Re}$	$S_{2\Re} + jS_{1\Im}$	-	$jS_{2\Im}$
$b_1b_2b_3b_4$	111100	$S_{1\Re} + jS_{1\Im}$	$S_{1\Re} + jS_{1\Im}$	$S_{2\Re} + jS_{2\Im}$	$S_{2\Re}$
$b_1b_2b_3b_4$	111101	$S_{1\Re} + jS_{1\Im}$	$S_{1\Re} + jS_{1\Im}$	$S_{2\Re}$	$S_{2\Re} + jS_{2\Im}$
$b_1b_2b_3b_4$	111110	$S_{1\Re} + jS_{1\Im}$	$S_{1\Re}$	$S_{1\Re} + jS_{1\Im}$	$S_{2\Re} + jS_{2\Im}$
$b_1b_2b_3b_4$	111111	$S_{1\Re} + jS_{1\Im}$	$S_{1\Re} + jS_{1\Im}$	$S_{2\Re} + jS_{2\Im}$	$S_{2\Re} + jS_{2\Im}$

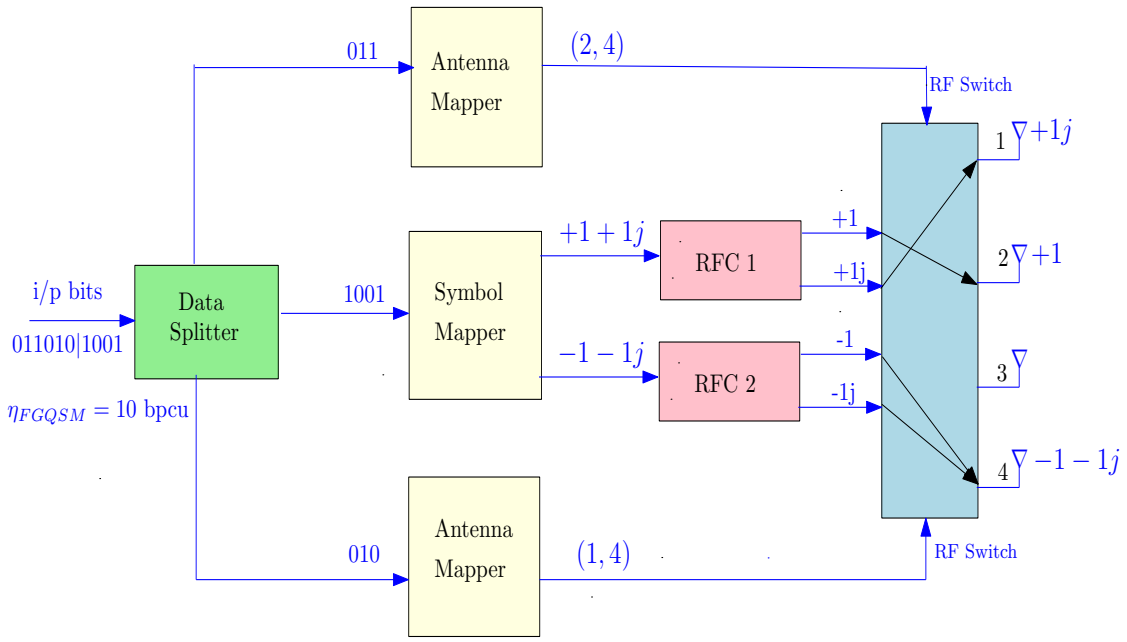

Fig. 6.2 FGQSM transmission with $N_T = 4$ and $M = 4$

is given as, $\mathbf{S} = [+1j \quad +1 \quad 0 \quad -1-1j]^T$. Similarly, other possible transmitted vectors are given in Table. 6.4.

6.2.2 FGQSM System Model

Assume $N_R \times N_T$ FGQSM system being N_R receive and N_T transmit antennas. Let the input signal $\mathbf{S}$ is transmitted over frequency-flat Rayleigh fading channel, $\mathbf{H}$. The channel gains of $\mathbf{H}$ and the coefficients of $\mathbf{n}$ are given as i.i.d $h_{N_R,N_T} \sim \mathcal{CN}(0,1)$ and $n_{N_R,1} \sim \mathcal{CN}(0,\sigma_n^2)$. Let $\mathbf{h}_{l_{q\Re}}$ and $\mathbf{h}_{l_{q\Im}}$ be the $l_{q\Re}^{th}$ and $l_{q\Im}^{th}$ columns of $\mathbf{H}$, respectively, i.e. $\mathbf{h}_{l_{q\Re}} = [h_{1,l_{q\Re}}, \cdots, h_{N_R,l_{q\Re}}]^T$ and $\mathbf{h}_{l_{q\Im}} = [h_{1,l_{q\Im}}, \cdots, h_{N_R,l_{q\Im}}]^T$; $q = 1, \cdots, N_C$. Therefore, the received signal can be given as,

$$\begin{aligned} \mathbf{y} &= \mathbf{HS} + \mathbf{n} \\ &= \sum_{q=1}^{N_C} (\mathbf{h}_{l_{q\Re}} S_{q\Re} + \mathrm{j}\mathbf{h}_{l_{q\Im}} S_{q\Im}) + \mathbf{n} \end{aligned} \tag{6.6}$$

where $\mathbf{S}$ is the transmitted signal and $l_{q\Re}, l_{q\Im} = 1, \cdots, N_T$.

6.3 Fading Channels

6.3.1 Rayleigh Fading

The Rayleigh fading model can be used to statistically analyse radio signal. In multipath propagation, it performs best when there is no LOS path. The fading gains of $\mathbf{H}$ are considered as i.i.d. $\mathcal{CN}(0,1)$.

6.3.2 Rician Fading

Rician fading can be modelled when the multipath propagation consist dominant LOS path as well as scattered non-LOS paths. Rayleigh fading is the special case of Rician when the dominant LOS path is not present. The channel matrix for the Rician fading can be given as,

$$\mathbf{H} = \sqrt{\frac{K}{1+K}} \times 1_{N_R \times N_T} + \sqrt{\frac{1}{1+K}} \times \mathbf{H}' \tag{6.7}$$

where K defines the Rician factor, $\mathbf{H}'$ defines the channel matrix, where each entry follows i.i.d. $\mathcal{CN}(0,1)$, and $1_{N_R \times N_T}$ denotes the $N_R \times N_T$ dimension matrix, where each entry equal to 1.

Using ML detection method, we calculate the estimated antenna indices corresponding to data symbols is given as,

$$\left[\widehat{l}_{q\Re}, \widehat{l}_{q\Im}, \widehat{S}_{q\Re}, \widehat{S}_{q\Im}\right] = \underset{l_{q\Re}, l_{q\Im}, S_{q\Re}, S_{q\Im}}{\arg\min} \left\| \mathbf{y} - \sum_{q=1}^{N_C} \left(\mathbf{h}_{l_{q\Re}} S_{q\Re} + \mathrm{j}\mathbf{h}_{l_{q\Im}} S_{q\Im} \right) \right\|^2 \tag{6.8}$$

where $\widehat{l}_{q\Re}$ and $\widehat{l}_{q\Im}$ are estimated antenna indices correspond to symbols, $\widehat{S}_{q\Re}$ and $\widehat{S}_{q\Im}$.

6.4 FGQSM and F-QSM Systems with Imperfect CSI

This section presents the FGQSM and F-QSM performances under imperfect CSI. To illustrate the performance of FGQSM and F-QSM with imperfect channel $(\mathbf{H} + \delta\mathbf{H}) \in \mathbb{C}^{N_R \times N_T}$, the error channel $\delta\mathbf{H} \in \mathbb{C}^{N_R \times N_T}$ is employed along with Rayleigh channel $\mathbf{H} \in \mathbb{C}^{N_R \times N_T}$. The coefficients of $\delta\mathbf{H}$ follows i.i.d. $\mathcal{CN}(0, \sigma_e^2)$, where σ_e^2 defines the variance of $\delta\mathbf{H}$. In this section, we consider two distinct scenarios, 1). fixed σ_e^2: to determine the performance of FGQSM and F-QSM, the value of σ_e^2 is constant for different SNR values, and 2). variable σ_e^2: where the σ_e^2 is changes with different SNR values as $\sigma_e^2 = 1/(\gamma N)$, where the average SNR, $\gamma = E\left\{|S|^2\right\}/\sigma_n^2$ and N is the number of pilot symbols which are used to estimate the error channel [35].

The ML detection method makes a decision with imperfect channel $\mathbf{H} + \delta\mathbf{H}$. The ML detection for input signal $\mathbf{S}$ can be given as,

$$\hat{\mathbf{S}} = \arg\min_{\mathbf{S}} \|\mathbf{y} - (\mathbf{H} + \delta\mathbf{H})\mathbf{S}\|^2 \tag{6.9}$$

where $\hat{\mathbf{S}}$ is the estimated signal of $\mathbf{S}$.

6.5 Simulation Results

This section presents the the BER performance comparison of FGQSM and F-QSM systems with mGQSM, RC-mGQSM and QSM systems. Also, present the FGQSM and F-QSM performance under imperfect CSI conditions. Consider the coefficients of the channel $\mathbf{H}$ and noise $\mathbf{n}$ are follows $\mathcal{CN}(0, 1)$ and $\mathcal{CN}(0, \sigma_n^2)$, respectively. We consider 10^6 symbols to calculate BER for various SNRs. For all the computer simulations, we assume 4×4 system with $N_T = 4$ and $N_R = 4$ and compare all the schemes at BER of 10^{-4}. The doublet in the figures is denote as (N_T, M).

BER comparison of F-QSM, RC-mGQSM, QSM, and SM under uncorrelated Rayleigh

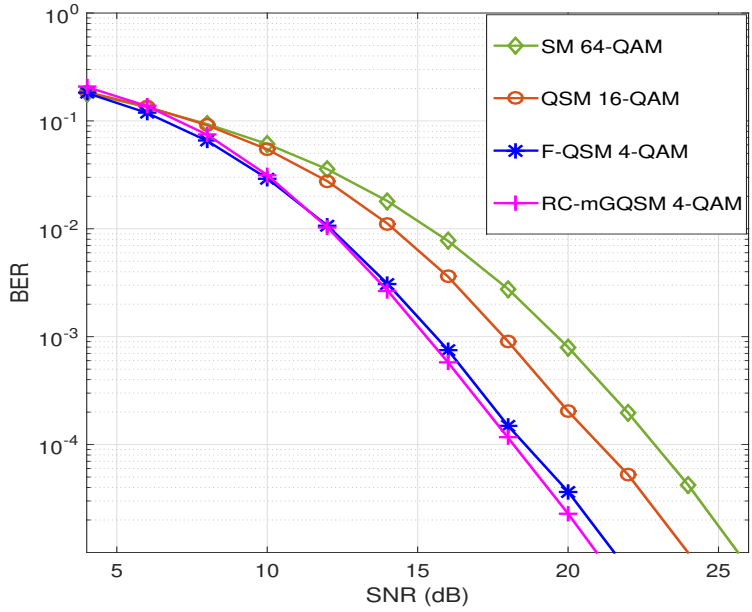

Fig. 6.3 BER versus SNR of F-QSM, RC-mGQSM, QSM, and SM systems over Rayleigh channel with same SE of 8 bpcu.

channel is shown in Fig. 6.3. These schemes are compared with the same SE of 8 bpcu. The F-QSM scheme outperform by $\sim$ 2.5 dB SNR of QSM and $\sim$ 4.5 dB SNR of SM. There is a small degradation of $\sim$ 0.5 dB SNR over RC-mGQSM. By comparing these schemes, F-QSM can deliver more spatial bits for a smaller number of transmitting antennas and lower order modulation, this mechanism decreases the complexity of F-QSM scheme.

Fig. 6.4 presents the BER versus SNR of F-QSM scheme under imperfect channel with variable σ_e^2. We compare the F-QSM performance with perfect CSI (P-CSI) to F-QSM with imperfect channel and number of pilot symbols N equal to 1, 3, and 10. The BER of F-QSM scheme degrades by $\sim$ 3.5 dB, $\sim$ 1.5 dB, and $\sim$ 0.5 dB SNRs with $N = 1$, $N = 3$ and $N = 10$, respectively. The performance of F-QSM with an imperfect channel approaches that of a perfect channel when N is increased.

The performance of F-QSM and QSM schemes under imperfect CSI are shown in Fig. 6.5 and 6.6, respectively. We compare the BER of both the schemes at SNR values of 16 dB, 18 dB, and 20 dB which is shown in Table. 6.5. We assume the values of error variance σ_e^2 as

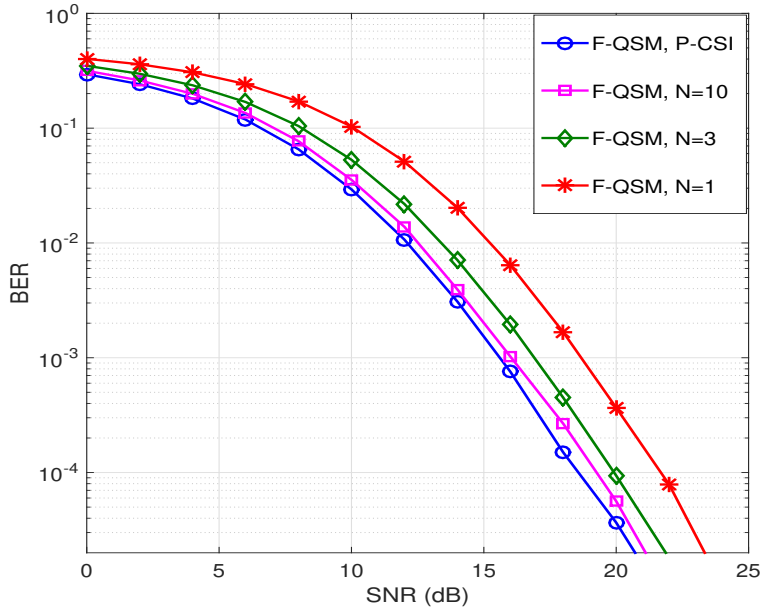

Fig. 6.4 BER versus SNR of F-QSM system under imperfect channel with $N = (1, 3, 10)$ and $\eta_{F-QSM} = 8$ bpcu.

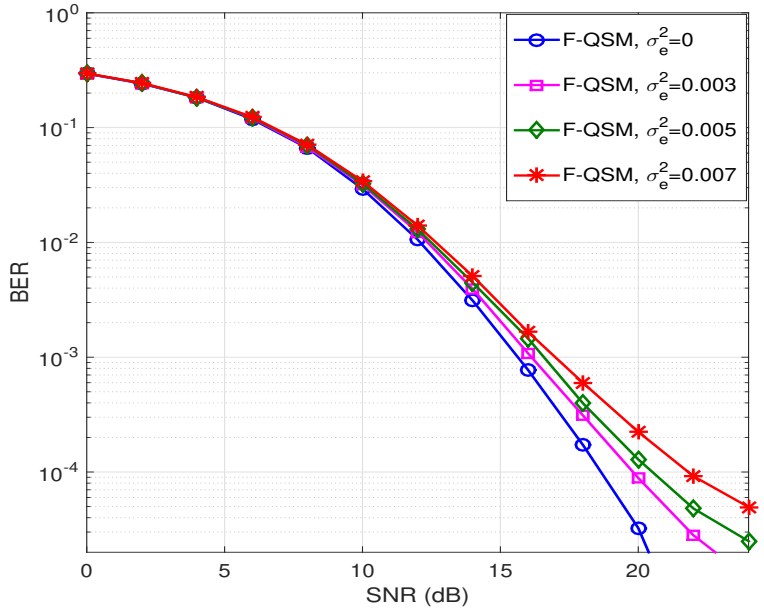

Fig. 6.5 BER versus SNR of F-QSM system with fixed error variance, $\sigma_e^2 = (0, 0.003, 0.005, 0.007)$ and $\eta_{F-QSM} = 8$ bpcu.

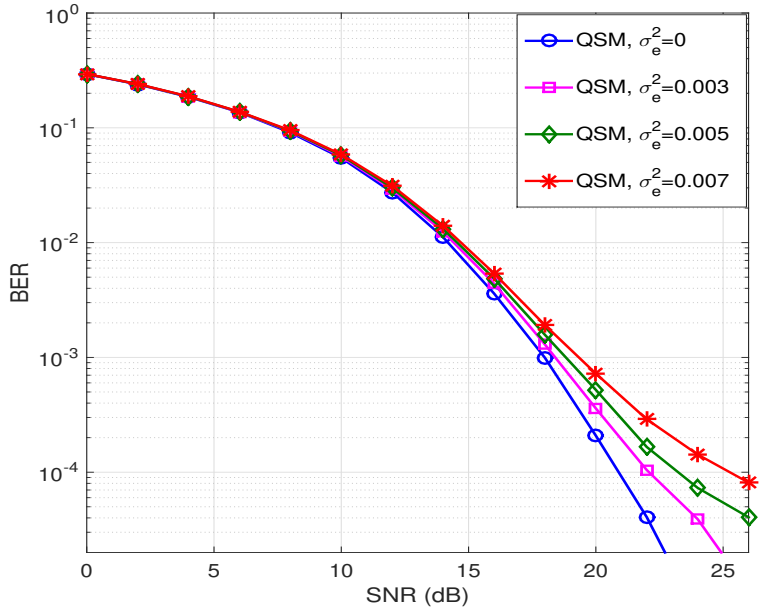

Fig. 6.6 BER versus SNR of QSM system with fixed error variance, $\sigma_e^2 = (0, 0.003, 0.005, 0.007)$ and $\eta_{QSM} = 8$ bpcu.

0, 0.003, 0.005, and 0.007. However, the value $\sigma_e^2 = 0$ becomes the perfect channel. At SNR of 16 dB, we observed the BER values for F-QSM and QSM schemes are 0.0014 and 0.0051, respectively and at 20 dB, the BER values are 0.0001 and 0.0005, respectively for $\sigma_e^2 = 0.005$. Hence, the F-QSM scheme performance better than QSM scheme under imperfect CSI. In F-QSM, the data can be transmitted through a variable number of antennas.

We calculate the computational complexity in terms of real valued multiplications. The computational complexity of the F-QSM and RC-mGQSM is calculated as $8N_R 2^{\eta_{F-QSM}}$ and $10N_R 2^{\eta_{RC-mGQSM}}$ [93], respectively. For 4×4 system and 4-QAM symbol, the complexity of RC-mGQSM is computed as 10240. Whereas, the complexity of F-QSM is 8092, which is approximately 21% less compared to the complexity of RC-mGQSM.

Fig. 6.7 shows the achievable SE of the FGQSM compared to the mGQSM, QSM, and SM respectively. The SE of FGQSM, mGQSM, QSM, and SM are calculated by assuming the fixed 4-QAM modulation scheme. Let $N_C = 2$ for FGQSM, mGQSM and $N_C = 1$ for QSM and SM. The achievable SE of the FGQSM is linearly proportional with N_T where as,

Table 6.5 BER Vs. SNR for imperfect CSI of F-QSM & QSM

SNR	**F-QSM** (BER)				**QSM** (BER)			
(dB)	$\sigma_e^2 = 0$	$\sigma_e^2 = 0.003$	$\sigma_e^2 = 0.005$	$\sigma_e^2 = 0.007$	$\sigma_e^2 = 0$	$\sigma_e^2 = 0.003$	$\sigma_e^2 = 0.005$	$\sigma_e^2 = 0.007$
16	0.0007	0.0010	0.0014	0.0016	0.0036	0.0043	0.0051	0.0054
18	0.0001	0.0003	0.0004	0.0005	0.0009	0.0012	0.0015	0.0019
20	3.25E-05	8.87E-05	0.0001	0.0002	0.0002	0.0003	0.0005	0.0007

the SE of mGQSM, QSM, and SM is logarithmically increase with N_T. For, $N_T = 16$, the SE of the FGQSM is 34 bpcu while the mGQSM, QSM, and SM systems achieve only 17 bpcu, 10 bpcu, and 6 bpcu SE, respectively. As a result, the proposed FGQSM achieves higher SE with smaller N_T than mGQSM, QSM, and SM.

BER comparison of proposed FGQSM, RC-mGQSM, F-QSM, and QSM over Rayleigh channel is shown in Fig. 6.8. These schemes are compared with the same SE of 10 bpcu. The FGQSM scheme outperform by $\sim$ 2 dB, $\sim$ 3.5 dB, $\sim$ 6 dB SNR values over RC-mGQSM, F-QSM, and QSM, respectively. By observing all these schemes, the FGQSM can deliver more number of spatial bits for a smaller N_T. In Fig. 6.9, BER results of FGQSM, mGQSM, and QSM are compared with different transmit antennas and same SE of 10 bpcu. We observed that the FGQSM performance degrades by $\sim$ 0.5 dB SNR for mGQSM and $\sim$ 2 dB SNR for QSM. In this scenario, the proposed FGQSM scheme requires only 4 transmit antennas whereas, mGQSM and QSM systems require 5 and 16 transmit antennas, respectively.

Figs. 6.10 and 6.11 shows the comparison of proposed FGQSM system with RC-mGQSM and QSM systems with Rician channel for $K = 3$ dB and $K = 5$ dB, respectively. Assume $N_C = 2$, 4-QAM ($M = 4$) for FGQSM system, 8-QAM ($M = 8$) for RC-mGQSM, and 64-QAM ($M = 64$) for QSM. By comparing performances of all these schemes for same SE of 10 bpcu, we found that FGQSM outperforms RC-mGQSM by $\sim$4.5 dB SNR and QSM by $\sim$7.5

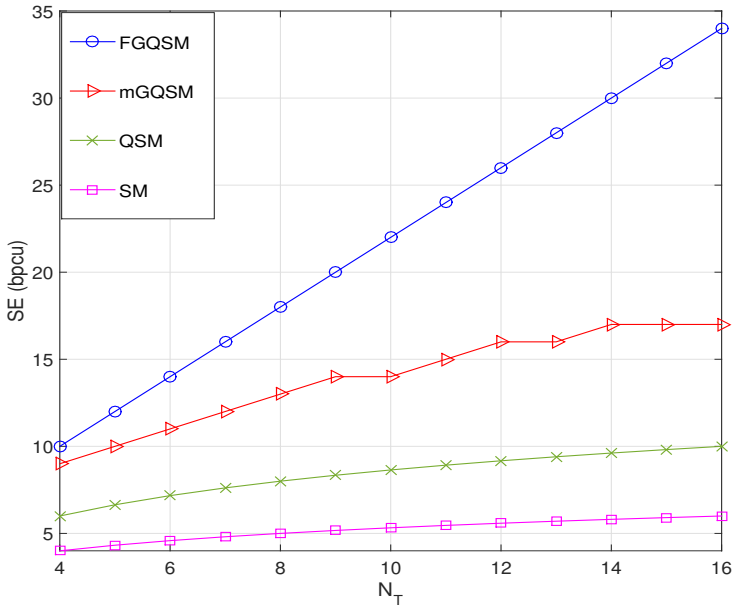

Fig. 6.7 Achievable SE for the proposed FGQSM is compared to mGQSM, QSM, and SM with different N_T values.

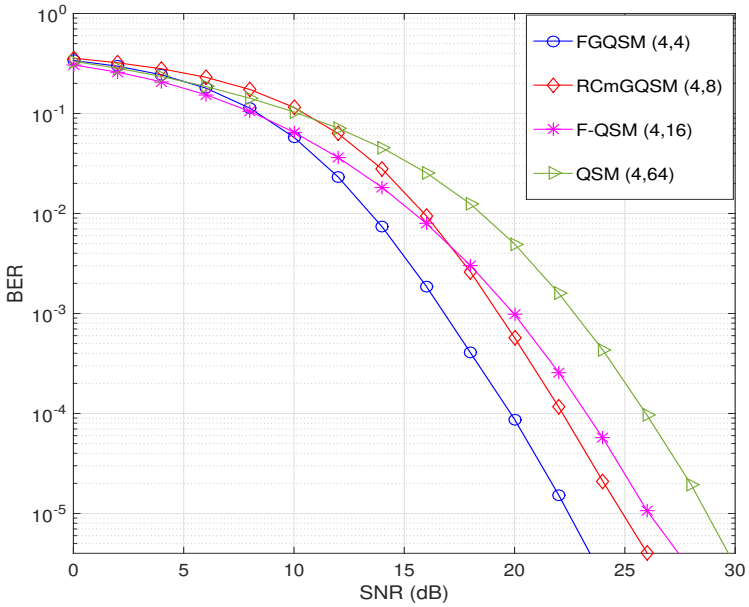

Fig. 6.8 BER Vs. SNR of FGQSM, RC-mGQSM, F-QSM and QSM systems over Rayleigh channel with the same SE of 10 bpcu.

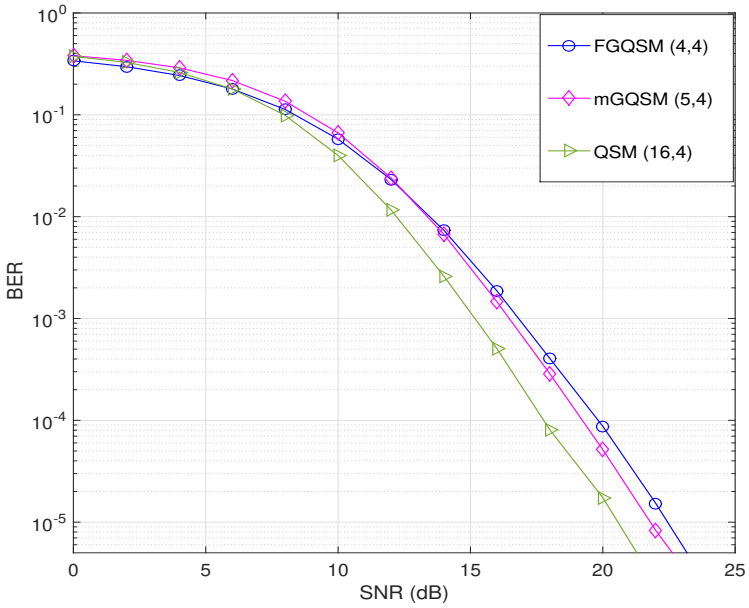

Fig. 6.9 BER Vs. SNR of FGQSM, mGQSM, and QSM systems over Rayleigh channel with different N_T values and same SE of 10 bpcu.

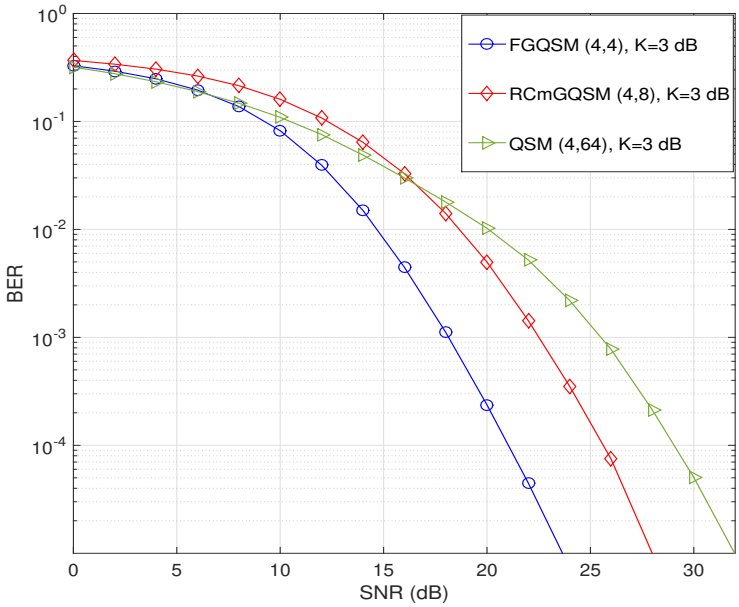

Fig. 6.10 BER Vs. SNR of FGQSM, RC-mGQSM, and QSM systems over Rician channel ($K = 3$) dB with same SE of 10 bpcu.

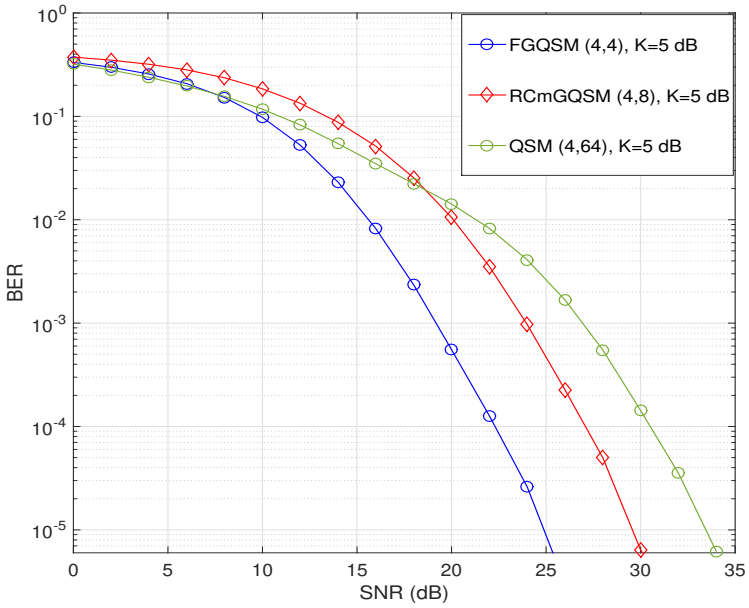

Fig. 6.11 BER Vs. SNR of FGQSM, RC-mGQSM, and QSM systems over Rician channel ($K = 5$) dB with same SE of 10 bpcu.

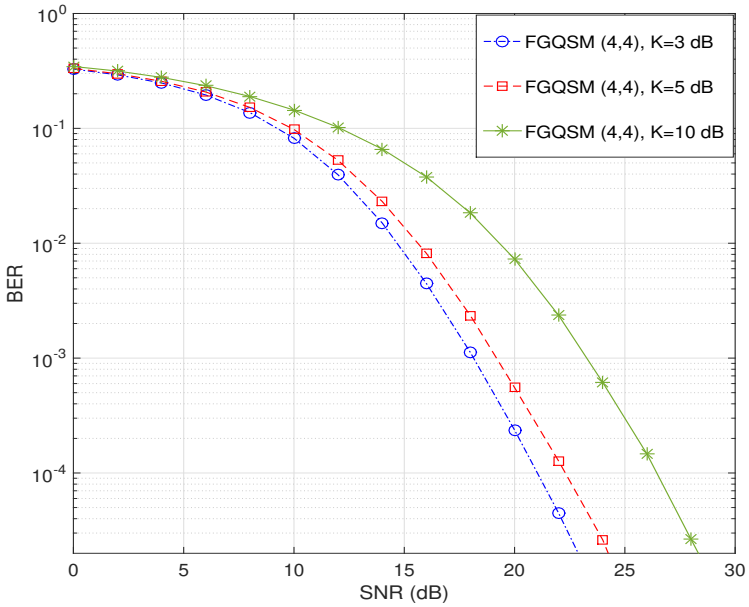

Fig. 6.12 BER Vs. SNR of FGQSM system over Rician channel ($K = 3, 5, 10$) dB with same SE of 10 bpcu.

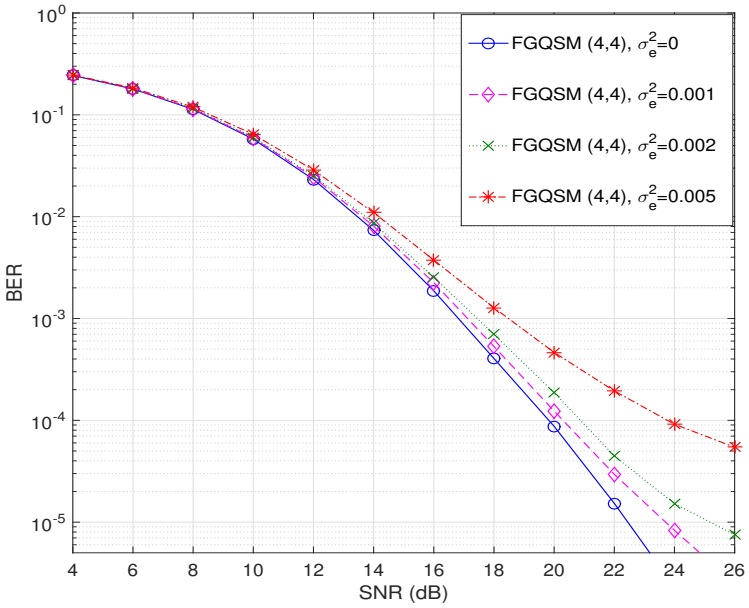

Fig. 6.13 BER Vs. SNR of FGQSM system with fixed error variance ($\sigma_e^2 = (0, 0.001, 0.002, 0.005)$ and $\eta_{FGQSM} = 10$ bpcu.

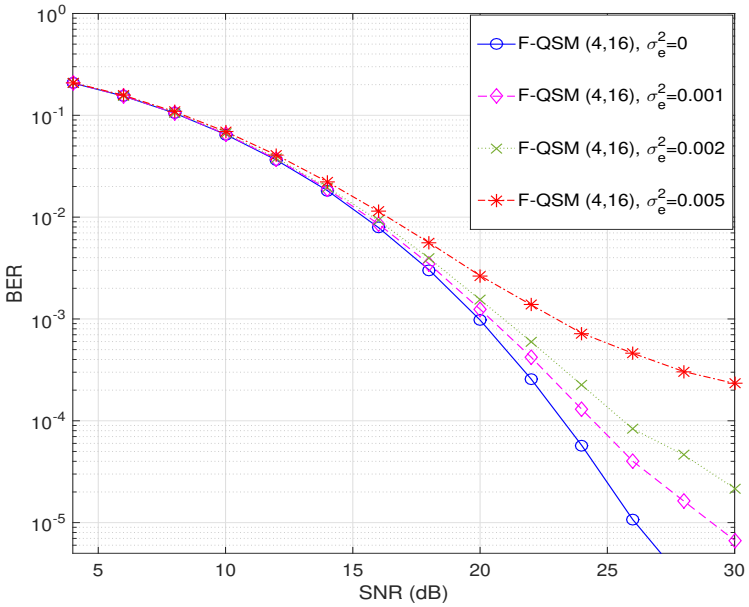

Fig. 6.14 BER Vs. SNR of F-QSM system with fixed error variance ($\sigma_e^2 = (0, 0.001, 0.002, 0.005)$ and $\eta_{F-QSM} = 10$ bpcu.

Table 6.6 BER Vs SNR for imperfect FGQSM and F-QSM

SNR	**FGQSM** (BER)				F-QSM (BER)			
(dB)	$\sigma_e^2 = 0$	$\sigma_e^2 = 0.001$	$\sigma_e^2 = 0.002$	$\sigma_e^2 = 0.005$	$\sigma_e^2 = 0$	$\sigma_e^2 = 0.001$	$\sigma_e^2 = 0.002$	$\sigma_e^2 = 0.005$
18	0.0004	0.0005	0.0006	0.0012	0.0030	0.0034	0.0039	0.0056
22	1.5E-05	2.9E-05	4.4E-05	0.0001	0.0002	0.0004	0.0006	0.0013
24	2.3E-06	8.3E-06	1.5E-05	9.1E-05	5.7E-05	0.0001	0.0002	0.0007

dB SNR values for $K = 3$ dB and $K = 5$ dB. The FGQSM performance over Rician channel with different values of K are shown in Fig. 6.12. Let us consider 4×4 FGQSM system with $N_C = 2$ and 4-QAM ($M = 4$). The performance of FGQSM is evaluated for different values of K. We observed the performance of FGQSM for $K = 3$ dB provide improvement by $\sim$1 dB SNR for $K = 5$ dB and by $\sim$6.5 dB SNR for $K = 10$ dB.

In Figs. 6.13 and 6.14, the FGQSM and F-QSM performances are presented under imperfect CSI conditions, respectively. We compare the BER of both the schemes at SNR of 18 dB, 22 dB, and 24 dB which is shown in Table. 6.6. We assume the values of error variance σ_e^2 as 0, 0.001, 0.002, and 0.005. However, the value $\sigma_e^2 = 0$ becomes the perfect channel. At SNR of 18 dB, observed BER values of FGQSM and F-QSM are 0.0006 and 0.0039, respectively. Similarly, at SNR of 24 dB, BER of FGQSM and F-QSM are 1.5×10^{-05} and 0.0002, respectively, for $\sigma_e^2 = 0.002$. Hence, the FGQSM scheme performance better than F-QSM scheme under imperfect channel conditions. In FGQSM, the data can be transmitted through a variable number of TACs.

6.6 Conclusion

In this chapter, the BER performance of the FGQSM and F-QSM are investigated over Rayleigh and Rician fading channels. A variable TACs are considered for the FGQSM and F-QSM transmission. The achievable SE of the proposed FGQSM is compared to various SMTs with different values of N_T. ML method is used to estimate the transmit antenna indices and data symbols. We compare the BER results of FGQSM system to mGQSM and F-QSM with various values of fading factor for Rician channel. For the Rayleigh channel, the FGQSM outperform by $\sim$ 2 dB, $\sim$ 3.5 dB, $\sim$ 6 dB SNR values over RC-mGQSM, F-QSM, and QSM, respectively. By observing all these schemes, the FGQSM can deliver more number of spatial bits for a smaller N_T. The BER results of FGQSM, mGQSM, and QSM are compared with different transmit antennas and observed that the FGQSM performance degrades by $\sim$ 0.5 dB SNR for mGQSM and $\sim$ 2 dB SNR for QSM. However, the proposed FGQSM requires only 4 transmit antennas whereas, mGQSM and QSM systems require 5 and 16 transmit antennas, respectively. Moreover, proposed FGQSM and F-QSM systems are investigated with imperfect channel conditions. The results demonstrating that the FGQSM outperforms F-QSM.

Chapter 7

Conclusions and Future Scope

7.1 Conclusions

In this thesis, the research has been oriented mainly on the SE improvement of various SM techniques. It contains seven chapters, including this as the last chapter.

In **Chapter 1**, introduction, background, and motivation for carrying out this research has been described.

In **Chapter 2**, the literature review on various SMTs have been provided. The transmission concepts of SM, GSM, MA-SM, QSM, and GQSM techniques are presented in order to enhance the SE and also provided the suitable examples for the data transmission.

In **Chapter 3**, the mGQSM and RC-mGQSM system performances illustrated under Nakagami-m, Rayleigh, and Rician fading channels. Using the ML-detection algorithm, the performance of the mGQSM and RC-mGQSM schemes are presented and compared with the performances of the GQSM, QSM, and SM schemes with various values for the Nakagami parameter and Rician factor. For m=4, the RC-mGQSM outperforms SM ($M = 64$) by ~ 1.5 dB and QSM ($M = 16$) by $\sim$2 dB SNRs. RC-mGQSM performance with 4-QAM modulation outperforms MA-SM ($M = 8$), QSM ($M = 16$), and GSM ($M = 64$) by $\sim$ 2 dB, 3 dB, and 5 dB SNRs, respectively. A low complexity detection method is presented for the RC-mGQSM

scheme. Also, study and compared the performances of the mGQSM and SM schemes under imperfect channel conditions.

In **Chapter 4**, the BER performances of the mGQSM and RC-mGQSM schemes are investigated under correlated Nakagami-m, Rayleigh, and Rician channels. ML method is used to compare the BER results of the mGQSM and RC-mGQSM to that of QSM and GQSM with various fading parameters of Nakagami and Rician channels. We observed that the proposed RC-mGQSM scheme outperforms QSM by $\sim$ 2 dB SNR for $K = 3$ dB and $\sim$ 1.5 dB SNR for $m = 2$. Under Rayleigh channel, the RC-mGQSM, GQSM, and QSM are compared with the fixed SE of 8 bpcu, we noticed that the RC-mGQSM gain 2 dB SNR over QSM and performance degrades by $\sim$ 0.5 dB SNR over GQSM. However, the RC-mGQSM uses more number of active antennas when compared to GQSM for the fixed system configuration. Furthermore, a low-complexity OB-MMSE detector is developed for the RC-mGQSM, and it is shown that the OB-MMSE detector achieves near-ML performance with reduced computational complexity of 47% when compared to the ML detector. Moreover, the mGQSM and QSM are evaluated and compared under imperfect CSI conditions. The study demonstrates that the mGQSM performs better than the QSM at high SNR values.

In **Chapter 5**, the BER results of mGQSM and RC-mGQSM systems are presented over uncorrelated and correlated Weibull fading channels. Using the ML detector, mGQSM and RC-mGQSM systems are illustrated and compared to QSM and GQSM systems. We considered Weibull non-fading and deep-fading environments with β equal to 5 and 0.5, respectively. The BER results of RC-mGQSM system are compared to that of QSM and GQSM. The RC-mGQSM outperforms QSM by $\sim$1.5 dB SNR and degrades $\sim$1.6 dB SNR over GQSM. The mGQSM outperforms QSM by $\sim$3 dB SNR and $\sim$4 dB SNR for correlated and uncorrelated Weibull channels, respectively. Furthermore, the mGQSM performance is demonstrated under imperfect CSI and compared to QSM. The computational complexity of the mGQSM increases with the SE.

In **Chapter 6**, the BER performance of the FGQSM and F-QSM are investigated over

Rayleigh and Rician fading channels. A variable TACs are considered for the FGQSM and F-QSM transmission. The achievable SE of the proposed FGQSM is compared to various SMTs with the different N_T values. For the Rayleigh channel, the FGQSM outperform by ~ 2 dB, ~ 3.5 dB, ~ 6 dB SNR values over RC-mGQSM, F-QSM, and QSM, respectively. By observing all these schemes, the FGQSM can deliver more number of spatial bits for a smaller N_T. The BER results of FGQSM, mGQSM, and QSM are compared with different transmit antennas and observed that the FGQSM performance degrades by ~ 0.5 dB SNR for mGQSM and ~ 2 dB SNR for QSM. However, the proposed FGQSM requires only 4 transmit antennas whereas, mGQSM and QSM systems require 5 and 16 transmit antennas, respectively. Moreover, proposed FGQSM and F-QSM systems are investigated with imperfect channel conditions. The results demonstrating that the FGQSM performance is better than F-QSM.

7.2 Future Scope

In this thesis, various fading channels are used to present the BER performances of mGQSM, RC-mGQSM, and FGQSM schemes. Furthermore, low complexity detection methods are used to investigate the performance of the RC-mGQSM scheme. This work can be further extended as follows.

- The computational complexity of the ML detection for the mGQSM scheme is increases by enhancing the SE. However, it requires near-ML low-complexity detection methods to further reduce the computational complexity.
- Massive MIMO systems can employ large number of transmit antennas (about 10 to 100 antennas) at the base station further to improve the SE.
- Point-to-multipoint or multi-user MIMO (MU-MIMO) communication can be investigated.

Bibliography

[1] D. Tse and P. Viswanath, *Fundamentals of wireless communication*. Cambridge university press, 2005.

[2] A. Chockalingam and B. S. Rajan, *Large MIMO systems*. Cambridge University Press, 2014.

[3] P. Wolniansky, G. Foschini, G. Golden, and R. Valenzuela, "V-blast: an architecture for realizing very high data rates over the rich-scattering wireless channel," in *1998 URSI International Symposium on Signals, Systems, and Electronics. Conference Proceedings (Cat. No.98EX167)*, pp. 295–300, 1998.

[4] R. Mesleh and A. Alhassi, *Space modulation techniques*. John Wiley & Sons, 2018.

[5] E. Basar, M. Wen, R. Mesleh, M. Di Renzo, Y. Xiao, and H. Haas, "Index modulation techniques for next-generation wireless networks," *IEEE Access*, vol. 5, pp. 16693–16746, 2017.

[6] X. Cheng, M. Zhang, M. Wen, and L. Yang, "Index modulation for 5g: Striving to do more with less," *IEEE Wireless Communications*, vol. 25, no. 2, pp. 126–132, 2018.

[7] Y.-T. Lai, Y.-R. Ciou, and J.-M. Wu, "Index modulation multiple access," in *2018 IEEE 29th Annual International Symposium on Personal, Indoor and Mobile Radio Communications (PIMRC)*, pp. 1–5, 2018.

[8] T. Mao, Q. Wang, Z. Wang, and S. Chen, "Novel index modulation techniques: A survey," *IEEE Communications Surveys & Tutorials*, vol. 21, no. 1, pp. 315–348, 2019.

[9] R. Y. Mesleh, H. Haas, S. Sinanovic, C. W. Ahn, and S. Yun, "Spatial modulation," *IEEE Transactions on Vehicular Technology*, vol. 57, no. 4, pp. 2228–2241, 2008.

[10] J. Jeganathan, A. Ghrayeb, and L. Szczecinski, "Spatial modulation: optimal detection and performance analysis," *IEEE Communications Letters*, vol. 12, no. 8, pp. 545–547, 2008.

[11] M. Di Renzo, H. Haas, A. Ghrayeb, S. Sugiura, and L. Hanzo, "Spatial modulation for generalized mimo: Challenges, opportunities, and implementation," *Proceedings of the IEEE*, vol. 102, no. 1, pp. 56–103, 2014.

[12] M. D. Renzo, H. Haas, and P. M. Grant, "Spatial modulation for multiple-antenna wireless systems: a survey," *IEEE Communications Magazine*, vol. 49, no. 12, pp. 182–191, 2011.

[13] P. Yang, M. Di Renzo, Y. Xiao, S. Li, and L. Hanzo, "Design guidelines for spatial modulation," *IEEE Communications Surveys & Tutorials*, vol. 17, no. 1, pp. 6–26, 2015.

[14] A. Younis, N. Serafimovski, R. Mesleh, and H. Haas, "Generalised spatial modulation," in *2010 conference record of the forty fourth Asilomar conference on signals, systems and computers*, pp. 1498–1502, IEEE, 2010.

[15] J. Fu, C. Hou, W. Xiang, L. Yan, and Y. Hou, "Generalised spatial modulation with multiple active transmit antennas," in *2010 IEEE Globecom Workshops*, pp. 839–844, 2010.

[16] J. Wang, S. Jia, and J. Song, "Generalised spatial modulation system with multiple active transmit antennas and low complexity detection scheme," *IEEE Transactions on Wireless Communications*, vol. 11, no. 4, pp. 1605–1615, 2012.

[17] T. Datta and A. Chockalingam, "On generalized spatial modulation," in *2013 IEEE Wireless Communications and Networking Conference (WCNC)*, pp. 2716–2721, 2013.

[18] M. Irfan and S. Aïssa, "Multiple active spatial modulation: A possibility of more than spatial multiplexing," *IEEE Wireless Communications Letters*, vol. 9, no. 3, pp. 294–297, 2020.

[19] R. Mesleh, S. S. Ikki, and H. M. Aggoune, "Quadrature spatial modulation," *IEEE Transactions on Vehicular Technology*, vol. 64, no. 6, pp. 2738–2742, 2015.

[20] Z. Yigit and E. Basar, "Low-complexity detection of quadrature spatial modulation," *Electronics Letters*, vol. 52, no. 20, pp. 1729–1731, 2016.

[21] Z. Yigit, E. Basar, and R. Mesleh, "Trellis coded quadrature spatial modulation," *Physical Communication*, vol. 29, pp. 147–155, 2018.

[22] F. R. Castillo-Soria, J. Cortez-González, R. Ramirez-Gutierrez, F. M. Maciel-Barboza, and L. Soriano-Equigua, "Generalized quadrature spatial modulation scheme using antenna grouping," *ETRI Journal*, vol. 39, no. 5, pp. 707–717, 2017.

[23] R. Abu-alhiga and H. Haas, "Subcarrier-index modulation ofdm," in *2009 IEEE 20th International Symposium on Personal, Indoor and Mobile Radio Communications*, pp. 177–181, 2009.

[24] E. Başar, m. Aygölü, E. Panayırcı, and H. V. Poor, "Orthogonal frequency division multiplexing with index modulation," *IEEE Transactions on Signal Processing*, vol. 61, no. 22, pp. 5536–5549, 2013.

[25] M. Wen, B. Ye, E. Basar, Q. Li, and F. Ji, "Enhanced orthogonal frequency division multiplexing with index modulation," *IEEE Transactions on Wireless Communications*, vol. 16, no. 7, pp. 4786–4801, 2017.

[26] M. Wen, E. Basar, Q. Li, B. Zheng, and M. Zhang, "Multiple-mode orthogonal frequency division multiplexing with index modulation," *IEEE Transactions on Communications*, vol. 65, no. 9, pp. 3892–3906, 2017.

[27] M. Wen, Q. Li, E. Basar, and W. Zhang, "Generalized multiple-mode ofdm with index modulation," *IEEE Transactions on Wireless Communications*, vol. 17, no. 10, pp. 6531–6543, 2018.

[28] J. Li, S. Dang, M. Wen, X.-Q. Jiang, Y. Peng, and H. Hai, "Layered orthogonal frequency division multiplexing with index modulation," *IEEE Systems Journal*, vol. 13, no. 4, pp. 3793–3802, 2019.

[29] J. Li, Y. Peng, Y. Yan, X.-Q. Jiang, H. Hai, and M. Zukerman, "Cognitive radio network assisted by ofdm with index modulation," *IEEE Transactions on Vehicular Technology*, vol. 69, no. 1, pp. 1106–1110, 2020.

[30] J. Li, Q. Li, S. Dang, M. Wen, X.-Q. Jiang, and Y. Peng, "Low-complexity detection for index modulation multiple access," *IEEE Wireless Communications Letters*, vol. 9, no. 7, pp. 943–947, 2020.

[31] B. Zheng, M. Wen, E. Basar, and F. Chen, "Multiple-input multiple-output ofdm with index modulation: Low-complexity detector design," *IEEE Transactions on Signal Processing*, vol. 65, no. 11, pp. 2758–2772, 2017.

[32] A. Alshamali and B. Quza, "Spatial modulation: Performance evaluation in nakagami fading channels," in *2009 5th IEEE GCC Conference & Exhibition*, pp. 1–4, 2009.

[33] A. Alshamali and B. Quza, "Performance of spatial modulation in correlated and uncorrelated nakagami fading channel.," *J. Commun.*, vol. 4, no. 3, pp. 170–174, 2009.

[34] R. Nunes, B. A. Angélico, and T. Abrão, "Impact of imperfect channel estimation on the performance of spatial modulation mimo systems," 2013.

[35] E. Basar, U. Aygolu, E. Panayirci, and H. V. Poor, "Performance of spatial modulation in the presence of channel estimation errors," *IEEE Communications Letters*, vol. 16, no. 2, pp. 176–179, 2011.

[36] M. Koca and H. Sari, "Performance of spatial modulation over correlated fading channels with channel estimation errors," in *2013 IEEE Wireless Communications and Networking Conference (WCNC)*, pp. 3937–3942, 2013.

[37] A. B. Saleem and S. A. Hassan, "On the performance of spatial modulation schemes in large-scale mimo under correlated nakagami fading," in *2020 IEEE 91st Vehicular Technology Conference (VTC2020-Spring)*, pp. 1–5, 2020.

[38] M. Di Renzo and H. Haas, "Bit error probability of sm-mimo over generalized fading channels," *IEEE Transactions on Vehicular Technology*, vol. 61, no. 3, pp. 1124–1144, 2012.

[39] N. Serafimovski, A. Younis, R. Mesleh, P. Chambers, M. Di Renzo, C.-X. Wang, P. M. Grant, M. A. Beach, and H. Haas, "Practical implementation of spatial modulation," *IEEE Transactions on Vehicular Technology*, vol. 62, no. 9, pp. 4511–4523, 2013.

[40] R. Mesleh, M. Di Renzo, H. Haas, and P. M. Grant, "Trellis coded spatial modulation," *IEEE Transactions on Wireless Communications*, vol. 9, no. 7, pp. 2349–2361, 2010.

[41] M. Lupupa and M. E. Dlodlo, "Performance of mimo system in weibull fading channel-channel capacity analysis," in *IEEE EUROCON 2009*, pp. 1735–1740, IEEE, 2009.

[42] R. Mudoi and R. Rongphar, "Performance analysis of tas/mrc-based mimo system over k fading channels," *International Journal of Systems, Control and Communications*, vol. 12, no. 4, pp. 279–290, 2021.

[43] O. S. Badarneh, F. S. Almehmadi, and T. Aldalgamouni, "On the performance analysis of wireless communication systems over α-μ/α-μ composite fading channels.," *Int. J. Ad Hoc Ubiquitous Comput.*, vol. 30, no. 3, pp. 137–149, 2019.

[44] A. Ghazizadeh, H. Mahlooji, A. T. Azar, M. Hamid, and M. Bastan, "Single-step change point estimation in nonlinear profiles using maximum likelihood estimation," *International Journal of Intelligent Engineering Informatics*, vol. 6, no. 6, pp. 527–547, 2018.

[45] R. Jindal and I. Singh, "A survey on database intrusion detection: approaches, challenges and application," *International Journal of Intelligent Engineering Informatics*, vol. 7, no. 6, pp. 559–592, 2019.

[46] A. M. Alshamali and M. S. Aloqlah, "Performance analysis of spatial modulation over weibull fading channels," *WSEAS Transaction on Communications*, vol. 11, no. 12, pp. 604–607, 2013.

[47] G. S. GD, S. Koila, N. Neha, and U. Sripati, "Performance of spatial-modulation and spatial-multiplexing systems over weibull fading channel," in *2015 international conference on computing and network communications (CoCoNet)*, pp. 389–394, IEEE, 2015.

[48] E. Basar, "Index modulation techniques for 5g wireless networks," *IEEE Communications Magazine*, vol. 54, no. 7, pp. 168–175, 2016.

[49] Y. Xiao, L. Xiao, L. Dan, and X. Lei, "Spatial modulaiton for 5g mimo communications," in *2014 19th International Conference on Digital Signal Processing*, pp. 847–851, IEEE, 2014.

[50] M. Wen, B. Zheng, K. J. Kim, M. Di Renzo, T. A. Tsiftsis, K.-C. Chen, and N. Al-Dhahir, "A survey on spatial modulation in emerging wireless systems: Research progresses and applications," *IEEE Journal on Selected Areas in Communications*, vol. 37, no. 9, pp. 1949–1972, 2019.

[51] J. Jeganathan, A. Ghrayeb, L. Szczecinski, and A. Ceron, "Space shift keying modulation for mimo channels," *IEEE Transactions on Wireless Communications*, vol. 8, no. 7, pp. 3692–3703, 2009.

[52] J. Jeganathan, A. Ghrayeb, and L. Szczecinski, "Generalized space shift keying modulation for mimo channels," in *2008 IEEE 19th International Symposium on Personal, Indoor and Mobile Radio Communications*, pp. 1–5, 2008.

[53] R. Y. Chang, S. J. Lin, and W. H. Chung, "New space shift keying modulation with hamming code-aided constellation design," *IEEE Wireless Communications Letters*, vol. 1, no. 1, pp. 2–5, 2012.

[54] H. W. Liang, R. Y. Chang, W. H. Chung, H. Zhang, and S. Y. Kuo, "Bi-space shift keying modulation for mimo systems," *IEEE Communications Letters*, vol. 16, no. 8, pp. 1161–1164, 2012.

[55] B. Vo and H. H. Nguyen, "Bi-generalized space shift keying over mimo channels," *IEICE Communications Express*, vol. 5, no. 4, 2016.

[56] R. Rajashekar, K. V. S. Hari, and L. Hanzo, "Antenna selection in spatial modulation systems," *IEEE Communications Letters*, vol. 17, no. 3, pp. 521–524, 2013.

[57] R. Rajashekar, K. V. S. Hari, K. Giridhar, and L. Hanzo, "Performance analysis of antenna selection algorithms in spatial modulation systems with imperfect csir," in *European Wireless 2013; 19th European Wireless Conference*, pp. 1–5, 2013.

[58] R. Rajashekar, K. V. S. Hari, and L. Hanzo, "Reduced-complexity ml detection and capacity-optimized training for spatial modulation systems," *IEEE Transactions on Communications*, vol. 62, no. 1, pp. 112–125, 2014.

[59] A. Younis, D. A. Basnayaka, and H. Haas, "Performance analysis for generalised spatial modulation," in *European Wireless 2014; 20th European Wireless Conference*, pp. 1–6, VDE, 2014.

[60] M. Koca and H. Sari, "Generalized spatial modulation over correlated fading channels: Performance analysis and optimization," in *ICT 2013*, pp. 1–5, 2013.

[61] Y. Xiao, Z. Yang, L. Dan, P. Yang, L. Yin, and W. Xiang, "Low-complexity signal detection for generalized spatial modulation," *IEEE Communications Letters*, vol. 18, no. 3, pp. 403–406, 2014.

[62] H.-Y. Yoon and T.-H. Kim, "Low-complexity symbol detection for generalized spatial modulation mimo systems," in *2017 IEEE 86th Vehicular Technology Conference (VTC-Fall)*, pp. 1–5, 2017.

[63] C.-C. Cheng, H. Sari, S. Sezginer, and Y. T. Su, "Enhanced spatial modulation with multiple signal constellations," *IEEE Transactions on Communications*, vol. 63, no. 6, pp. 2237–2248, 2015.

[64] M. M. Alwakeel, "Quadrature spatial modulation performance analysis over rician fading channels.," *J. Commun.*, vol. 11, no. 3, pp. 249–254, 2016.

[65] A. Younis, R. Mesleh, and H. Haas, "Quadrature spatial modulation performance over nakagami- m fading channels," *IEEE Transactions on Vehicular Technology*, vol. 65, no. 12, pp. 10227–10231, 2016.

[66] M. Yacoub, G. Fraidenraich, and J. Santos Filho, "Nakagami-m phase-envelope joint distribution," *Electronics Letters*, vol. 41, no. 5, pp. 259–261, 2005.

[67] R. Mesleh and S. S. Ikki, "On the impact of imperfect channel knowledge on the performance of quadrature spatial modulation," in *2015 IEEE Wireless Communications and Networking Conference (WCNC)*, pp. 534–538, 2015.

[68] A. Afana, I. Atawi, S. Ikki, and R. Mesleh, "Energy efficient quadrature spatial modulation mimo cognitive radio systems with imperfect channel estimation," in *2015 IEEE international conference on ubiquitous wireless broadband (ICUWB)*, pp. 1–5, IEEE, 2015.

[69] R. Mesleh and O. S. Badarneh, "Quadrature spatial modulation in correlated η-μ fading channels with imperfect channel state information," in *2017 International Conference on Wireless Communications, Signal Processing and Networking (WiSPNET)*, pp. 887–892, IEEE, 2017.

[70] O. S. Badarneh and R. Mesleh, "Performance of quadrature spatial modulation with imperfect channel information over correlated α-μ fading channels," in *2016 IEEE Wireless Communications and Networking Conference*, pp. 1–5, IEEE, 2016.

[71] R. Mesleh, S. S. Ikki, and H. M. Aggoune, "Quadrature spatial modulation–performance analysis and impact of imperfect channel knowledge," *Transactions on Emerging Telecommunications Technologies*, vol. 28, no. 1, p. e2905, 2017.

[72] A. Afana, E. Erdogan, and S. Ikki, "Quadrature spatial modulation for cooperative mimo 5g wireless networks," in *2016 IEEE Globecom Workshops (GC Wkshps)*, pp. 1–5, IEEE, 2016.

[73] I. Al-Nahhal, O. A. Dobre, and S. S. Ikki, "Quadrature spatial modulation decoding complexity: Study and reduction," *IEEE Wireless Communications Letters*, vol. 6, no. 3, pp. 378–381, 2017.

[74] A. Younis, N. Abuzgaia, R. Mesleh, and H. Haas, "Quadrature spatial modulation for 5g outdoor millimeter–wave communications: Capacity analysis," *IEEE Transactions on Wireless Communications*, vol. 16, no. 5, pp. 2882–2890, 2017.

[75] O. S. Badarneh and R. Mesleh, "A comprehensive framework for quadrature spatial modulation in generalized fading scenarios," *IEEE Transactions on Communications*, vol. 64, no. 7, pp. 2961–2970, 2016.

[76] J. Li, X. Jiang, Y. Yan, W. Yu, S. Song, and M. H. Lee, "Low complexity detection for quadrature spatial modulation systems," *Wireless Personal Communications*, vol. 95, no. 4, pp. 4171–4183, 2017.

[77] V. B. Kumaravelu, G. Jaiswal, V. V. Gudla, G. Ramachandra Reddy, and A. Murugadass, "Modified spatial modulation: an alternate to spatial multiplexing for 5g-based compact wireless devices," *Arabian Journal for Science and Engineering*, vol. 44, pp. 6693–6709, 2019.

[78] G. Jaiswal, V. V. Gudla, V. B. Kumaravelu, G. R. Reddy, and A. Murugadass, "Modified spatial modulation and low complexity signal vector based minimum mean square error detection for mimo systems under spatially correlated channels," *Wireless Personal Communications*, vol. 110, no. 2, pp. 999–1020, 2020.

[79] B. Vo and H. H. Nguyen, "Improved quadrature spatial modulation," in *2017 IEEE 86th Vehicular Technology Conference (VTC-Fall)*, pp. 1–5, IEEE, 2017.

[80] T. Holoubi, S. Murtala, N. Muchena, and M. Mohaisen, "On the performance of improved quadrature spatial modulation," *ETRI Journal*, vol. 42, no. 4, pp. 562–574, 2020.

[81] Z. Yigit and E. Basar, "Double spatial modulation: A high-rate index modulation scheme for mimo systems," in *2016 International Symposium on Wireless Communication Systems (ISWCS)*, pp. 347–351, 2016.

[82] G. S. GD, K. Shriharsha, M. Raghavendra, and U. S. Acharya, "A comprehensive framework for double spatial modulation under imperfect channel state information," *Physical Communication*, vol. 25, pp. 519–526, 2017.

[83] T. Holoubi, S. Murtala, N. Muchena, and M. Mohaisen, "Double quadrature spatial modulation," *International Journal of Internet, Broadcasting and Communication*, vol. 11, no. 3, pp. 27–33, 2019.

[84] W. Zhao, Z. Huang, F. Huang, and Y. Zhan, "Double generalized spatial modulation," *Transactions on Emerging Telecommunications Technologies*, vol. 33, no. 1, p. e4386, 2022.

[85] M. Mohaisen and S. Lee, "Complex quadrature spatial modulation," *Etri Journal*, vol. 39, no. 4, pp. 514–524, 2017.

[86] M. Mohaisen, "Increasing the minimum euclidean distance of the complex quadrature spatial modulation," *IET Communications*, vol. 12, no. 7, pp. 854–860, 2018.

[87] M. Mohaisen, "Generalized complex quadrature spatial modulation," *Wireless Communications and Mobile Computing*, vol. 2019, 2019.

[88] S. Murtala, N. Muchena, T. Holoubi, M. Mohaisen, and K.-S. Choi, "Parallel complex quadrature spatial modulation," *Applied Sciences*, vol. 11, no. 1, p. 330, 2020.

[89] J. Li, S. Dang, Y. Yan, Y. Peng, S. Al-Rubaye, and A. Tsourdos, "Generalized quadrature spatial modulation and its application to vehicular networks with noma," *IEEE Transactions on Intelligent Transportation Systems*, vol. 22, no. 7, pp. 4030–4039, 2021.

[90] J. Li, M. Wen, X. Cheng, Y. Yan, S. Song, and M. H. Lee, "Generalized precoding-aided quadrature spatial modulation," *IEEE Transactions on Vehicular Technology*, vol. 66, no. 2, pp. 1881–1886, 2017.

[91] S. Guo, H. Zhang, P. Zhang, S. Dang, C. Liang, and M.-S. Alouini, "Signal shaping for generalized spatial modulation and generalized quadrature spatial modulation," *IEEE Transactions on Wireless Communications*, vol. 18, no. 8, pp. 4047–4059, 2019.

[92] J. An, C. Xu, Y. Liu, L. Gan, and L. Hanzo, "The achievable rate analysis of generalized quadrature spatial modulation and a pair of low-complexity detectors," *IEEE Transactions on Vehicular Technology*, vol. 71, no. 5, pp. 5203–5215, 2022.

[93] K. Gunde and K. Hari, "Modified generalised quadrature spatial modulation," in *2019 National Conference on Communications (NCC)*, pp. 1–5, 2019.

[94] M. Elsayed, H. S. Hussein, and U. S. Mohamed, "Fully generalised spatial modulation," in *2018 35th national radio science conference (NRSC)*, pp. 274–282, IEEE, 2018.

[95] I. E Shaalan, S. Dawod, and S. M Abuelenin, "Fully generalized spatial modulation utilizing transmit antenna grouping," *Port-Said Engineering Research Journal*, vol. 25, no. 1, pp. 49–58, 2021.

[96] H. S. Hussein and M. Elsayed, "Fully-quadrature spatial modulation," in *2018 IEEE international black sea conference on communications and networking (BlackSeaCom)*, pp. 1–5, IEEE, 2018.

[97] H. S. Hussein, M. Elsayed, and U. S. Mohamed, "Fully-quadrature spatial modulation over rician fading channels," in *2018 International Japan-Africa Conference on Electronics, Communications and Computations (JAC-ECC)*, pp. 39–42, IEEE, 2018.

[98] V. V. Gudla, S. Gamini, V. B. Kumaravelu, and F. R. C. Soria, "Performance evaluation of fully quadrature spatial modulation under various channel fading scenarios," in *2022 2nd International Conference on Artificial Intelligence and Signal Processing (AISP)*, pp. 1–5, 2022.

[99] R. Mesleh, O. Hiari, A. Younis, and S. Alouneh, "Transmitter design and hardware considerations for different space modulation techniques," *IEEE Transactions on Wireless Communications*, vol. 16, no. 11, pp. 7512–7522, 2017.

[100] Y. Celik, "Fully improved quadrature spatial modulation," *Arabian Journal for Science and Engineering*, vol. 46, no. 10, pp. 9639–9647, 2021.

[101] H. S. Hussein, M. Elsayed, U. S. Mohamed, H. Esmaiel, and E. M. Mohamed, "Spectral efficient spatial modulation techniques," *IEEE Access*, vol. 7, pp. 1454–1469, 2018.

[102] J.-P. Kermoal, L. Schumacher, K. I. Pedersen, P. E. Mogensen, and F. Frederiksen, "A stochastic mimo radio channel model with experimental validation," *IEEE Journal on selected areas in Communications*, vol. 20, no. 6, pp. 1211–1226, 2002.

[103] A. Van Zelst and J. Hammerschmidt, "A single coefficient spatial correlation model for multiple-input multiple-output (mimo) radio channels," *Proc. 27th General Assembly of the Int. Union of Radio Science (URSI)*, 2002.

[104] A. M. Abu-Hudrouss, M. . -T. O. E. Astal, A. H. Al Habbash and S. Aïssa, "Signed quadrature spatial modulation for MIMO systems," *IEEE Transactions on Vehicular Technology*, vol. 69, no. 3, pp. 2740–2746, 2020.

[105] A. M. Abu-Hudrouss, H. S. Al Nahhal, I. A. Mousa and K. B. A. Issa, "A study of low complexity antenna selection algorithms for signed quadrature spatial modulation," *International Conference on Promising Electronic Technologies (ICPET)*, pp. 56–60, 2020.

[106] M. Alshawaqfeh, A. Gharaibeh and R. Mesleh, "Optimal low complexity detector for signed quadrature spatial modulation MIMO system," *IEEE Journal on Selected Areas in Communications*, vol. 40, no. 10, pp. 2855–2864, 2022.

[107] A. H. A. Habbash, A. M. Abu-Hudrouss, M. T. O. E. Astal, M. A. Albreem and S. S. Ikki, "Extended signed quadrature spatial modulation system with multi-user support," *IEEE Transactions on Broadcasting*, vol. 67, no. 4, pp. 868–878, 2021.

[108] O. Hiari and R. Mesleh, "Novel transmitter designs for variant signed quadrature space modulation techniques," *IEEE Systems Journal*, vol. 16, no. 2, pp. 3437–3445, 2022.

[109] T. Y. Elganimi and K. M. Rabie, "Multidimensional generalized quadrature index modulation for 5G wireless communications," *IEEE 93rd Vehicular Technology Conference (VTC2021-Spring)*, pp. 1–6, 2021.

[110] V. V. Gudla, S. Gamini, V. B. Kumaravelu and F. R. C. Soria, "Performance evaluation of fully quadrature spatial modulation under various channel fading scenarios," *2nd International Conference on Artificial Intelligence and Signal Processing (AISP)*, pp. 1–5, 2022.

[111] M. Yan, Z. Bai, K. Pang, B. Li, P. Ma and X. Hao, "Antenna grouping based generalized spatial modulation system," *IEEE/CIC International Conference on Communications in China (ICCC)*, pp. 574–578, 2021.

[112] M. A. Kurt and E. Başar, "Transmit antenna grouping quadrature spatial modulation for MIMO systems," *29th Signal Processing and Communications Applications Conference (SIU)*, pp. 1-4, 2021.

[113] N. Sibanda, H. Xu, and N. Pillay, "Error performance analysis of generalized quadrature spatial modulation using H-8QAM," *Scientific Reports*, vol. 12, no. 1, p.20634, 2022.

List of Publications

Inernational Journals

1 K. Gunde and A. Sundru, "Modified Generalised Quadrature Spatial Modulation Performance over Nakagami-m Fading Channel," International Journal of Communication Systems (IJCS), Wiley, vol. 34, no. 16, e4944, 2021. [SCIE, Wiley]

2 K. Gunde and A. Sundru, "Performance of Modified Generalised Quadrature Spatial Modulation over Correlated Fading Channels with Imperfect Channel Information," Transactions on Emerging Telecommunications Technologies, Wiley, vol. 33, no. 9, e4563, 2022. [SCIE, Wiley]

3 K. Gunde and A. Sundru, "On the Performance of Modified Generalised Quadrature Spatial Modulation under Correlated Weibull Fading," International Journal of Intelligent Engineering Informatics, vol. 10, no. 3, pp. 183-195, 2022. [ESCI, Inderscience]

4 K. Gunde and A. Sundru, "Fully Generalised Quadrature Spatial Modulation Performance with Variable Transmit Antenna Combinations," Wireless Personal Communications, Springer. [Under Review]

Book Chapters

5 K. Gunde and A. Sundru, "Modified Generalised Quadrature Spatial Modulation Performance over Weibull Fading Channel," International Conference on Communication and Computational Technologies (ICCCT), pp. 79-88, 27-28 Feb, 2021. [Book Chapter, Algorithms for Intelligent Systems (AIS), Springer]

6 K. Gunde and A. Sundru, "Fully Quadrature Spatial Modulation Performance with Imperfect Channel Information," International Conference on Computational Electronics for Wireless Communications (ICCWC), pp. 527-535, 9-10 June, 2022. [Book Chapter, Lecture Notes on Networks and Systems (LNNS), vol. 554, Springer]